FACULTY OF SCIENCES

HYDROGEOLOGICAL INVESTIGATION AND RECHARGE ESTIMATION OF GUMERA RIVER CATCHMENT IN LAKE TANA BASIN, NORTHERN ETHIOPIA.

Annelies Van Landtschoote
Student number: 01201129

Promotor: Prof. Dr. Kristine Walraevens

Jury: Marc Van Camp, Prof. Dr. Wim Cornelis

Master's dissertation submitted in partial fulfilment of the requirements for the degree of Master of Science in Geology

Academic year: 2016 - 2017

GHENT UNIVERSITY

KU LEUVEN

Preface – Acknowledgements

I would like to thank Prof. Dr. Kristine Walraevens to give me the opportunity to perform a thesis in hydrogeology and for her consistent advice and guidance with this final work. I am very thankful to have the opportunity improving my knowledge in hydrogeology.

I am very thankful to Marc Van Camp for his observations and guidance throughout my collected data. He improved my knowledge with his advice and great ideas.

I would like to thank Fenta to provide all the necessary financial and material for the fieldwork.

I am very thankful to Ashebir and Alemu for their guidance and suggestions during fieldwork and to be the translator if it was necessary. They continued with the monitoring of the wells when I left Ethiopia. They provided me the necessary data and information and together with Melese, they immersed me into the Ethiopian culture.

Many thanks go to Binyam. He brought me safely everywhere in the catchment and tried to enter in poorly accessible areas.

I am very thankful to Jessica, Melese and Alebachew to give me an unforgettable time in Ethiopia.

I would like to express my deepest gratitude to my parents, my sister and friends for their believe and infinite support in me.

Table of Contents

1. Introduction

1.1. Background

Water is one of the most important resources on earth. It is affecting every aspect of human life and dominates the functioning of terrestrial and aquatic ecosystems. Ethiopia is located in East-Africa and consists of 12 river basins (Fig. 1.1). Temperature and rainfall patterns vary across the country due to large topographic variations and differences in response to regional and global weather mechanisms (Korecha and Barnston, 2007). Higher precipitation mainly occurs in the western basins while the central and eastern basins have to deal with water shortages (Ludi et al., 2013). The population of Ethiopia is generally a poor, fast growing and largely rural population of which the agriculture is heavily dependent on the rainy season. (Ludi et al., 2013). Currently, frequent droughts and poverty have increased the demand for irrigation and hydropower development which enhances the utilization of water. According the World Health Organization, a large part of the Ethiopian population is living below the national poverty line. One of the severe needs is the access to safe water and good sanitation. Of the total population only 57,3 % is using improved drinking water sources and only 28 % makes use of improved sanitation facilities (WHO, 2016). A productive water use enhances the diet and increases the earnings, leading to improved food and livelihood security. Safe water, used for domestic purposes, decreases the risk of diseases related to poor water quality, sanitation and hygiene (Van Koppen et al., 2009). The geology, geomorphology, and climate are mainly influencing the groundwater occurrence determining the water quality, availability and storage. The water resources available in Ethiopia indicate a large variation in spatial and temporal distribution. Due to the increasing population, the agricultural activity has intensified resulting in extensive vegetation and land degradation (Kebede et al., 2006). This causes reductions in infiltration capacity and groundwater recharge, together with an increase in surface runoff and erosion. The main challenge of the water management sector is to improve a sustainable use of groundwater without affecting the social and economic development and to attenuate the impacts of runoff, drought, flood events and other natural hazards (Ludi et al., 2013).

(a) (b)

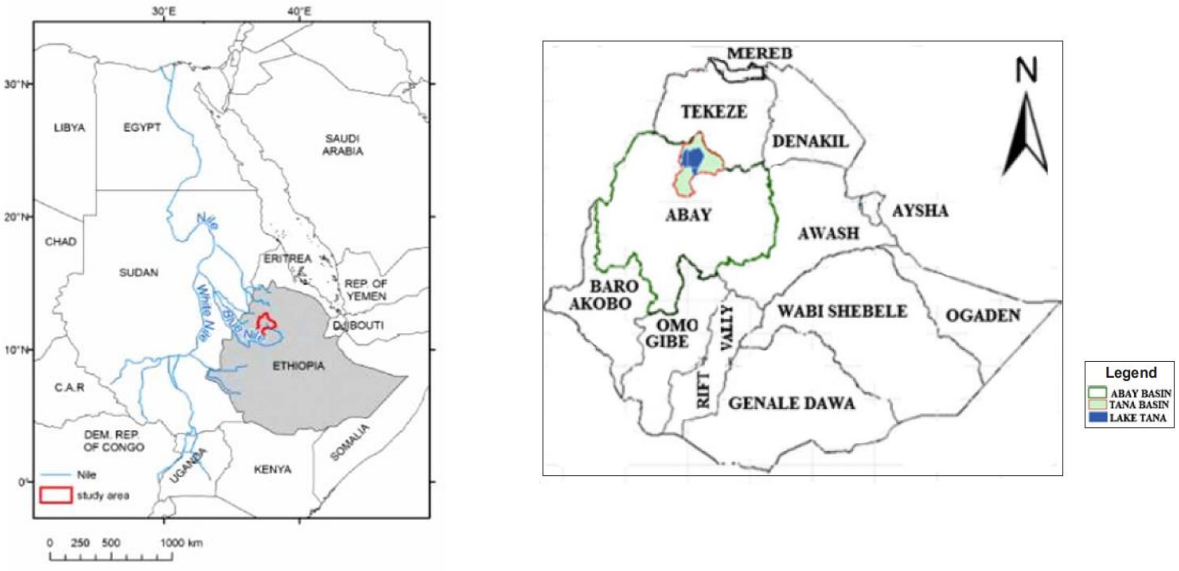

Fig. 1.1: (a) Ethiopia is located in East-Africa. The study area is situated at the northwestern side of the country (adapted from Poppe et al. (2013)). (b) Ethiopia contains 12 basins. Lake Tana Basin is a sub-basin of the Blue Nile River Basin (Abay Basin) (adapted from Jemberie et al. (2016)).

Boreholes, springs and wells provide the access to groundwater for the rural population. An increase of groundwater withdrawal makes aquifers vulnerable to changes in weather conditions and contamination. Surface subsidence and compaction can be the result of groundwater extraction reducing the aquifer storage (Sum et al., 1999). These events can have large consequences for the rural population. If groundwater extraction surpasses the recharge rate, the base flow in rivers and streams decreases as a result of the lowered water tables (Jones and Mulholland, 2000). It is therefore important to distinct renewable and nonrenewable groundwater and to determine the hydraulic characteristics of the aquifer for water management and policy. The refilling of renewable aquifers depends on the current precipitation and is susceptible to changes in the quantity and quality of recharge water (White et al., 1995). Groundwater recharge is therefore one of the most dominating factors contributing to a sustainable yield of groundwater and surface water exploitation. The water resources in Ethiopia are abundant compared with many countries in sub-Saharan Africa with roughly an average total surface flow of 122 billion m^3/year and estimated renewable groundwater resources of 2.6 billion m^3 (Ludi et al., 2013). To assess the available water resources, it is essential to understand the controlling factors of the groundwater system.

Lake Tana Basin is located at the northwestern side of Ethiopia (Fig. 1.1; Fig. 1.2). It is one of the sub-basins of the Blue Nile River Basin (or Abay Basin) draining an area of 15 077 km^2. With its 3077 km^2, Lake Tana is the largest lake in the country and the source of the Blue Nile River. Gumera catchment is situated at the eastern side of Tana basin and is one of the major catchments around Lake Tana having an important contribution to the water supply of the lake. Drained by the perennial Gumera River, this catchment is known for its great potential for irrigation, high value crops and livestock production. Feasibility studies for irrigation such as the 'Gumera Irrigation Project' have been performed where an irrigable area of 14 000 ha was estimated (Alemayehu et al., 2010). Small – scale irrigation schemes occur already in the floodplain (Derib, 2015).

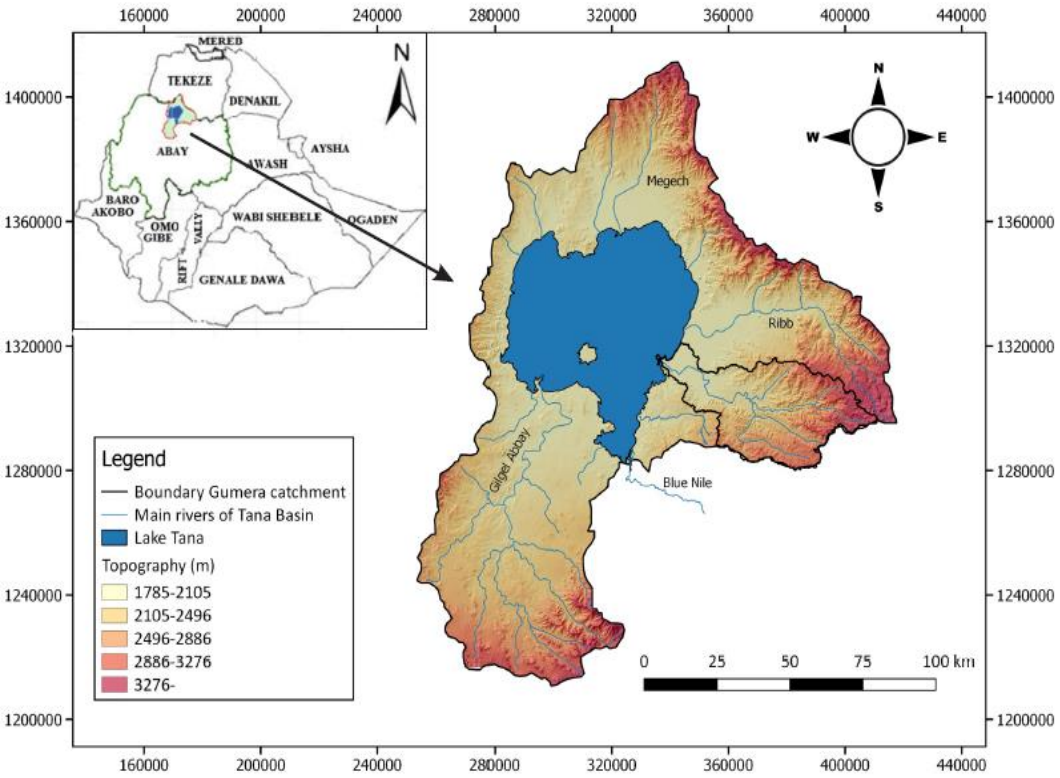

Fig.1.2: Gumera catchment is located at the eastern side of Lake Tana Basin.

1.2. Previous studies

Many studies have been performed on the Blue Nile basin and Lake Tana basin because of the importance of the Blue Nile River. During the last decades several studies highlighted the impact of climate change in the two basins using Soil Water Assessment Tools (SWAT) (Setegn et al., 2011; Wagena et al., 2016; Ayele et al., 2016; Woldesenbet et al., 2017). Several water balance models were developed for Lake Tana basin (Dessie et al., 2015; Kebede et al., 2005; Chebud and Melesse, 2009). Runoff mechanisms and rainfall-runoff processes in Gumera catchment were investigated by Dessie et al. 2014a, b and Mamo and Jain 2013. Derib (2015) estimated the water balance of the catchment. Seyoum et al. (2013) forecasted the precipitation for rainfall-runoff predictions in Ribb and Gumera catchments. There are fewer studies available of the separate catchments as most studies focus on Lake Tana Basin in general. The groundwater recharge and its contribution to the Tana basin were investigated for Gilgel Abay, Gumera, Ribb and Megech Rivers (Abiy et al., 2016) but generally the groundwater system in Gumera catchment is poorly investigated.

1.3. Objectives

The general objective of this study is to investigate the hydrogeological characteristics of Gumera catchment and to perform recharge estimations. This will be achieved analyzing the following subjects:

- Characterization of the structure of the groundwater reservoir
- Estimation and comparison of the groundwater recharge by four methods: base flow separation, chloride mass balance, soil moisture balance and water fluctuation method.
- Determination of hydraulic parameters
- Determination of the regional and local groundwater flow
- Determination of the water chemistry and evaluation of the water quality

2. Study area

2.1. Location

Gumera catchment is located in the South Gondar zone which is part of the Amhara Region covering an area of 1531 km² (Fig. 2.1). The catchment extends from 335448 m to 411665 m longitude and 1295832 m to 1316817 m latitude. The elevation ranges from more than 3600 m in the highland to around 1800 m in the floodplain. An undulating and rugged topography is dominating the catchment containing steep slopes in the mountainous region in the east and more gentle slopes towards Lake Tana (Mamo and Jain, 2010). Some gravel roads provide access to the deeper part of the catchment, but generally the accessibility of the catchment is poor.

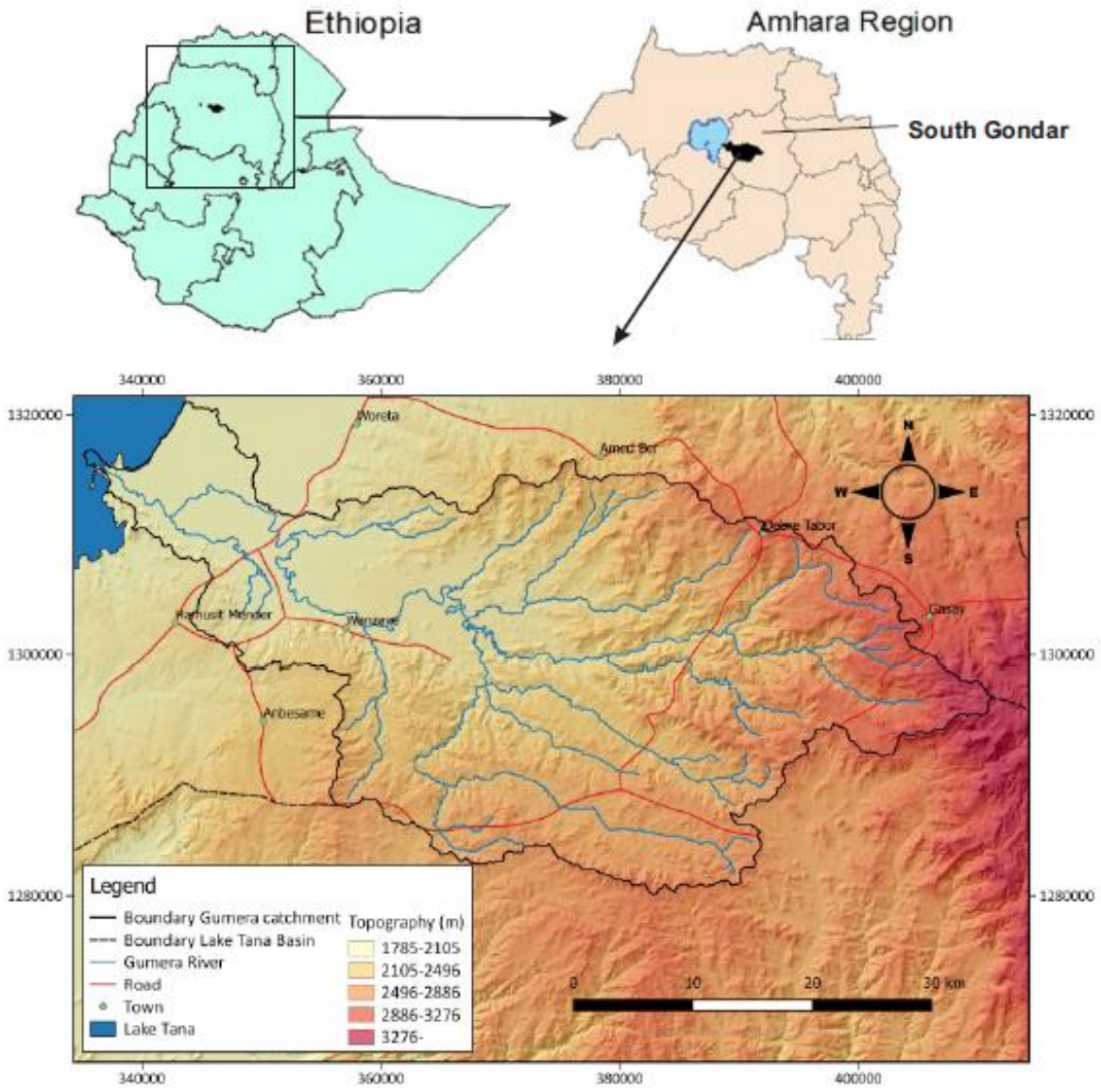

Fig. 2.1: Gumera catchment located at the eastern side of Lake Tana in Amhara Region (modified after Wubie et al. (2016)).

2.2. Geology

Complex lithological and tectonic structures are characterizing Tana Basin. In the Late-Jurassic, marine limestone was deposited which indicated that the northwestern Ethiopian plateau was below sea level. Continental-fluvial sandstone was covering the marine deposits during the Cretaceous (Gani and Abdelsalam, 2006). The Ethiopian plateau is located at the western side of the Afar Depression and the tectonically active Main Ethiopian Rift (Fig. 2.2). It has a mean elevation of 2.5 km but the uplift history is poorly understood and heavily debated (Gani et al., 2007). It is thought that a combination of the rising Afar mantle plume and flank uplift of the Main Ethiopian Rift has caused the uplift during the Eocene and Early-Oligocene (Sengör, 2001; Davis and Slack, 2002; Beyene and Abdelsalam, 2005). Extensive Tertiary continental flood basalts were covering the plateau 30 Ma years ago (Hoffman et al., 2004). The rising Afar mantle plume caused fault formation in the deeper part of the Ethiopian lithosphere resulting to a collapse that initiated the formation of the Afar Depression 24 Ma years ago (Beyene and Abdelsalam, 2005). The developments of several large shield volcanoes followed this intense and active volcanic period. Mount Guna and Mount Choke are shield volcanoes surrounding the Tana Basin respectively in the east and southeast (Kieffer et al., 2004; Chorowicz et al., 1998). The West Tana escarpment is bordering the west side of the basin. According to Chorowicz et al. (1998), Tana Basin is perched on a topographic height on this volcanic plateau. Fault-bounded grabens are characterizing Tana Basin forming a triple junction at Lake Tana. The Debre Tabor graben is located in the east of the basin and is recently reactivated. The Dengel Ber graben is situated south-southwest and is buried. The third graben, the Gondar graben, has a north-northwest direction and is exposed. The grabens were active during the mid-Tertiary flood basalt flows and were fed by an extensive dike and pipe network (Chorowicz et al., 1998). The Tana grabens have an important contribution in controlling the groundwater flow path (Kebede et al., 2005). According to Poppe et al. (2013), Lake Tana was formed through a combination of epirogenetic subsidence resulting from the convergence of three grabens (Chorowicz et al., 1998) and a Quaternary lava barrier blocking the southern outlet of the lake (Mohr, 1968). The subsidence was initiated before the termination of the mid–Tertiary flood volcanism (Chorowicz et al., 1998). Graben faults reactivation occurred in the Late Miocene – Quaternary resulting in subsequent subsidence followed by lacustrine deposits and olivine basalt flows, overlying unconformaby the faulted mid-Tertiary basalts (Chorowicz et al., 1998).

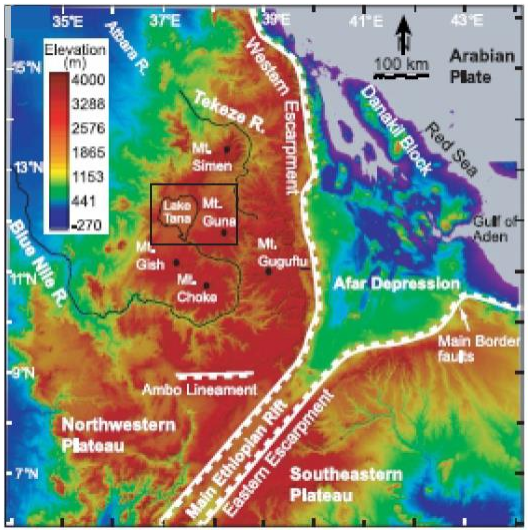

Fig. 2.2: The Ethiopian plateau with the Afar Depression and the tectonically active Main Ethiopian Rift (adapted from Gani et al. (2007)).

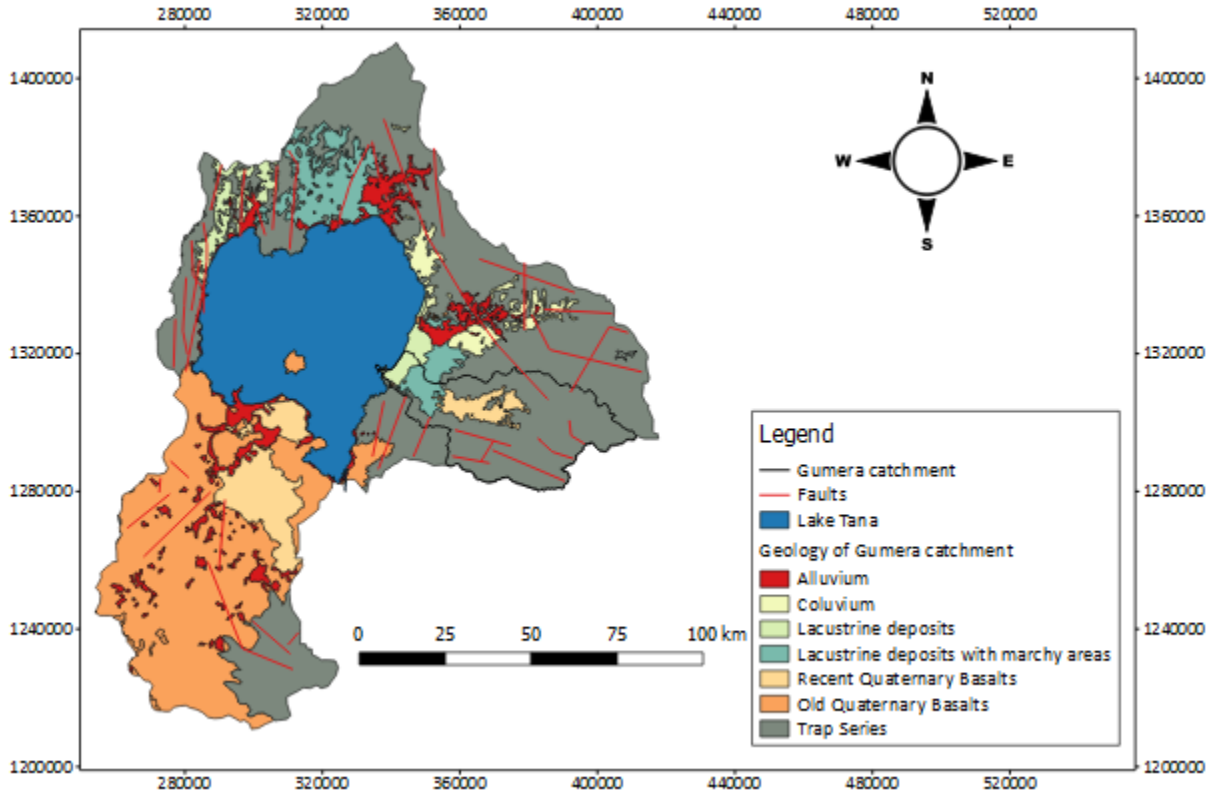

Fig. 2.3: The geological formations of Tana Basin.

Table 2.1 and figure 2.3 provide an overview of the different formations and their environmental settings. The Tertiary flood basalts, also known as the Trap series, have a thickness ranging from 1000-1500 m (Hofmann et al., 1997). SOGREAH (2012) has described the volcanic formations more in detail. Based on the formation age, the Tertiary flood basalts are divided in four formations: Ashangi, Amba-Aiba, Alaji and Termaber Formation. The Ashangi Formation represents the Lower Basalt sequence and consists of deeply weathered basalts and pyroclastic material. It corresponds to the oldest flood basalt of which the Eocene age is still debated (Chorowicz et al., 1998; SOGREAH, 2012). The Amba – Aiba, Alaji, form the Middle Basalt sequence. The Amba - Aiba Formation was deposited during 32 – 25 Ma. It contains layered, aphyric basalts and can unconformably overlie the Ashangi Formation. The Alaji Formation contains aphyric flood basalts with rhyolite and trachyte plugs and was deposited 32 – 15 Ma years ago. The Termaber Formation represents the Upper Basalt sequence and overlays the Amba - Aibi Formation unconformably. It consists of rhyolite-trachyte flows with alternating scoriaceous lava flows and large amounts of tuffs. It has an alkaline affinity. This formation can be easily recognized in the field due to the occurrence of red paleosoils. It covers large areas of the Tana basin and was deposited 30 – 13 Ma years ago (SOGREAH, 2012). The dominated mineral geochemistry of the northern Ethiopian plateau consists generally of pyroxene, olivine and feldspar (Fenta et al., 2016).Tana Basin contains furthermore Quaternary sediments and Quaternary volcanic rocks. The Quaternary volcanic formations occur in relatively flat and gently sloping areas. They are known as the Aden Series. Aphanitic, compacted basalts are characterizing old Quaternary volcanic rocks and are mainly exposed south and southwest of Lake Tana. Recent Quaternary volcanic formation covers small areas over the whole Tana Basin. They consist of porphyritic and moderately to highly vesicular and fine scoriaceous basalts. An

undulating and blocky topography is characterizing this latter formation (SOGREAH, 2012). The Quaternary sediments are composed of alluvial, colluvial and lacustrine deposits whereby the latter refers to the early higher lake level (Poppe et al., 2013). During the maximum extent of the lake, lacustrine plains (e.g. Fogera) were formed and erosion occurred in the higher parts resulting in the infilling of river valleys and basins (Poppe et al., 2013; SOGREAH, 2012). Currently, mountain regions are bordering the west and north-west part of the basin. The largest floodplain areas are located at the north and eastern side of the lake and are characterized by areas subjected to floods, permanent and seasonal swamps (Dessie et al., 2014a).

Serie	Group	Formation	Geology	Deposition age	Environmental setting
-	Quaternary sediments	Colluvial deposits	Clay and silt	Quaternary	Run off
		Lacustrine deposits	Clay and silt		Extent of Lake Tana
		Fluvial deposits	Sand and gravel beds		Erosion highlands and Mt Guna
Aden Series	Quaternary volcanics	Recent Quaternary Basalts	Vesicular and scoriaceous basalts	No detailed data	Local volcanoes
		Old Quaternary Basalts	Aphanitic, compacted basalts	No detailed data	
Trap series	Upper Basalt Sequence	Termaber Basalts	Rhyolite - trachyte basalts, scoriaceous basalts, tuff	30-13 Ma	Mainly Shield Volcanoes
	Middel Basalt Sequence	Alaji Basalts	Aphyric basalts rhyolite and trachyte plugs	32-15 Ma	Main Ethiopian Rift, Shield volcanoes
		Amba –Aiba Basalts	Layered aphyric basalts	32-25 Ma	Afar mantle plume, Main Ethiopian Rift
	Lower Basalt Sequence	Ashangi Basalts	Deeply weathered basalts, Pyroclastic material	Eocene age still debated	

Table 2.1: Overview of the different formation in Lake Tana.

The Termaber Formation is the dominant geological formation in Gumera catchment covering the highlands and the border of the central part of the catchment (Fig. 2.4). The inner central part of the catchment consists of recent Quaternary volcanic material. The floodplain consists of alluvial deposits respectively fluvial and lacustrine sediments. Thick sand and gravel beds occur in compacted silty clay layers. The sand and sandy gravel beds have a thickness of 24 m and 12 m respectively. Guna volcano is located at the eastern boundary of Tana basin. Steep slopes are characterizing the Tertiary volcano of about 10.7 Ma generating strong erosion resulting in coarse alluvial deposits in the floodplain. Lacustrine sediments occur at the surface of the floodplain. The faults in Gumera catchment are all concentrated in the Termaber basalts lowering the areas located at the western side of the faults. They have WNW-ESE and NNE-SSW orientations.

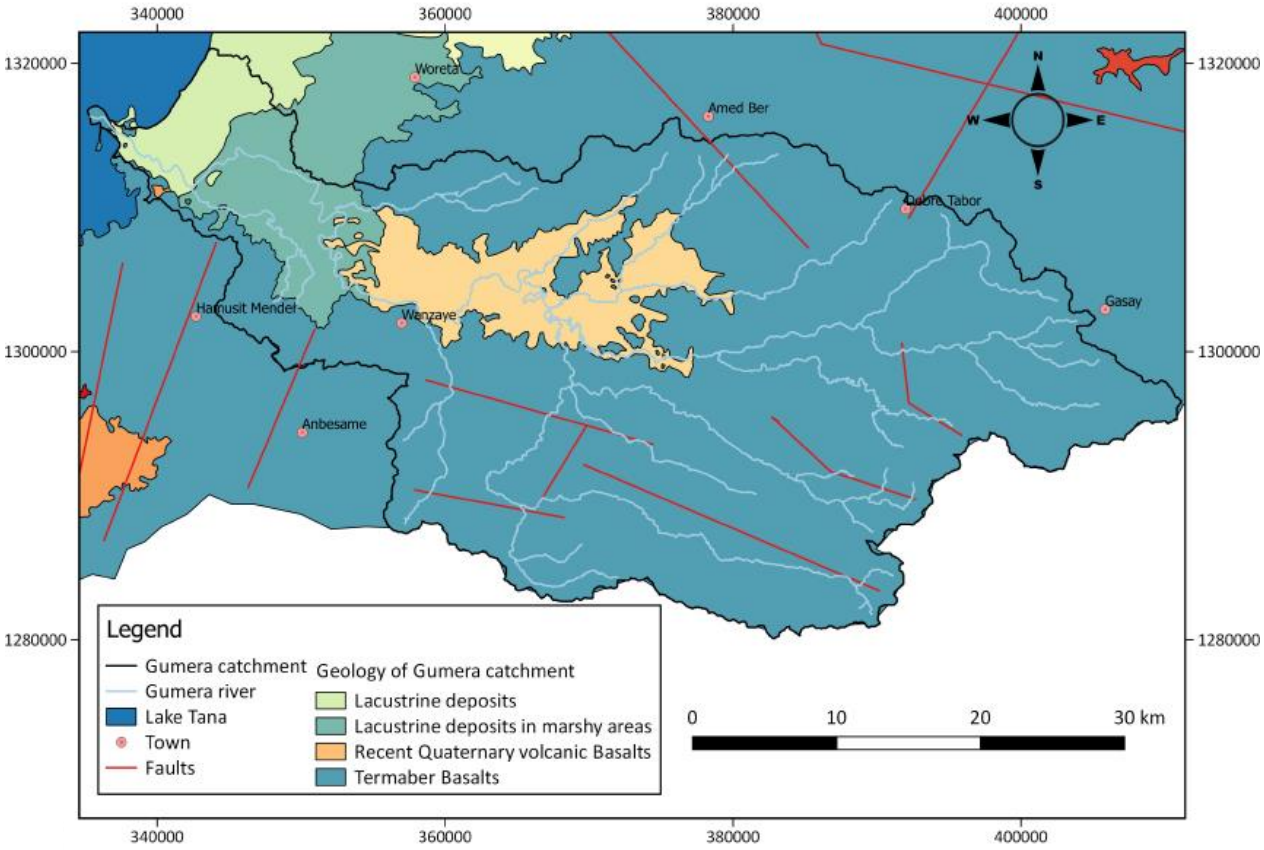

Fig. 2.4: Geological formations occurring in Gumera catchment.

2.3. Hydrogeology

According to Kebede (2013), different aquifer categories are distinguished based on the geology of the basin. The Lower Basalt sequence forms the least productive aquifer compared to the younger flood basalts. Contact springs may occur at the boundary between the Lower and Middle Basalt sequence but generally springs are rare in the Ashangie Formation. Springs occurs in wetlands and at the margin of cliffs. Groundwater appears in joints, fractures and scoriaceous layers. The Quaternary basalts are highly productive. Discharge develops mainly at rivers and fractured springs (Kebede, 2013).

2.4. Soil and land use

According to the Food and Agriculture Organization of the United Nations (FAO) and related literatures, Gumera catchment contains four major soil units (Chesworth, 2008; Schad and Spaargaren, 2006). The classification is based on the soil properties defined in terms of diagnostic horizons, properties and materials.

Lithic Leptosols are typically formed on hard rocks in extensive mountain ranges which are affected by strong erosion. They are very young and shallow soils with minimal development. Pedogenetic features are rarely visible. The depth to the hard rock is often less than 10 cm which has a limited effect to root growth. Leptosols have resource potential for forest land and wet-season grazing. Excessive internal drainage is characterizing the soil. They occur in the highlands at the easternmost side of the catchment.

Pedogenetic processes are characterizing Chromic Luvisols and Haplic Luvisols resulting in a differentiation between the topsoil and subsoil with respectively lower and higher clay content. They occur commonly in flat or gently sloping regions with distinct dry and wet seasons. This soil type is typical for an intermediate stage of weathering. Luvisols are fertile soils and are used for many agricultural purposes because of their greatest capacity for available water storage. Generally, they are characterized by of a good drainage network. They dominated in the central part of the catchment.

Eutric Vertisols are soils with a high clay-content containing high proportion of expanding clay minerals and causing deep cracks during the dry season. They have agricultural potential but an adapted management is required for a sustainable production. Large areas are still unused for agriculture and are restricted to intensive grazing. Due to the dominating swelling clays, a narrow available soil moisture range occurs. Vertisols occurs typical in lower landscape positions. The alternating wet-dry conditions had a limited effect on the root growth. They are characterized by a poor drainage network. This soil type occurs in the floodplain.

According to Mamo and Jain (2010), the eastern side of the catchment consists of clay and clayey loam, the central part and western part contains mainly clay to silty clay.

The indigenous vegetation cover occurs almost only around churches and in the extreme highland area of the catchment. Most of it was transformed to cultivated land as a result of the population growth and increasing demand of land use. Approximately 75 % of the catchment is intensively cultivated (Asres and Awulachew, 2010). Moderate cultivation is dominating the remaining part. The cultivated and urban areas were expanded with 22 % in the last 48 years. Forest, shrub, grass and wetland were decreased with respectively 85.3 %, 91.39 %, 76.15 % and 72.54 % (Wubie et al., 2016). Moderately deep rooted crops like teff, maize, barley and wheat are the major cultivated crops. Other land cover types are shrublands, grasslands and the cultivation of vegetables.

2.5. Climate and meteorology

The climate in Ethiopia has a large spatial and temporal variability. Temperature and rainfall patterns vary across the country due to the large topographic variations and differences in response to regional and global weather mechanisms. Seasonal changes in large-scale circulations are determining the spatial and temporal rainfall variations in Ethiopia of which the seasonal north-south movement of the intertropical convergence zone (ITCZ) has an important contribution. The main precipitation occurs during the most northern position of the ITCZ. Dry periods dominate from November to February when the ITCZ is located south of Ethiopia. Although, Korecha and Barnston (2007) suggested that the El Niño-Southern Oscillation (ENSO) mainly determines the distribution and intensity of the precipitation with a decrease in average annual rainfall during warm El Niño events. Local climate factors near Africa and the Atlantic and Indian Oceans reinforce the rainy season. Intense variations in annual rainfall distributions together with strong monthly and seasonal rainfall variability make it difficult to detect long-term trends. The low lying areas in the southeast and northeast parts of the country have an annual rainfall of less than 600 mm while areas with an elevation higher than 3200 m receive an annual rainfall of more than 1400 mm (Mason et al., 2013). According to Jemberie et al. (2016), the precipitation varies with latitude and longitude in Tana Basin. Lower rainfall occurs in the northern part whereas the highest rainfall is observed in the southern part of the basin. The main precipitation appears between June and September and accounts for 50 – 80 % of the total annual rainfall (Korecha and Barnston, 2007). November, December, January and February are generally characterized as dry periods. Sporadic precipitation occurs during March, April and May (Fig. 2.5b). Kim et al. (2008) forecasted an increase in annual precipitation in the highlands of Ethiopia in the coming decades. The mean annual precipitation in Tana basin ranges from 1251 mm to 1685 mm based on data collected in Bahir Dar during 2000-2014 (Fig. 2.5a). The temperature and precipitation vary from year to year, no clear trend is visible (Fig. 2.5a). The lowest average temperature occurs in 2007. There is a large temperature difference between the day and the night. The maximum and minimum monthly temperature ranges between 24.5-30.3 °C and 8.1-15.2 °C, respectively. The average annual temperature is 19.9 °C with May and April as the warmest months (Fig. 2.5b).

(a)

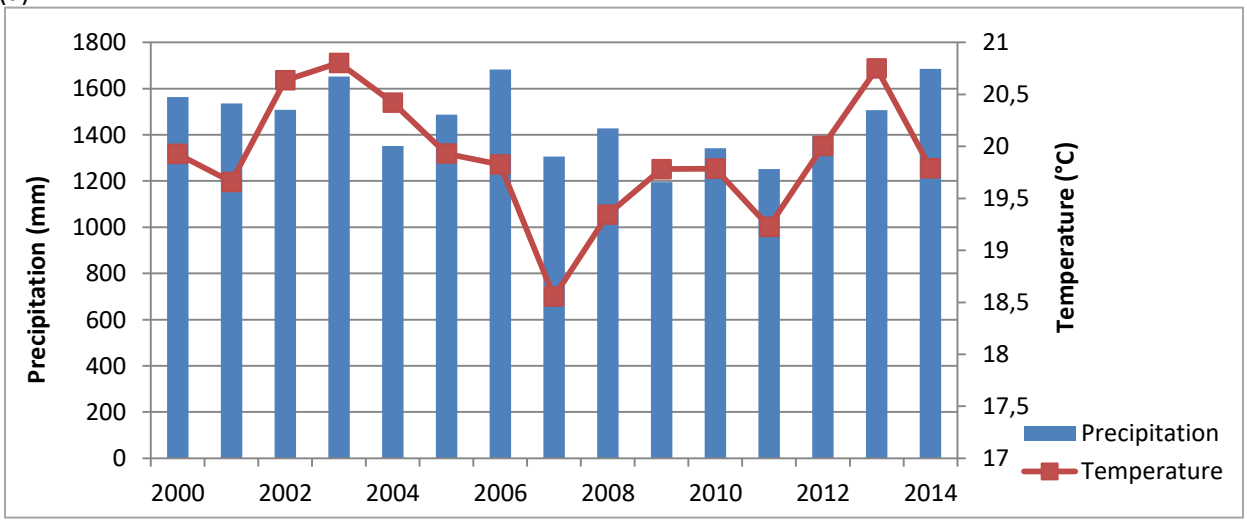

(b)

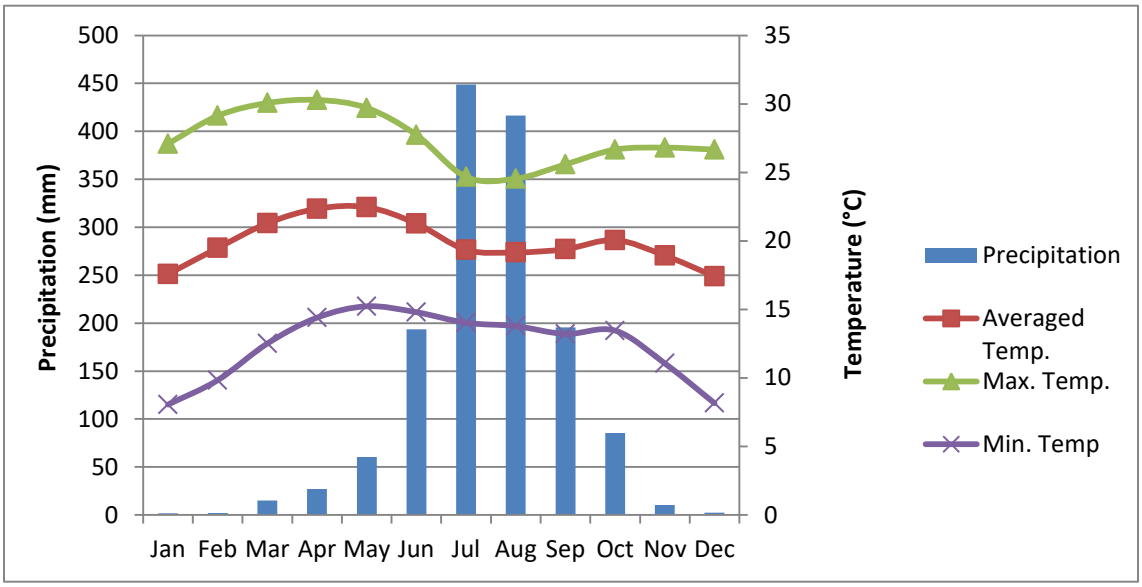

Fig. 2.5: (a) The mean annual precipitation and temperature evolution for 2000-2014 collected in Bahir Dar. (b) The evolution of the average monthly temperature and precipitation during the year.

2.6. Hydrography

Lake Tana is the largest lake in Ethiopia with an area of 3077 km^2. It is very shallow with an average depth of 9 m. The lake has one natural outlet located at its southern tip which corresponds with the headwater from the Blue Nile. The outflow varies with the rainfall variability (Kebede et al., 2006). Additionally, a tunnel outlet is recently constructed in the southwest and is used for hydropower purposes. The natural outflow provided 7 % of the Blue Nile flow at the Ethiopian-Sudanese border (Conway, 2000). A flow regulation system regulates the lake level since 1995 at the outlet to the Blue-Nile River (Abate et al., 2015). Numerous rivers are feeding the lake but 93% of the inflow is determined by four permanent rivers: Gilgel-Abay, Rib, Gumera and Megech (Kebede et al., 2006). There are no large rivers flowing at the western side of the lake.

The origin of the Gumera River is located in Mount Guna. The river flows westward over a distance of approximately 132 km. Gumera catchment contains many intermittent and perennial streams and springs. At Wanzaye in the central, lower part of the catchment, there is a thermal spring located. Faults and dikes networks enable the appearance of thermal waters at the surface (Kebede, 2013).

Flooding on the alluvial plain has become a frequent phenomenon. Abate et al. (2015) investigated the morphological changes of Gumera River channel over 50 years. They concluded that the lower reach has undergone the major changes. There, the meandering of the river has slightly increased during 1980-2006. The sediment deposition in the river and on the riverbanks is related to the anthropogenic impacts linked with irrigation activities and dikes. Land degradation in the upper catchment and the backwater effect due to the artificial regulation of the lake level since 1995 also contribute to the sediment deposition (Abate et al., 2015). Increasing sedimentation reduces the flood carrying capacity of the Gumera River, although minor channel narrowing and shifting of river banks occurs (Abate et al., 2015).

3. Material and methods

3.1. Topography

The created topographic maps are based on the Shuttle Radar Topography Mission (SRTM) digital elevation data having a resolution of 30 m x 30 m. They are provided by the United States Geological Survey (USGS). The maps are developed in Essen QGIS 2.14.11. The drainage network is generated after applying a GRASS-tool and is visually verified. The used geographic datum is WGS 1984 spheroid. The projection is the Universal Transverse Mercator, zone 37N. The elevations, collected from GPS data during fieldwork are verified for several locations and compared with the elevations provided by Google Earth and the obtained digital elevation map to determine the accuracy of the measurements. The used GPS type is Garmin GPSMAP 64s. The elevations are expressed in m referring to Meter Above Sea Level.

3.2. Meteorological data

Meteorological parameters are obtained from two meteorological stations located at Bahir Dar and Debre Tabor. Bahir Dar is situated near the outlet of the Blue Nile River. Debre Tabor is located at the northern boundary of Gumera and Ribb catchment (Fig. 2.1).

The precipitation together with the maximum and minimum temperature belongs to daily meteorological parameters registered at Bahir Dar. They contain 14 years of data collected from 2000-2014. Missing data are replaced using the monthly arithmetic mean. The data from Debre Tabor are derived from the CLIMWAT 2.0 software. They provide only average monthly precipitation data for one year. In the upstream part of the catchment, daily rainfall measurement has been performed from 30th of July till 7th of December 2016. Other daily precipitation data from 30th of July till 30th of August 2016 are provided for Infranz catchment and for the floodplain at Ribb catchment. Infranz catchment is located southwest of Bahir Dar. Ribb catchment is situated at the north of Gumera catchment. The spatial correlation between these three latter catchments is determined.

3.3. Hydrostratigraphical model

To characterize the structure of the groundwater reservoir, several cross-sections are made based on the geological map provided by the Geological Survey of Ethiopia. Springs together with the information collected in the field and borehole data, are incorporated in the sections. A conceptual hydrostratigraphical model is created together with the corresponding recharge/discharge mechanisms characterizing the catchment. The different aquifers are determined describing the permeability, porosity type, extent of the flow system and the continuity based on the cross-sections and fieldwork. The visualizations are performed in CorelDRAW.

3.4. Monitoring of groundwater hydraulic heads

Information of springs and hand dug wells are collected during the fieldwork conducted in July and August. In total 39 springs and 33 hand dug wells are mapped and described. For each hand dug well, the groundwater depth is measured. From the 33 hand dug wells, 9 wells were measured weekly from the 27th of May 2016 till the 11th of March 2017. For the monitoring wells, a detailed description is provided based on oral information of the owner. Two Electrical Conductivity (EC) and pH-measurements are performed for the weekly visited wells. The description of the springs defines the type of spring, the surrounding geology, vegetation and land use

Two divers are installed in the catchment, one is located in the highlands, the other one in the floodplain. The water level is monitored every 30 minutes. A barometric compensation is performed using the data derived from a barometric diver located at Bahir Dar. The atmospheric pressure is measured every 30 minutes.

3.5. Surface water discharge measurements

Daily river discharge measurements are performed at the bridge of Gumera River near the road to Gondar and Bahir Dar from 1980-2014. For every month the minimum, maximum and averaged discharge is provided. Based on the present data, runoff and runoff coefficients are determined. The evolution minimum discharge is investigated.

Precipitation, runoff and groundwater discharge contribute to surface water discharge. To calculate the runoff, the base flow is firstly determined. If the minimum discharge is used, the runoff coefficients will show an underestimation during the rainy season. Base flow is defined as the drainage of groundwater from the aquifer storage after the occurrence of groundwater recharge (Zhu et al., 2010).The minimum discharge is reliable as base flow for October, November, winter and spring seasons because there is almost no precipitation during these periods that can contribute to runoff. The rainy season in Tana Basin occurs in July, August and September. During these months, the minimum discharge represents an overestimation of the base flow due to the contribution of precipitation and runoff. The base flow for September and August is estimated by extrapolating the recession slope of the minimum discharge values from October, November and December. The base flow value for July is estimated calculating the arithmetic mean of June and August. Subtracting the monthly average discharge with the monthly average base flow generates the runoff. The runoff coefficients are determined based on the average monthly precipitation data from Debre Tabor. After dividing the runoff with the area and adjusting the units to mm, the runoff is divided with the precipitation generating the runoff coefficients. The arithmetic average is calculated for every season to compare the obtained coefficients with the runoff coefficients from Jemberie et al. (2016).

3.6. Hydraulic parameters

Quantitative information concerning the hydraulic properties of the basin is essential to control the development of the groundwater system. The specific yield, the transmissivity and the hydraulic conductivity are determined based on a pumping test and continuous monitoring of the groundwater level. The latter is performed with a diver and contains data from 29th of July 2016 till the 10th of February 2017. The pumping test is conducted on 19th of August 2016. Continuous monitoring and the pumping test are both performed in monitoring well 5 (GUM-05) in the upper part of the catchment (400870 E, 1296665 N; Fig. 4.1).

3.6.1. Specific yield and recession rate

The specific yield (S_y) and the groundwater recession rate are determined based on diver data combined with daily meteorological information. A barometric compensation has been performed for the diver data. The diver has its own meteorological station of which the precipitation is daily measured during 30th of July till 7th of December. The monitoring measurements are continued till the 10th of February. Several assumptions have been made:

- The precipitation infiltrates immediately into the groundwater storage during the measured period.
- No precipitation reaches the groundwater table during the three assumed recession periods.

The specific yield is expressed as the volume percentage of water that is drained due to gravitation (V_w) from a saturated volume of matrix (V_t) (Kruseman and de Ridder, 1990).

$$S_y = \frac{V_w}{V_t} \qquad (3.1)$$

The determination of S_y is based on the water table fluctuation (WTF) method (cfr 3.8.4). This method assumes that an increase of groundwater recharge causes a rise in groundwater level (dh) over a certain time period (Healy and Cook, 2002). The recharge (R) is obtained using the following equation:

$$\mathrm{R} = S_y * \frac{dh}{dt} \qquad (3.2)$$

Redefining the formula, gives the specific yield:

$$S_y = \mathrm{R} * \frac{dt}{dh} \qquad (3.3)$$

The recharge is estimated using the following equation assuming no occurrence of runoff.

$$R = P - PET \qquad (3.4)$$

P represents the precipitation (mm) and PET the potential evapotranspiration (mm). Different recession slopes are characterized in the diver data. For each slope, the groundwater velocity and the groundwater recession rate are determined. The groundwater velocity is calculated with the following equation:

$$\mathrm{v} = \frac{dh}{dt} \qquad (3.5)$$

The groundwater recession rate is determined with the WTF formula but is defined for a decrease in groundwater level using the previously calculated specific yields and groundwater velocities.

$$\text{Recession rate} = S_y * \frac{dh}{dt} \qquad (3.6)$$

In the last step, a linear regression is performed to estimate the groundwater depth at which the recession rate is 0 and to determine the maximum recession rate occurring in the aquifer.

During the calculation, the diver readings measured at 4:00 AM are taken. In Ethiopia, there is a large difference in daily minimum and maximum temperature, inducing water table fluctuations near the soil surface due to evapotranspiration. Healy and Cook (2002) assumed no occurrence of evapotranspiration between midnight and 4:00 AM. The specific yield is primarily used in unconfined aquifers to express the storage of water in its upper part (Şen, 2014).

3.6.2. Pumping test

A pumping test is performed at the same location at which the specific yield is estimated (monitoring well 5). Every three seconds, the diver performs a measurement. After pumping, the water level starts to rise again till its initial water level. The initial water table measured from the ground level was 0,43 m. The test had a total duration of 1:46:30 resulting in 3,15 m drawdown. The discharge was 3,4 l/s. The pumping test was shortly interrupted 3 times. Because the well started to partially collapse, the pumping was stopped earlier to avoid a complete collapse. The recovery is continuous measured for 18 hours long. The residual drawdown (s') is calculated as the difference between the initial water level and the water level measured after cessation of pumping at a certain time t' (Kruseman and de Ridder, 1990). The recovery of the pumping test is used to calculate the transmissivity and the hydraulic conductivity. Both hydraulic parameters indicate the ability of the aquifer to transport water. The hydraulic conductivity is defined for a unit saturated thickness while the transmissivity takes into account the complete saturated thickness of the aquifer (Kruseman and de Ridder, 1990).

The hydraulic parameters are calculated with Theis recovery method. The calculations are performed manual and with an aquifer test analysis software known as MLU Software (Hemker and Post, 2011). For the manual calculations the Jacob simplification of the Theis recovery method is applied. The Jacob simplification neglects the width of the well. These two approaches are used to verify the reliability of the calculated values together with previously estimated parameters provided by the Amhara National Regional State Water Resource.

The Theis recovery method is suitable in unconfined aquifers for late-time recovery data assuming a constant discharge rate and a constant, equal storativity during pumping and recovery (Kruseman and de Ridder, 1990). According to Theis (1935), a semi-logarithmic plot of s' vs. t/t' is represented. The parameter t represents the time in days since the start of pumping. The parameter t' refers to the time in days since the cessation of pumping. In the Jacob simplification of the Theis recovery method, this will generate a straight line of which the slope is defined as:

$$\Delta s' = \frac{2.3*Q}{4\pi T} \qquad (3.7)$$

$\Delta s'$ is the residual drawdown difference per log cycle of t/t' in m. Q is the rate of discharge in m³/day(d). T represents the transmissivity in m²/d. Redefining this equation expresses the transmissivity (m²/d):

$$T = \frac{2.3*Q}{4\pi\Delta s'} \qquad (3.8)$$

The hydraulic conductivity (m/d) is obtained dividing the transmissivity with the depth (D) of the well in m.

$$K = \frac{T}{D} \qquad (3.9)$$

MLU Software stands for Multi-Layer Unsteady state Software and is described as an aquifer test analyses software (Hemker and Post, 2011). It considers the hydrogeological structure of the substrate as a sequence of 2D water-bearing permeable layers (aquifer) and semi-pervious layers (aquitard). MLU is based on the Theis recovery method and simulates the drawdown in the pumping well using analytical formulas, the hydraulic parameters and a constant discharge rate. The depth and radius of the pumping well need to be specified. Due to the large amount of diver data, only the measurements performed at an interval of five minutes are used as drawdown observations. In the MLU analysis, the hydrological parameters of the imported aquifers and aquitards are calculated automatically but can be changed manually, attempting to calibrate the simulated drawdown with the observed drawdown. If a good fit between the observed and simulated drawdown is obtained, the calibration is completed and the hydrological parameters of the aquifers can be derived.

3.7. Groundwater flow

The piezometric map is created in QGIS based on the digital elevation model (DEM) with a regression approach. The average groundwater depth of the monitoring wells is calculated together with the measured distance of these wells to the closest river in Google Earth. The relationship between the groundwater depth and the distance to the river is determined. The obtained direction coefficient is used for further calculations. The distance to the river of the whole catchment is approached using the distance matrix tool and the river shape file in QGIS. The outcome is multiplied with the direction coefficient generating the depth of the groundwater level occurrence. The result is subtracted from the DEM creating the piezometric map. Equipotential lines are created in QGIS to approach the estimated piezometric surface at a certain area. The groundwater flow is visualized on regional and local scale.

3.8. Groundwater recharge

Groundwater recharge is defined as the downward flow of water that is added to the groundwater reservoir and that joins the regional groundwater system (De Vries and Simmers, 2002). The precipitation firstly has to attain the field capacity of the soil moisture storage and exceeding the potential evapotranspiration before it starts to percolate into the groundwater layers. The soil moisture storage is described as the amount of water that is stored in the plants root zone. The soil is at field capacity when the excess water is drained away under gravitational forces. The deeper the plant root zone, the larger the volume of water incorporated in the soil will be. This reduces the amount of water that can infiltrate to the groundwater reservoir. The rooting depth and soil texture are the major components controlling the soil moisture storage (Bakundukize et al., 2011). The amount of water that reaches the water-table generally depends on the intensity and duration of the precipitation, the soil-moisture conditions of the unsaturated layers, the water table depth and the soil texture. The recharge is estimated and compared using the base flow calculation, chloride mass balance, soil-moisture balance and water table fluctuation methods.

3.8.1. Base flow separation

Base flow is an indirect parameter for recharge assuming the base flow as the drainage of groundwater from the aquifer storage after the occurrence of groundwater recharge (Zhu et al., 2010). The baseflow separation is already explained in section 3.5 to estimate the runoff. The base flow in dry season corresponds to the measured monthly minimum discharge while for the rainy season corrections need to be performed due to the contribution of precipitation and runoff. Extrapolations based on the monthly minimum discharge from October, November and December approaches a monthly base flow value for August and September. For July, the monthly base flow is estimated using the arithmetic mean of June and August. To approach the annual recharge, the estimated monthly base flow is firstly divided with the area. Adding the monthly values, give the annual recharge based on the base flow separation method.

3.8.2. Chloride Mass Balance method

Eriksson and Khunakasem (1969) developed the Chloride Mass Balance (CMB) method assuming chloride as a conservative tracer. It compares chloride concentrations in rainfall samples with chloride concentrations in groundwater. Precipitation and aerosols are considered to be the only source of the chloride-concentrations in groundwater. The recharge is estimated using the following equation:

$$R = P_{eff} \frac{Cl_p}{Cl_{gw}} \qquad (3.10)$$

P_{eff} is the mean annual effective precipitation (mm), R is the total recharge (mm), Cl_p is the mean chloride concentration in precipitation (mg/L) and Cl_{gw} is the mean chloride concentration in shallow groundwater (mg/L) (Ting et al., 1996; Demlie, 2014). The effective precipitation is calculated as precipitation – runoff. The recharge is calculated for the annual precipitation data from Bahir Dar and Debre Tabor. 11 rain samples were collected in the eastern and southern part of Tana basin together with 17 spring samples, 12 samples from shallow hand dug wells and 2 samples from hand pumps taken within Gumera catchment. The arithmetic-geometric averages are determined for the rain samples, the springs and the well samples respectively. Firstly, the arithmetic (a_1) and geometric (g_n) averages for the chloride concentrations are calculated using the following equations where N refers to the number of samples:

$$a_1 = \frac{1}{\mathrm{N}}(\mathrm{x}_1 + \mathrm{x}_2 + \cdots + \mathrm{x}_N) \qquad (3.11)$$

$$g_1 = \sqrt[N]{x_1 x_2 \ldots . x_N} \qquad (3.12)$$

Then, two sequences are defined using a_1 and g_1 with n the index in the sequence:

$$a_2 = \frac{1}{2}(a_1 + g_1)$$

$$g_2 = \sqrt{a_1 g_1}$$

...

$$a_{n+1} = \frac{1}{2}(a_n + g_n) \qquad (3.13)$$

$$g_{n+1} = \sqrt{a_n g_n} \qquad (3.14)$$

The two sequences converge to a similar outcome which is defined as the arithmetic-geometric average. The same method is applied for the bromide -concentrations in the springs, wells and rain samples.

3.8.3. Soil moisture balance: Thornthwaite method

The temperature and precipitation data used for this study are collected at the meteorological station of Bahir Dar. The effective precipitation is derived after multiplying the determined runoff coefficients with the monthly precipitation values.

Firstly, the potential evapotranspiration is calculated. This is the amount of water that can evaporate under certain conditions assuming no control on the water supply. The calculation is based on the Thornthwaite equation. This is a simple empirical formula taking into account the average monthly temperature data, the actual number of days in the month and the number of daylight hours. The latter is a function of the longitude (Pereira and De Camargo, 1988). The equation is expressed as follows:

$$\mathrm{PET} = 16\left(\frac{L}{12}\right)\left(\frac{N}{30}\right)\left(10\frac{T}{I}\right)^{a} \qquad (3.15)$$

PET is the estimated potential evapotranspiration (mm/month), N is the number of days in the month, L is the average day length of the month (hours) and T is the average daily temperature of the month (°C). The parameter 'I' is the temperature-efficiency index or heat index. It is calculated as the sum of 12 monthly values of the heat index i. Parameter 'a' is a function of the heat index I.

$$\mathrm{i} = \left(\frac{T}{5}\right)^{1.514} \qquad (3.16)$$

$$\mathrm{I} = \sum_{i=1}^{12} i \qquad (3.17)$$

$$\mathrm{a} = 0.000000675I^3 - 0.0000771I^2 + 0.01792I + 0.49239. \qquad (3.18)$$

The plant available water expresses the differences in water content between field capacity and permanent wilting point for a certain rooting depth. It is calculated as follows:

$$\mathrm{PAW} = 10\ (\mathrm{FC} - \mathrm{PWP})\ \mathrm{Zr} \qquad (3.19)$$

Where PAW is the plant available water (mm), FC is the field capacity (vol%), PWP is the permanent wilting point (vol%) and Zr is the rooting depth (m). The field capacity and the permanent wilting point are derived from the Hydraulic Properties Calculator developed by the USDA Agricultural Research Service in cooperation with the Washington State University. The PAW is calculated for several rooting

depths and soil textures, due to the large variation in rooting depth and the occurrence of several soil textures.

An excel sheet is used to determine the parameters. The monthly effective precipitation and calculated PET values for 2000-2014 are used as input data. Also the PAW, initial moisture and runoff percentage need to be defined at the beginning of the calculations. The excel sheet automatically determines the accumulated potential water loss (APWL) and the soil moisture storage (S) together with estimations of the actual evapotranspiration (AET) and the monthly recharge. The actual evapotranspiration is the amount of water that is removed from the soil due to evaporation and transpiration. It varies with the temperature and the moisture availability during the year (Bakundukize et al., 2011). In the rainy season, when the soil is at field capacity and the amount of effective precipitation is larger than the PET, the AET is at its maximum value. This maximum value is than equal to PET. During this situation the aquifer is recharged. If PET is larger than precipitation, the aquifer is no longer recharged. The water used for evapotranspiration is taken from precipitation and from the soil moisture storage until it is depleted. As already mentioned above, the heavy rain periods in northern Ethiopia occur during June, July, August and September. Because the initial soil moisture content is unknown, the calculation is started in May assuming a complete depletion of the soil moisture storage at the end of the dry season. There is the uncertainty about the different rooting depths and the exact percentage of the respective land use types. A range in recharge is therefore calculated together with their corresponding PAW values to reduce these uncertainties.

3.8.4. Water table fluctuation method

As already explained in section 3.6., the water table fluctuation method is based on the assumption that an increase of groundwater recharge causes a rise in the groundwater level (Healy and Cook, 2002). The recharge is estimated using the following equation:

$$\mathrm{R} = S_y * \frac{dh}{dt} \qquad (3.20)$$

Where R is the recharge occurring between a certain time interval t (m), S_y is the specific yield (dimensionless), dh is the water-table peak over a certain time period (m). It is assumed that groundwater recharge and discharge are the only components causing the water table fluctuations and that the specific yield is constant over the time period. The specific yield is determined in section 4.6 for the Termaber Basalt. For the floodplain, the specific yield is based on Johnson (1967). The water table fluctuations are derived from the diver data located in the highlands and in the floodplain together with manual groundwater level measurements.

3.9. Hydrochemistry

The physical and chemical properties of the surrounding rocks together with the type of anthropogenic activity at the surface are affecting the quality and the geochemical characteristics of the (ground-) water (Şen, 2014). The concentrations of the dissolved constituents vary with pH, salinity and with the amount of recharge water reaching the groundwater table. Chemical analyses of groundwater samples enable the interpretation of the water quality. The evolution of the groundwater properties can be determined related with the geology, anthropogenic activity and different groundwater flow paths in the catchment.

In total 31 water samples of which 17 springs, 12 wells and 2 hand pumps were collected between 3th and 15th of August 2016. 30 sample sites were performed in total because one spring was sampled twice due to a wrong sample naming. 5 samples were located in the highlands, 20 samples in the central part of the catchment and 6 in the lowlands. In situ measurements have been conducted in the field assessing the temperature, EC and pH. The water samples were collected in clean polyethylene bottles. The bottles

were firstly rinsed three times with the sample water before being filled completely. They were stored under cool conditions. The chemical analyses were performed in the Laboratory for Applied Geology and Hydrogeology at Ghent University, Belgium. The cation-concentration of Na^+, K^+, Ca^{2+}, Mg^{2+}, Fe^{2+}/Fe^{3+}, Mn^{2+}, Al^{3+}, Sr^{2+} and Li^+ were analyzed with the Atomic Absorption Spectroscopy (AAS). Spectrophotometry was used to determine the NH_4^+, Cl^-, SO_4^{2-}, NO_3^-, NO_2^- and PO_4^{3-}-concentrations. HCO_3^- is measured performing titration. The CO_3^{2-}-concentration is not measured because every sample had a pH lower than 8.2. The F^- and Br -concentrations were analyzed using selective electrodes. EC and pH were determined with an EC-electrode and pH-electrode respectively. The Total Dissolved Solids (TDS) was calculated as the sum of the cations and anion concentrations. Finally, the electrical balance was estimated together with the corresponding error values for each sample.

To interpret the groundwater quality and the evolution of the groundwater properties, a Piper diagram, a variant of the Schoeller diagram and several cross-plots are created. The Piper diagram is developed using the Groundwater Chart Program provided by the USGS. A Piper diagram allows a graphical visualization of the hydrochemical analyses of the water sample. The cations and anions are represented separately in ternary plots. A variant of the Schoeller diagram is created in R. A Schoeller diagram enables the comparison of many samples on a single graph and shows the total anion-cation concentration on a logarithmic scale. The created diagram differs from the original Schoeller diagram because the concentrations are expressed in mg/l instead of meq/l.

4. Results

4.1. Topography

The accuracy of the elevations derived from GPS data are verified for several locations comparing the elevations with data from Google Earth and the DEM (Table 4.1). Figure 4.1 shows the different locations on the topographic map. The elevation difference between Google Earth and the DEM map is little. The difference in elevation between the GPS data and the DEM or between the GPS data and Google Earth shows a broader range with a large deviation for GUM-05.

Comparison of the different elevations (m)						
Well	GPS (h_3)	Google Earth (h_1)	DEM (h_2)	h_1-h_2	h_3-h_2	h_3-h_2
GUM-01	1803	1800	1798	2	5	3
GUM-02	1825	1828	1828	0	-3	-3
GUM-03	1939	1944	1940	4	-1	-5
GUM-04	2232	2232	2228	4	4	0
GUM-05	2462	2614	2609	5	-147	-152
GUM-06	2461	2443	2443	0	18	18
GUM-07	2347	2349	2347	2	0	-2
GUM-08	2399	2397	2394	3	5	2
GUM-09	1819	1822	1820	2	-1	-3

Table 4.1: Comparison of the GPS-data with the DEM and Google Earth.

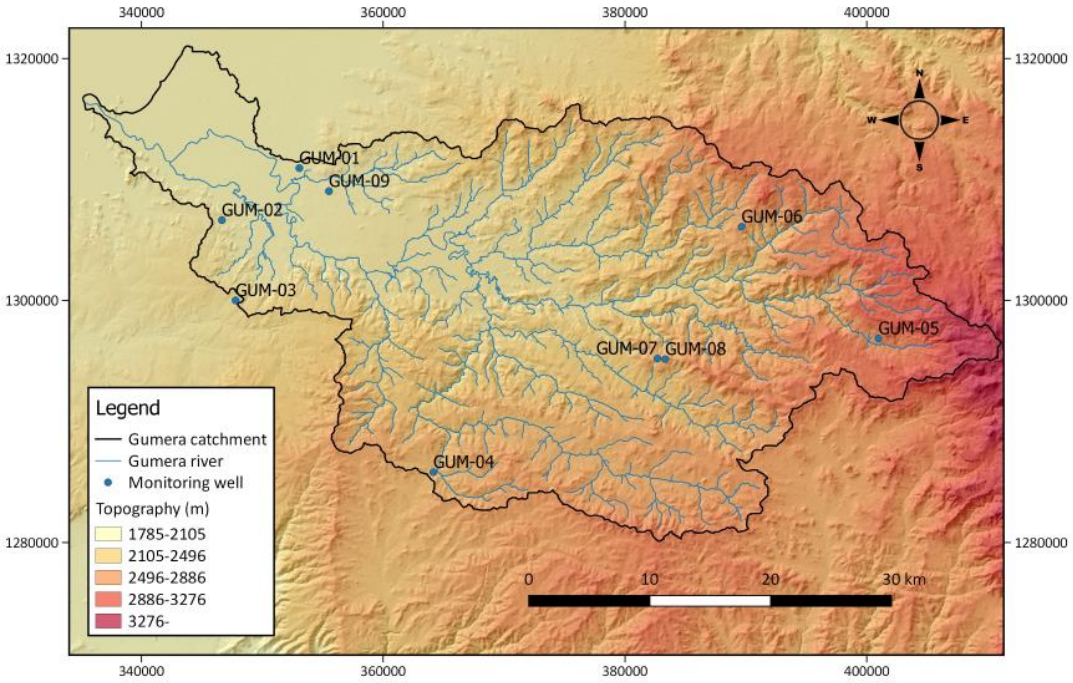

Fig. 4.1: The different locations of the verified elevations.

4.2. Meteorological data

Table 4.2a represents the monthly average rainfall for Bahir Dar and Debre Tabor. The collected rainfall in Debre Tabor is higher compared with Bahir Dar. There is a large temperature difference between day and the night-time (Table 4.2b). The maximum and minimum monthly temperature ranges between 24,5-30,3 °C and 8,1-15,2 °C, respectively. The average annual temperature is 19,9 °C with May and April as the warmest months.

The correlation coefficients between the different catchments are determined based on daily rainfall data. The meteorological stations at Gumera and Ribb are located 52 km away from each other while the distance between the stations at Gumera and Infranz is 95 km (Table 4.3). The measurements performed at the highlands in Gumera catchment indicate no correlation with Infranz catchment. There is maybe a correlation between Ribb and Gumera catchment (Fig. 4.2; Table 4.3).

(a)

Average precipitation (mm/month)		
Month	Debre Tabor	Bahir Dar
Jan	6,00	1,8
Feb	11,00	2,1
Mar	42,00	15,0
Apr	46,00	27,0
May	93,00	60,6
Jun	180,00	193,5
Jul	501,00	448,8
Aug	476,00	416,4
Sep	193,00	195,7
Oct	66,00	85,5
Nov	21,00	10,5
Dec	16,00	2,6
Total	1651,00	1459,54

(b)

Temperature °C			
Month	Max	Min	Average
Jan	27,09	8,06	17,57
Feb	29,13	9,84	19,48
Mar	30,06	12,52	21,29
Apr	30,29	14,40	22,35
May	29,71	15,23	22,47
Jun	27,74	14,80	21,27
Jul	24,67	14,03	19,35
Aug	24,54	13,78	19,16
Sep	25,59	13,21	19,40
Oct	26,67	13,46	20,06
Nov	26,81	11,06	18,93
Dec	26,67	8,16	17,41
Average	27,41	12,38	19,90

Table 4.2: (a) The monthly average precipitation. Bahir Dar receives less precipitation compared with Debre Tabor. (b) The maximum, minimum and average temperatures observed at Bahir Dar.

(a)

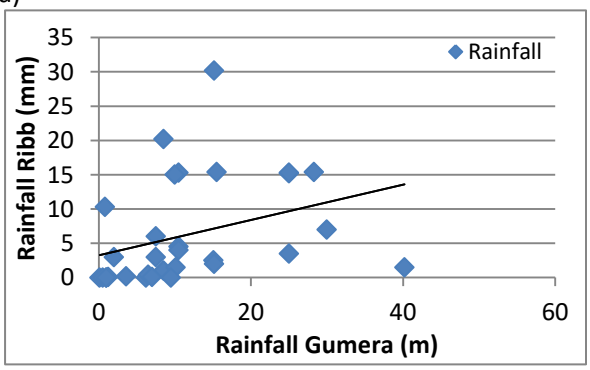

(b)

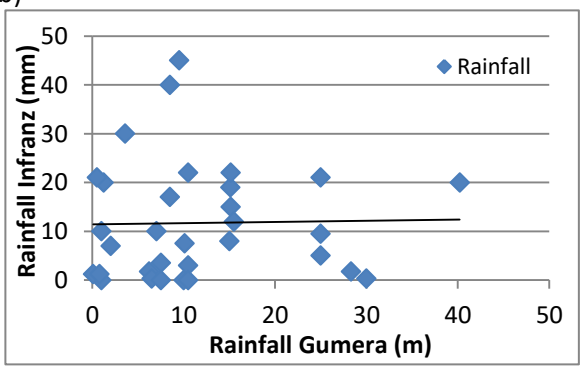

Fig. 4.2: Crossplots from the daily rainfall measurements for Gumera, Infranz and Ribb catchment.

Compared catchments	Correlation coefficients	Distance (km)
Gumera_Infranz	0,021329	95,562
Gumera_Ribb	0,334788	52,055

Table 4.3: Representation of the correlation coefficients and the distance between the different catchments.

4.3. Hydrostratigraphical model

The structure of the groundwater reservoir is determined based on several cross-sections (Fig. 4.3). Generally, two different flow systems are distinguished. One appears near the surface while the other occurs at larger depths. The shallow groundwater flow seems subjected to a shorter travel distance. It appears to the surface as springs or contributes to river valleys (Fig. 4.3). The local topography is affecting the groundwater flow in the subsurface. The deeper groundwater flow indicates the regional groundwater flow and occurs in the deeper parts of the groundwater reservoir. The term regional refers to catchment scale.

(a)

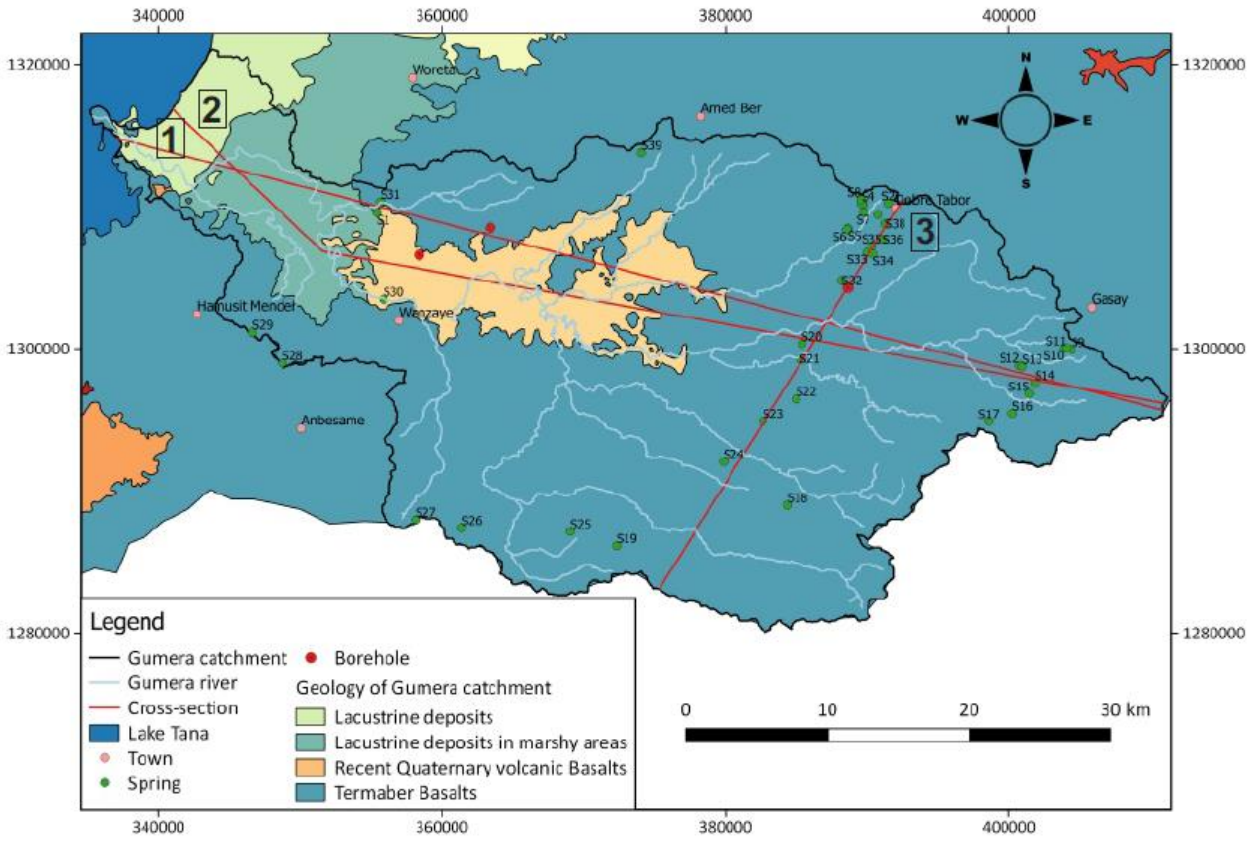

b)

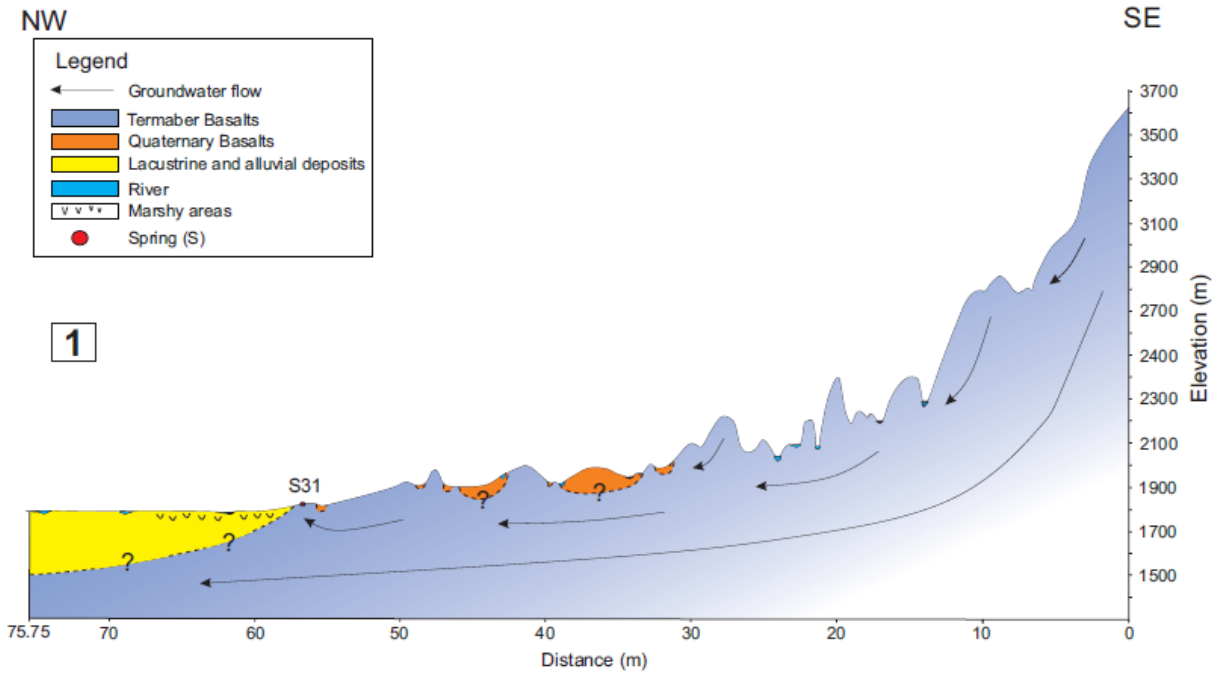
NW
SE
Legend
Groundwater flow
Termaber Basalts
Quaternary Basalts
Lacustrine and alluvial deposits
River
Marshy areas
Spring (S)
1
S31
?
3700
3500
3300
3100
2900
2700
2400
2300
2100
1900
1700
1500
Elevation (m)
75.75
70
60
50
40
30
20
10
0
Distance (m)

c)

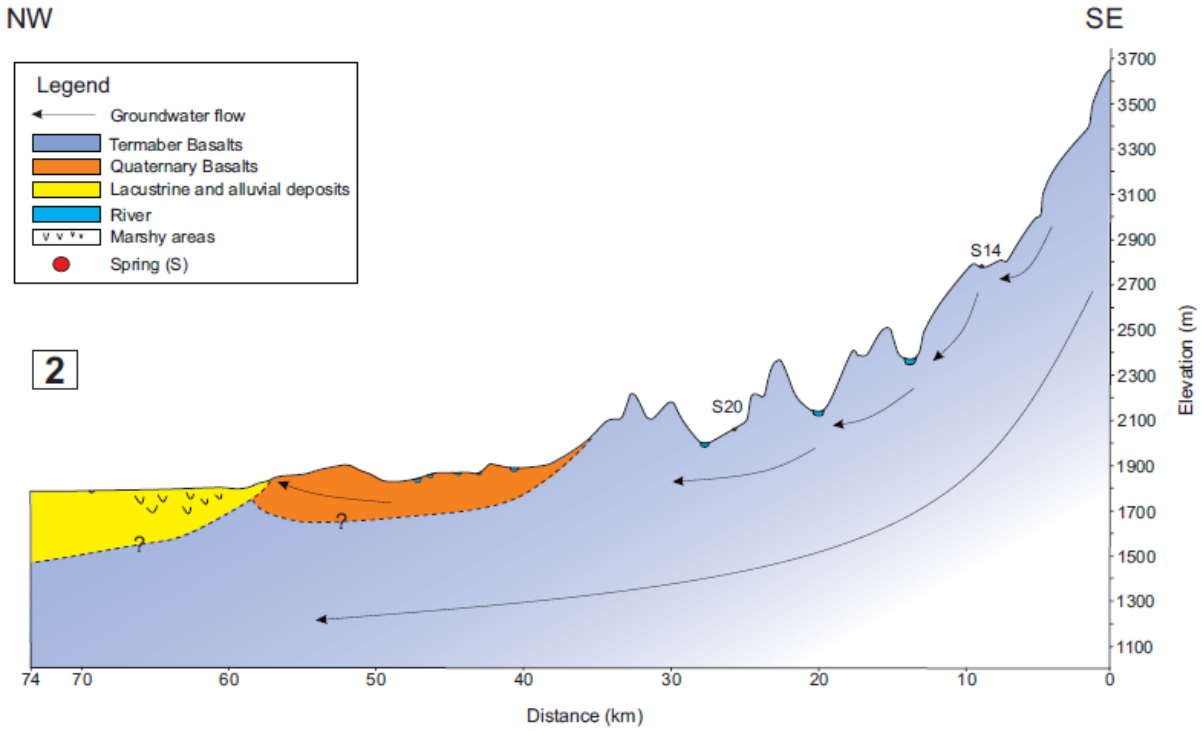
NW
SE
Legend
Groundwater flow
Termaber Basalts
Quaternary Basalts
Lacustrine and alluvial deposits
River
Marshy areas
Spring (S)
2
S14
S20
?
3700
3500
3300
3100
2900
2700
2500
2300
2100
1900
1700
1500
1300
1100
Elevation (m)
74
70
60
50
40
30
20
10
0
Distance (km)

(d)

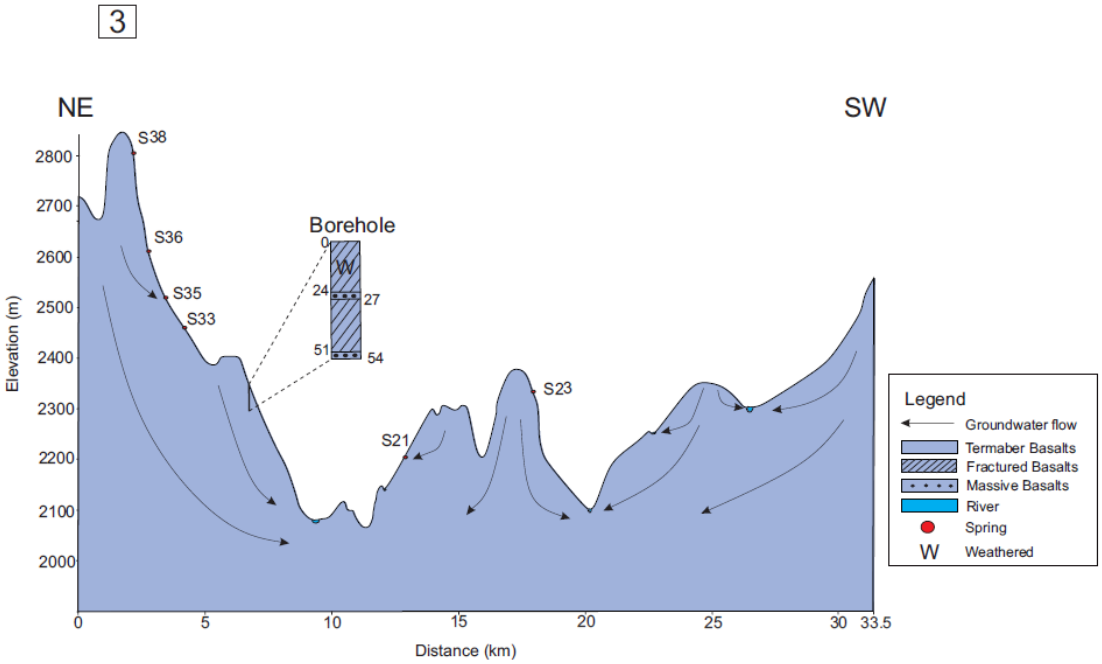

Fig. 4.3: Several cross-sections throughout the catchment representing the large variety in groundwater flow.

Based on the large variation in groundwater flow paths, a hydrostratigraphical model is created with the corresponding recharge/discharge mechanisms characterizing the catchment (Fig. 4.5). In line with the geology and geomorphology, the catchment contains at least five different aquifer types. For each aquifer type the permeability, the porosity type, the extent of the flow system and the continuity of the aquifers are determined. In general, two porosity types are distinguished, primary and secondary porosity affecting both the permeability of the geological formation. Primary porosity refers to the initial porosity during deposition and occurs in the catchment as intergranular porosity. This term is described as the porosity between grains or vesicles, for sediments and volcanic deposits respectively. Secondary porosity is defined as the porosity created after deposition occurring mainly in Gumera catchment as fractures.

Table 4.4 provides a short description of several aquifer types that are discussed below. The Termaber Basalt Aquifer is the dominating aquifer with a regional extent of the flow system. The lithology is variable consisting of weathered and/or fractured basalts alternating with tuff layers or massive, hard rock as observed in the available information of the boreholes and during fieldwork (Fig. 4.3d). This aquifer has generally a low permeability containing fractures as secondary porosity. The Termaber Basalt Aquifer is a connected/continuous aquifer which means that the Termaber Basalt aquifer contributes to the same regional flow system. A medium permeability is characterizing the Quaternary Basalt Aquifer due to the presence of scoriaceous and fractured basalts (Fig. 4.4a). The aquifer contains primary and secondary porosity dominated by intergranular porosity and fractures respectively. The flow system of this aquifer is rather locally and discontinuous as indicated in cross-section 1 in figure 4.3b. It occurs in the central - lower part of the catchment (Fig. 4.5). The permeability of the Lacustrine -Alluvial Aquifer is varying with the lithology. The lacustrine deposits, dominated by silt and clay, are overlying fluvial deposits around 6 m depth as indicated in the log report of a borehole in Woreta reaching a depth of 88 m. As already mentioned in section 2.2, thick sand and gravel beds alternates with compacted clay layers. The sand and sandy gravel beds have a thickness of 24 m and 12 m respectively. Fractured

vesicular basalts appear at a depth of 84 m. Woreta is located at the onset of the floodplain in Ribb-catchment (Fig. 4.3a). Geophysical survey is performed at the lacustrine plain to identify the underlying volcanic formation and to estimate the thickness of the lacustrine-alluvial deposits. Based on results obtained from the Controlled Source Audio Magneo-telluric (MT) prospection, SOGREAH (2012b) estimated the maximum alluvial thickness at 330 m in the central part of the plain. The thickness of the Lacustrine-Alluvial Aquifer is expected to increase toward Lake Tana to a depth of 350-450 m based on extrapolation. It decreases towards the plain boundaries. An increase of finer sediments at the subsurface is expected towards the lake shore. The subsurface has a low permeability influenced by the silt-clay layers. Medium to high porosity is characterizing the interbedded alluvial layers. Intergranular porosity is dominating this lowland aquifer. The extent of the flow system is local but continuous (Fig. 4.3b,c). This aquifer type only occurs in the lowlands but the entire floodplain area is connected/continuous. Hill Top Aquifers are dominating the more central parts of the catchment consisting of fine sediments. They have a low to medium permeability consisting of intergranular porosity. The flow system occurs more locally and the different Hill Top Aquifers are generally disconnected/discontinuous with other hill top aquifers. The last aquifer type, the River Valley Aquifer has a medium to high permeability due to the occurrence of coarse river sediments (Fig. 4.4b). The different River Valley Aquifers are generally connected but the extent of the flow system is more local. Intergranular porosity is controlling the primary porosity in this continuous aquifer.

(a) (b)

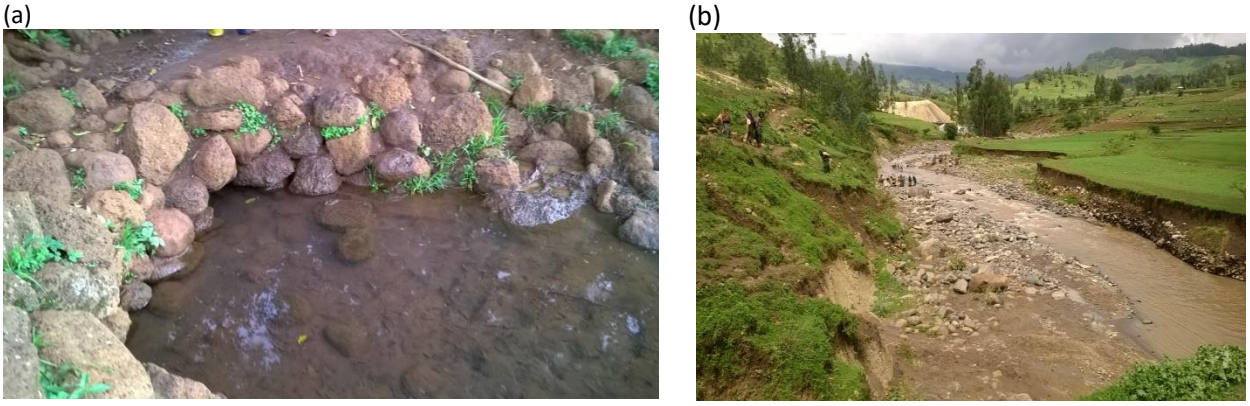

Fig. 4.4: (a) The exposed volcanic formation of the Quaternary Basalt Aquifer (b) Medium to coarse sediments are dominating the river beds of the River Valley Aquifer.

Each aquifer is characterized by its own recharge/discharge mechanisms (Fig. 4.5 and Table 4.5). In general, evapotranspiration occurs in every aquifer type. The recharge occurring in the Termaber Basalt aquifer derives from precipitation and leakage form Hill top Aquifers. Recharge due to precipitation is defined as diffuse recharge. The groundwater leaves this aquifer as discharge towards Lake Tana or to river valleys. The Quaternary Basalt Aquifer receives most recharge from precipitation. Discharge appears in local river valleys. Diffuse recharge occurs in Lacustrine - Alluvial Aquifers together with sporadic recharge during flooding events. The groundwater leaves the system in Lake Tana or to the river in summer. The water table rises in summer due to the heavy rainfall. Most of the lacustrine plain is then flooded. The river is then gaining water from the aquifer. The Hill Top Aquifer receives its recharge from precipitation. Discharge appears as springs and runoff together with percolation to the Termaber Basalt Aquifer. Diffuse recharge and mountain front recharge provide the recharge occurring in the River Valley Aquifer. This latter term is defined as the contribution of mountain regions to recharge in adjacent aquifers, in this case the river valley (Wilson and Guan, 2004). The groundwater leaves this local aquifer as river discharge.

Aquifer Name	Lithology	Permeability	Porosity type	Extent flow system	Continuity
Termaber Basalt Aquifer	Basalts Weathered Fractured Hard rock	Low	F	R	C
Quaternary Basalt Aquifer	Basalts, Scoriaceous fractured	Medium	F + I	L	D
Lacustrine - Alluvial Aquifer	Fine sediments (clay / silt), sand, sandy gravel	Low to Medium-high	I	L	C
Hill Top Aquifer	Fine sediments (silt/fine sand)	Low to medium	I	L	D
River Valley Aquifer	Medium to coarse sediments	Medium to high	I	L	C

Table 4.4: Description of the lithology of the different aquifers with its characteristic features. F = Fractures, I = Intergranular porosity, R = Regional, L = Local, C = Continuous / Connected, D = Discontinuous / Disconnected.

Aquifer Name	Recharge	Discharge
Termaber Basalt Aquifer	Diffuse recharge from precipitation Leakage from Hill top aquifers	Lake Tana, River valley
Quaternary Basalt Aquifer	Diffuse recharge from precipitation	Local river valley
Lacustrine - Alluvial Aquifer	Diffuse recharge from precipitation Sporadic recharge due to flooding	Lake Tana, River (summer)
Hill Top Aquifer	Diffuse recharge from precipitation	Springs, Percolation to Termaber Basalt aquifer, Evapotranspiration Runoff
River Valley Aquifer	Mountain front recharge Local diffuse from precipitation	River

Table 4.5: The different recharge/discharge mechanisms for each determined aquifer.

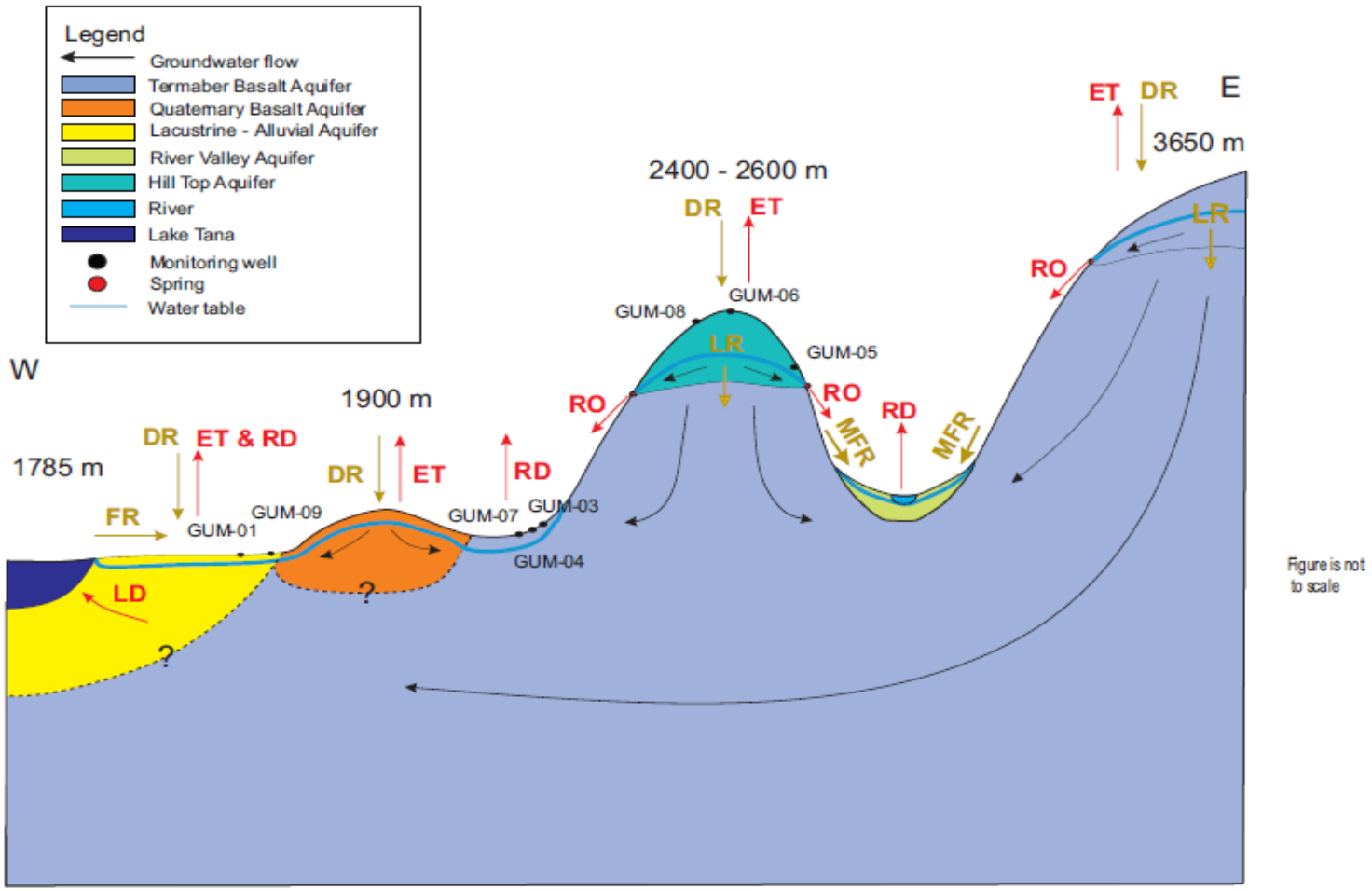

Fig. 4.5: Hydrostratigraphical model with the different recharge/discharge mechanisms for each aquifer type. DR = diffuse recharge, MFR = Mountain Front Recharge, LR = Leakage recharge, FR = Flooding recharge, LD = Lake discharge ET = Evapotranspiration, RD = River Discharge and RO = runoff. Monitoring well 2 is not on the hydrostratigraphical model. The figure is not to scale.

4.4. Monitoring of groundwater hydraulic heads

4.4.1. Monitoring wells and diver measurements

A small description of the monitoring wells is provided in table 4.6. All the monitoring wells are hand dug type wells (Fig. 4.10a). Stones or tires are supporting the wall in some cases but generally they consist of an earth wall. GUM-02 and GUM-04 are public wells having less provided information while the remaining wells are located on private area. The depth of the monitoring well ranges between 6 and 15 m. No well runs dry in winter season. The purposes vary depending on the location and wall supporting system. GUM-01 is not used for drinking purposes because of the tires used as wall supporting system. The amount of water withdrawn every day differs depending on day and season. On Friday, a lot of water is withdrawn for domestic purposes.

Figure 4.6 represents the evolution of the groundwater depth in the nine monitoring wells indicating a simultaneous response at the beginning of the rainy season. For most of the monitoring wells, the difference between the minimum and maximum water table depth ranges between three and four meters except for GUM-03, GUM-04, GUM-07 (Table 4.7). The difference between the maximum and minimum water depth of the GUM-09 is slightly higher compared to the general trend (Table 4.7). The deepest average groundwater depth occurs in GUM-06 and GUM-08 followed by GUM-03 (Table 4.7).The average groundwater depth for all the monitoring wells during the measured period is 5.9 m. There is a poor relationship between the elevation and groundwater depth (Fig. 4.7a). Figure 4.7b shows the poor relationship between the average groundwater depth of each monitoring with its closest distance to the valley.

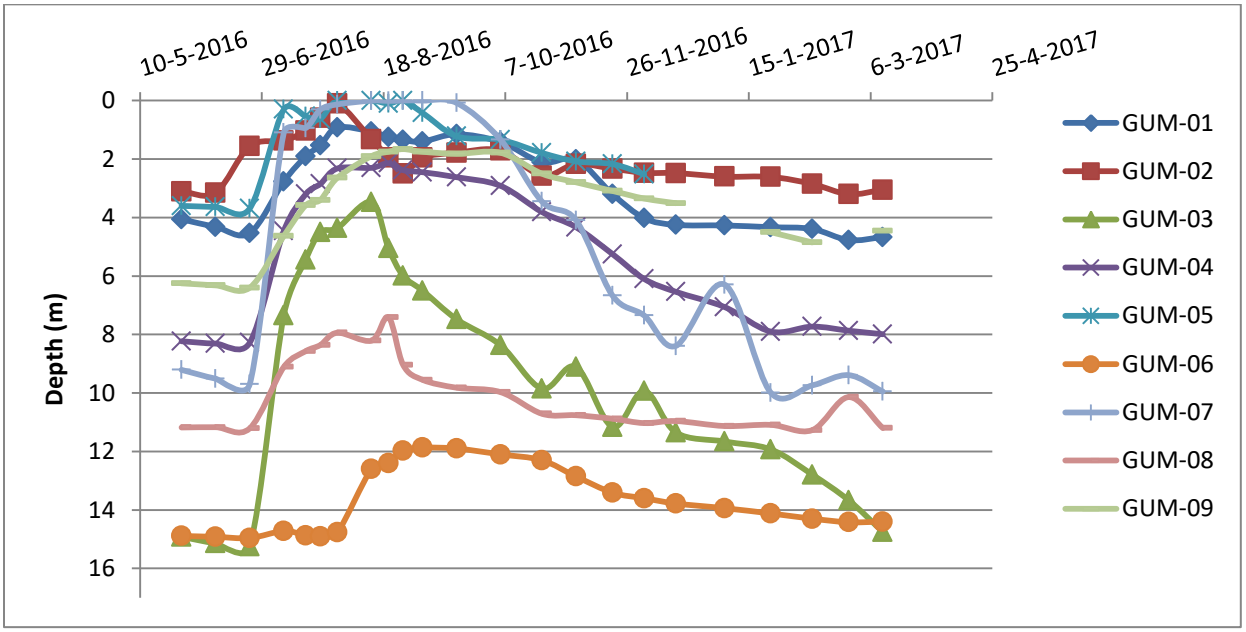

Fig. 4.6: Evolution of the groundwater depth.

(a)

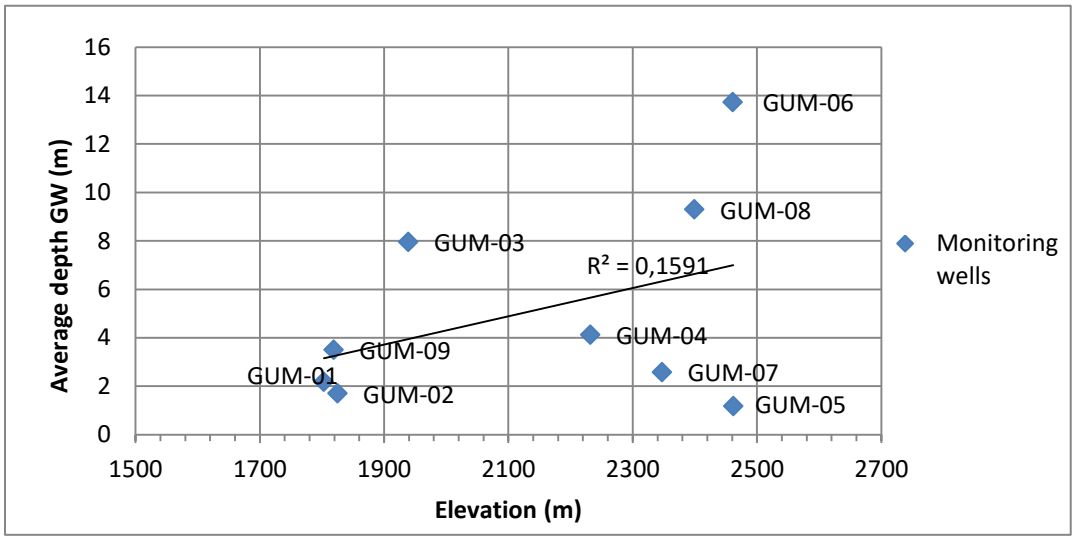

(b)

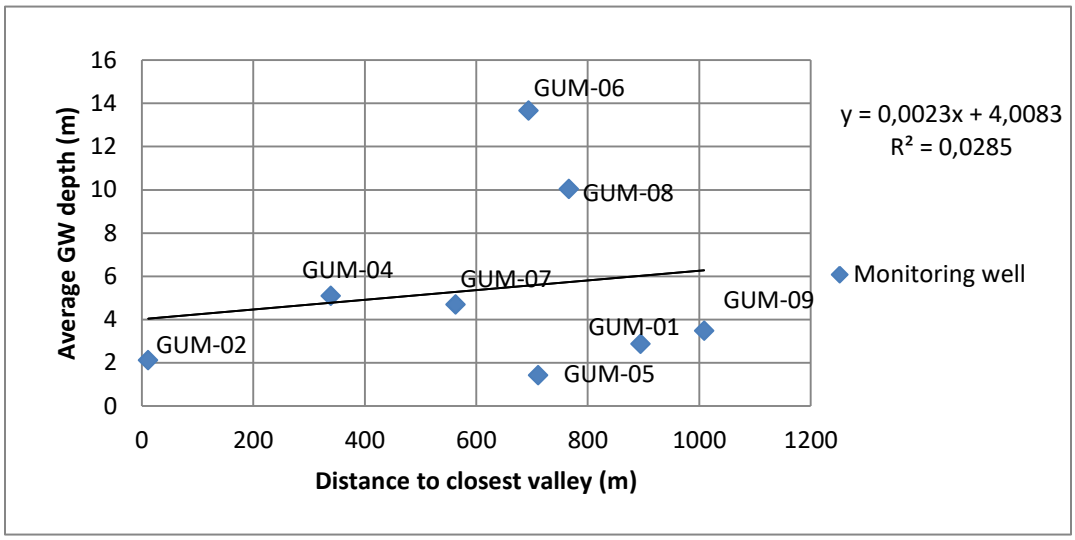

Fig. 4.7: (a) shows the poor relationship between the average groundwater depth and the elevation. (b) represents the poor relationship between the average groundwater depth of each monitoring with its closest distance to the valley.

ID_well	GUM-01	GUM-02	GUM-03	GUM-04	GUM-05	GUM-06	GUM-07	GUM-08	GUM-09
Depth (m)	7	NK	16	NK	6	15	10	11	8,5
Run dry	not really*	NK	no	NK	NK	no	(dug this year)	no	no
Withdraw (l/day)	50	100-200	500 -700	NK	60 (dry season)	NK	100-250	300	20
Wall supporting	Tires	Earth	Earth	Stones	Earth	Earth	Earth	Earth	Earth
Use	D,L	D	D, L , I	L	L,I,D	NK	D, L	D,L	D,I
Private - Public well	Private	Public	Private	Public	Private	Private	Private	Private	Private

*Around April: the well is dry in the evening but recovered in the night

Domestic purposes	D
Livestock	L
Irrigation	I
Not Know	NT

Table 4.6: Description of the monitoring wells based on oral information.

W-Id	Easting	Northing	Elevation (m)	Max water depth (m)	Date of max water depth	Min water depth (m)	Date of min water depth	Difference (m)	Average water depth(m)
GUM-01	352978	1310739	1803	4,77	25-2-2017	0,92	30-7-2017	3,85	2,86
GUM-02	346561	1306439	1825	3,2	25-2-2017	0,1	30-7-2017	3,1	2,11
GUM-03	347703	1299802	1939	15,25	24-6-2016	3,47	13-8-2017	11,78	9,57
GUM-04	364059	1285613	2232	8,31	27-5-2016	2,14	20-8-2016	6,17	5,09
GUM-05	400870	1296665	2462	3,69	24-6-2016	0	30-7-2016	3,69	1,41
GUM-06	389559	1305899	2461	14,96	24-6-2016	11,87	3-9-2016	3,09	13,65
GUM-07	382602	1295007	2347	9,99	24-1-2016	0	13-8-2016	9,99	4,68
GUM-08	383239	1294956	2399	11,27	10-2-2016	7,41	20-8-2016	3,86	10,03
GUM-09	355418	1308829	1819	6,4	24-6-2016	1,66	26-8-2016	4,74	3,47
Diver 1	400870	1296665	2462	2,94	10-2-2017	0	21-8-2016	2,94	-
Diver 2	352660	1310704	1803	3,51	29-1-2017	0	30-9-2016	3,51	-

Table 4.7: The monitoring wells with their corresponding maximum, minimum and average depth to water.

Two divers are installed in the catchment. Diver 1 is located in the highlands in GUM-05. Diver 2 is situated in the floodplain. Figure 4.8 shows the evolution of the groundwater level since 20th of August till 10th of February. Diver 2 is used for irrigation from 6th November on. The large fluctuations observed in diver 2 are due to pumping. The groundwater recovers to its original level during the night. The groundwater level in in the floodplain reacts differently comparing the groundwater level in the highland. The groundwater level is in both divers at the surface at the beginning of the measurements (19 -7-2016). The groundwater in the highlands leaves the groundwater reservoir earlier compared with the floodplain, 21th of August and 30th of September respectively. The groundwater level decreases immediately in the highlands when no precipitation occurs. The difference between the minimum and maximum water table depth is 2,94 m for diver 1 (Table 4.7). For diver 2 the water table difference is 3,51 m (Table 4.7). After a certain time period, the groundwater seems to stay at a constant level. Figure 4.9 shows the differences in hydraulic heads plotted on the map.

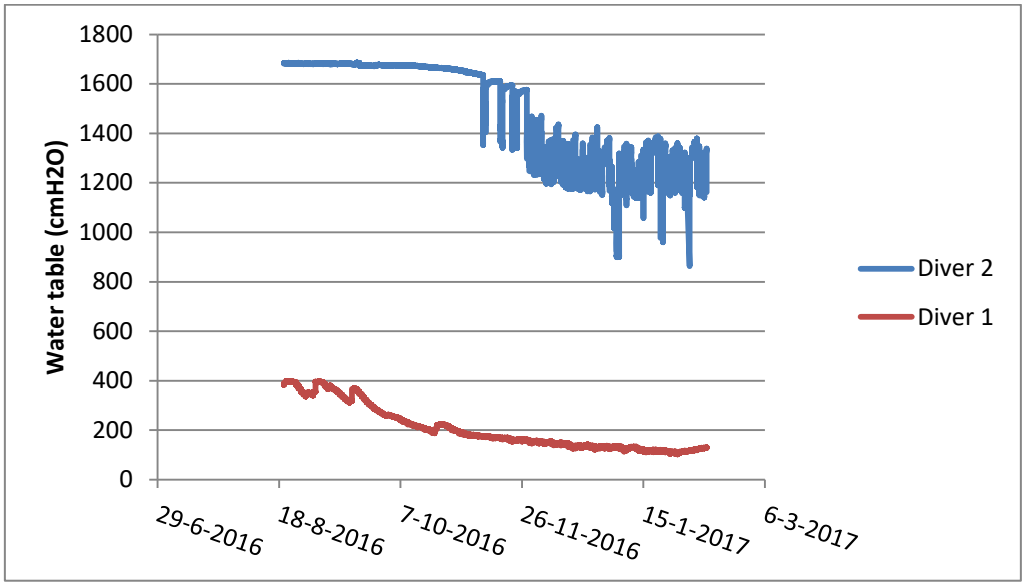

Fig. 4.8: The diver measurements for the floodplain (diver 2) and the highlands (diver 1).

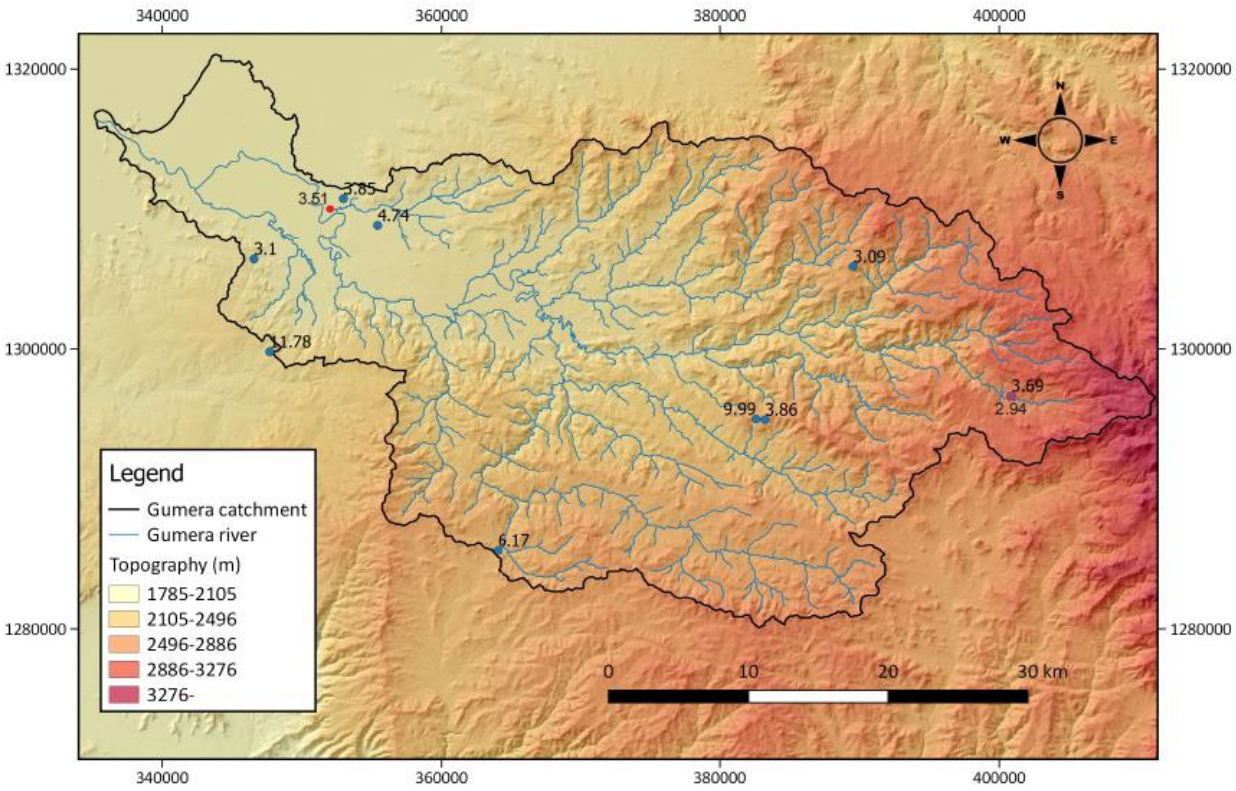

Fig.: 4.9: The differences in hydraulic heads plotted on the map.

4.4.2. Inventorizing wells and springs

Different types of springs are characterizing the catchment. Most of them are diffuse springs but some fractured springs occur near Debre Tabor (Fig. 4.11b). Contact springs appear very often at the boundary between fractured basalts and compacted tuff layers or in the rainy season between the soil and the underlying bedrock. Many springs in Gumera catchment are enhanced springs (Fig. 4.11c). The discharge of the springs is generally low. Some springs are used for religious purposes and are demarcated (Fig. 4.10d).

(a)

(b)

(c) (d)

Fig. 4.10: (a) Hand dug well, (b) Fracture spring, (c) Enhanced spring, (d) Holy spring.

Figure 4.11 shows the inventorized springs and wells. They are divided in several groups based on their location in the catchment (Table 4.8). The name GIW refers to Gumera Inventorized Well. The name GUM indicates a monitoring well. Few hand dug wells occur in the highest part of the catchment (Group 1). Springs appear frequently but not all of them are used for drinking purposes. Many springs are developed in the area around Debre Tabor (Group 2). More downstream of the western river generated around Debre Tabor, springs and wells are absent due to the presence of massive basalts. Spring 33 and 34 (S33 & S34) are fractured springs. Group 3 consists of many enhanced springs. The occurrence of spring 23 (S23) is expected at lower elevations following the morphology. Fault rock and fault breccia are characterizing the local surrounding area concluding that a dyke system is probably damming the water. Group 4 contains enhanced and contact springs. Fractures are surrounding spring 26 (S26). This is an enhanced spring of which the discharge is lower than expected. The water follows the direction of the fractures and not from the intergranular permeability. Most of the water flows down to lower elevations. Spring 27 (S27) and spring 19 (S19) are contact springs. Fractured basalts are overlying compacted tuff layers. Tuff outcrops around well 17 (GIW17). The lower part of the catchment contains many wells (Group 5). Spring 30 (S30), located south-east of the floodplain, is a thermal spring close to the river bank of Gumera River. Well 17 (GIW) is located on a little hill. It was the only well on the hill area that doesn't run dry in the winter. Spring 1 (S1) is located in the Quaternary Basalts and supply the local village with freshwater all year around. Based on oral information of the rural people, several springs occur a few kilometers upstream from spring 1. The local name for that area is Bebeks. Unfortunately, the area is poorly accessible.

Group	Well	Spring	Location
1	GIW12, GIW13, GUM-05	S9, S10, S11, S12, S13, S14, S15, S16, S17	Eastern part
2	GIW10, GIW11, GIW19, GIW20, GIW21, GIW22, GIW24, GUM-06	S2, S3, S4, S5,S6,S7, S8, S32, S33, S34, S35, S36, S37, S38, S39	Northern part
3	GIW 14, GIW15, GUM-07, GUM-08	S18, S20,S21, S22, S23, S24	Central higher part
4	GUM-08, GIW16, GIW17	S19, S25, S26, S27	Southern part
5	GIW1, GIW2, GIW3, GIW4, GIW5, GIW6, GIW7, GIW8, GIW9, GIW18, GIW23, GUM-01, GUM-02, GUM-03, GUM-09	S1, S28, S29, S31, S30	Lower part

Table 4.8: Classification of the inventrorized wells and springs based on their location in the catchment.

(a)

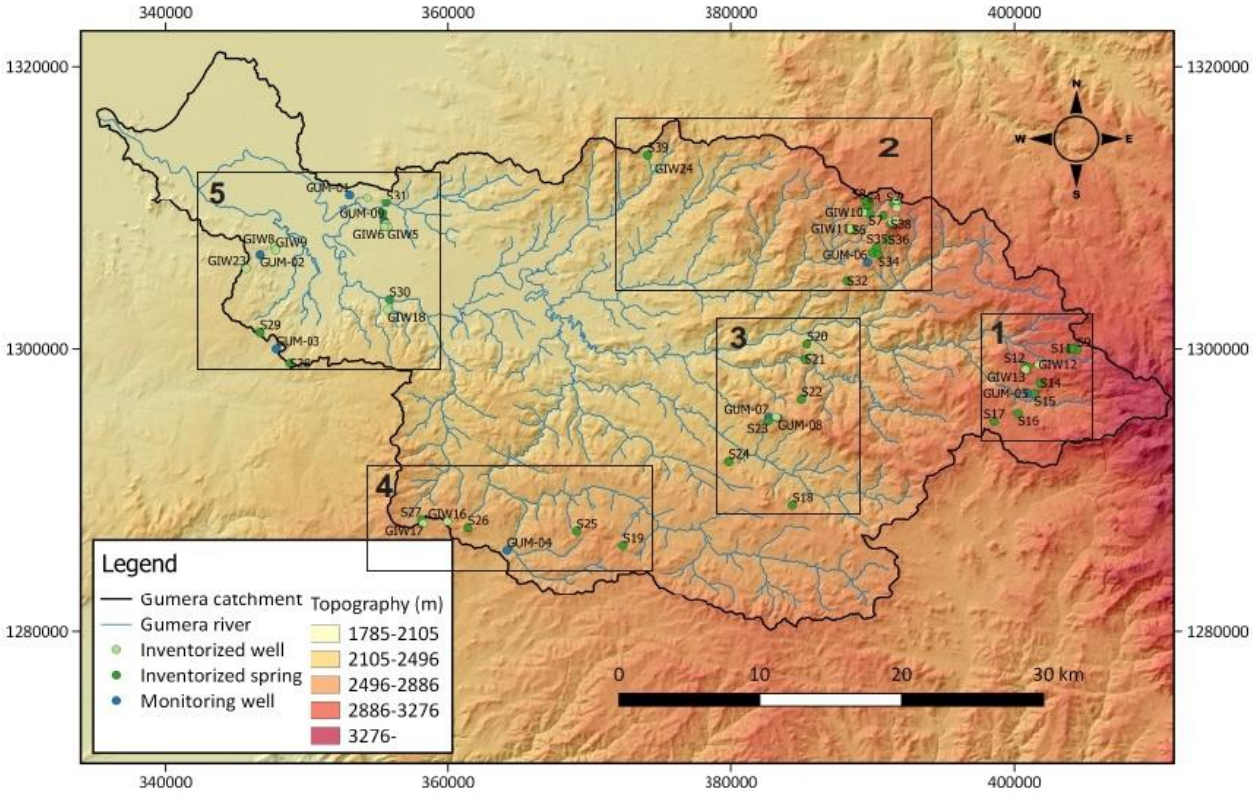

(b)

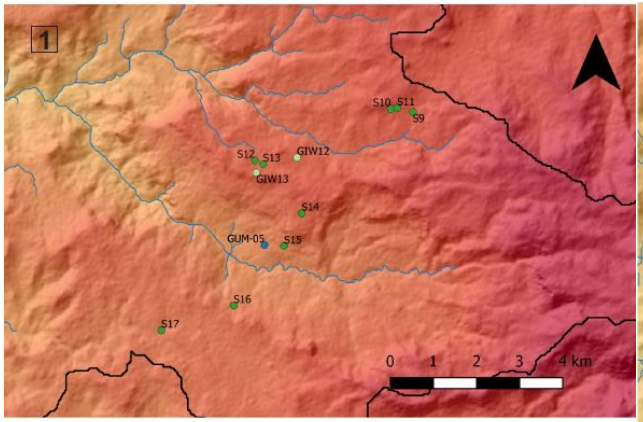

(c)

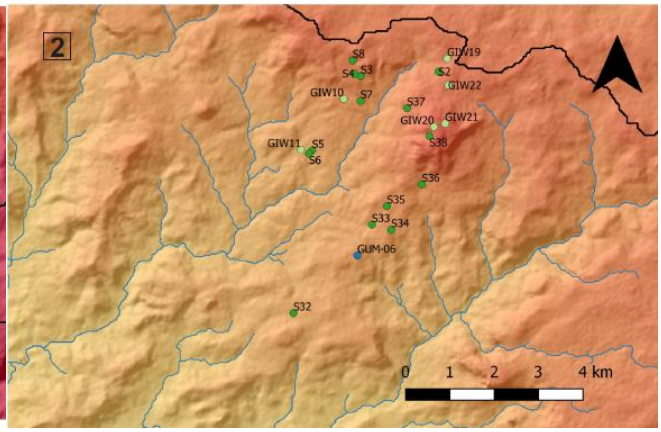

(d)

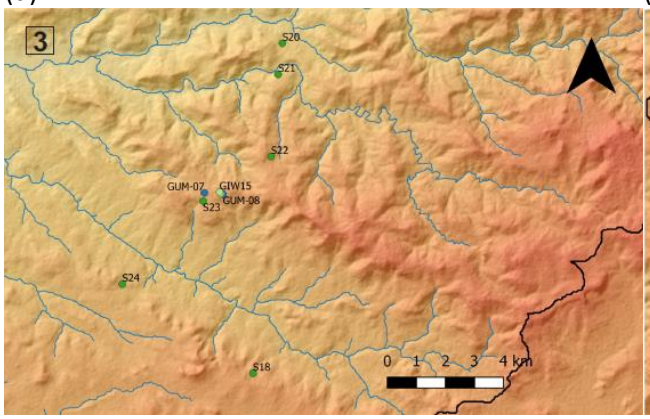

(e)

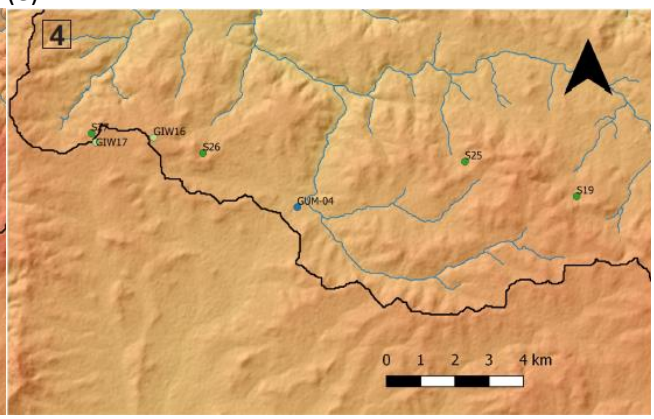

(f)

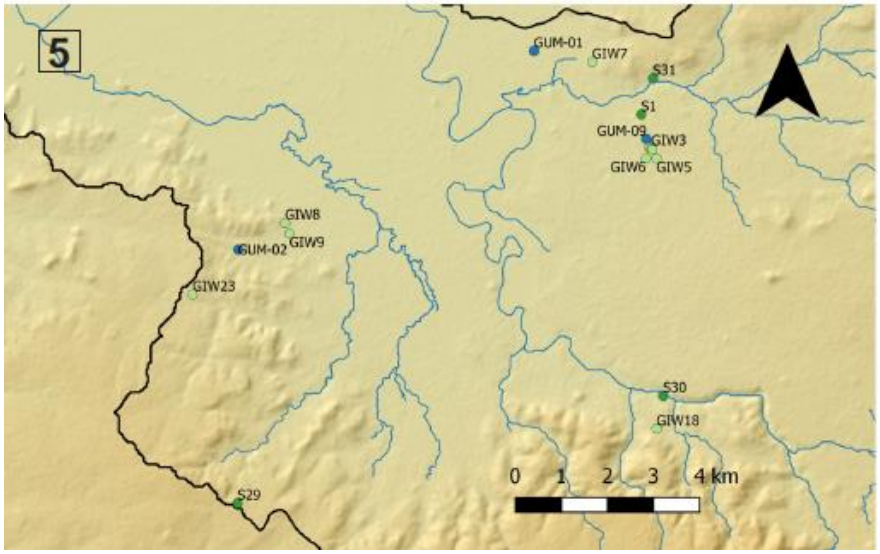

Fig. 4.11: Representation of the monitoring wells, inventorized wells and springs.

4.5. Surface water discharge measurements

Table 4.9 represents the determined base flow, runoff and runoff coefficients. The annual runoff is estimated to be 340,869 m³/s or 590,66 mm/year. This corresponds to 36 % of the annual precipitation and to 900 million m³/year runoff occurring in the catchment. The highest baseflow and runoff-values occur during August (Fig. 4.12). The largest runoff coefficient is represented in September (Fig. 4.12). Figure 4.13a and Figure 4.13b show the minimum discharge (Qmin) evolution from January to May and September to December during 1980-2014. From the year 1996 on, the minimum discharge from January to May in figure 4.13a seems increase for all the months. In 2003, 2005, 2007, 2012 and 2014 the minimum discharge in September is significantly higher compared with the other years (Fig. 4.13b).

	Baseflow (m³/s)	Runoff (m³/s)	Precipitation (mm/month)	Runoff (mm/month)	Runoff coeff.	Average runoff
Jan	2,80	0,76	6,00	1,33	0,22	0.10
Feb	1,95	0,40	11,00	0,64	0,06	
March	1,47	0,59	42,00	1,03	0,02	
April	1,09	0,75	46,00	1,26	0,03	0.06
May	1,49	1,03	93,00	1,81	0,02	
June	2,61	13,28	180,00	22,48	0,12	
July	11,31	80,48	501,00	140,81	0,28	0.50
Aug	19,00	135,22	476,00	236,57	0,50	
Sept	15,00	81,43	193,00	137,86	0,71	
Oct	13,39	20,79	66,00	36,37	0,55	0.37
Nov	7,91	3,95	21,00	6,69	0,32	
Dec	4,64	2,18	16,00	3,81	0,24	
Total	82,64	340,86	1651,00	590,66	0,36	

Table 4.9: Representation of the estimated baseflow, runoff and runoff coefficients.

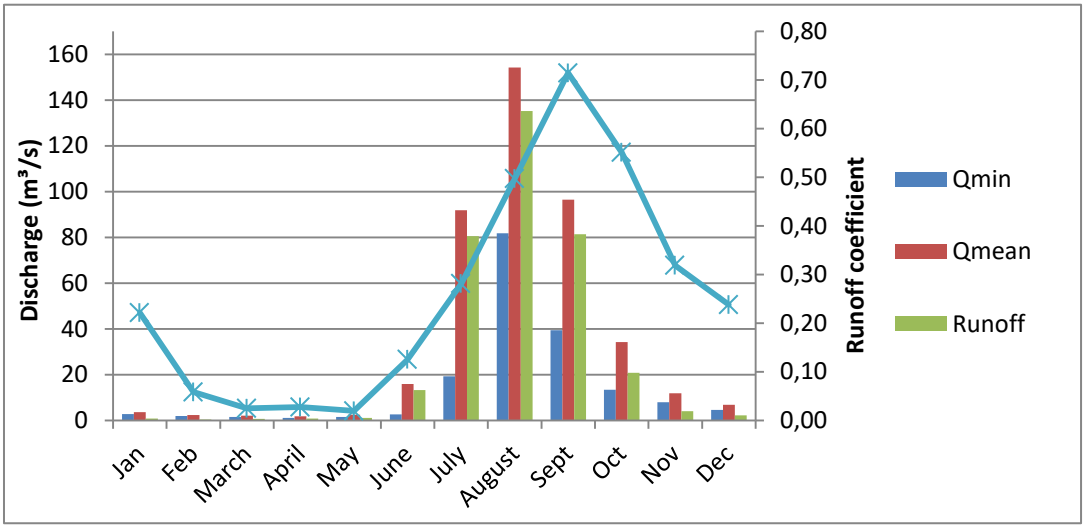

Fig. 4.12: The variations in discharge during the year with the estimated runoff and runoff coefficients.

(a)

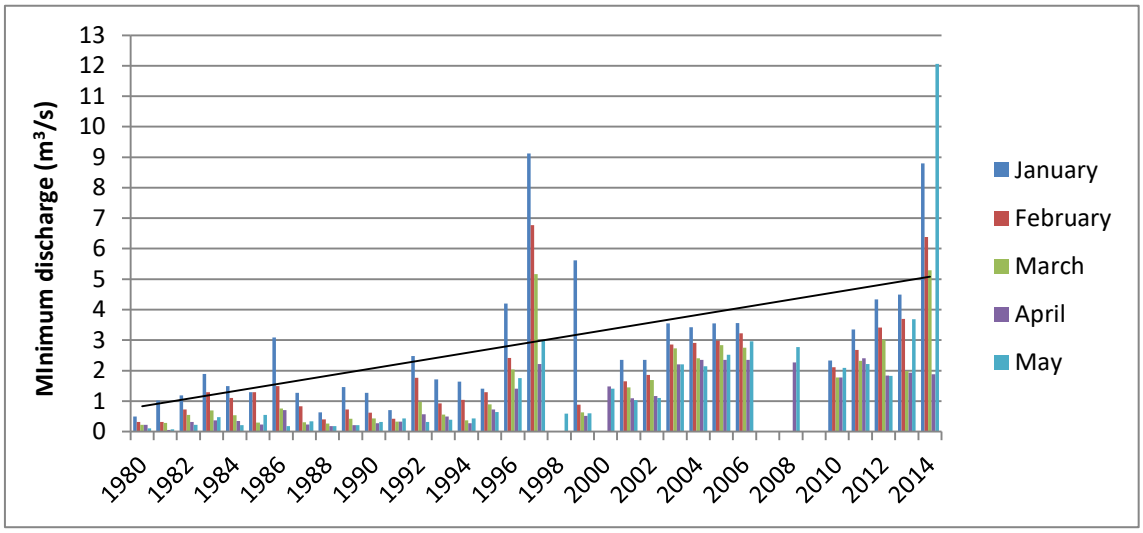

(b)

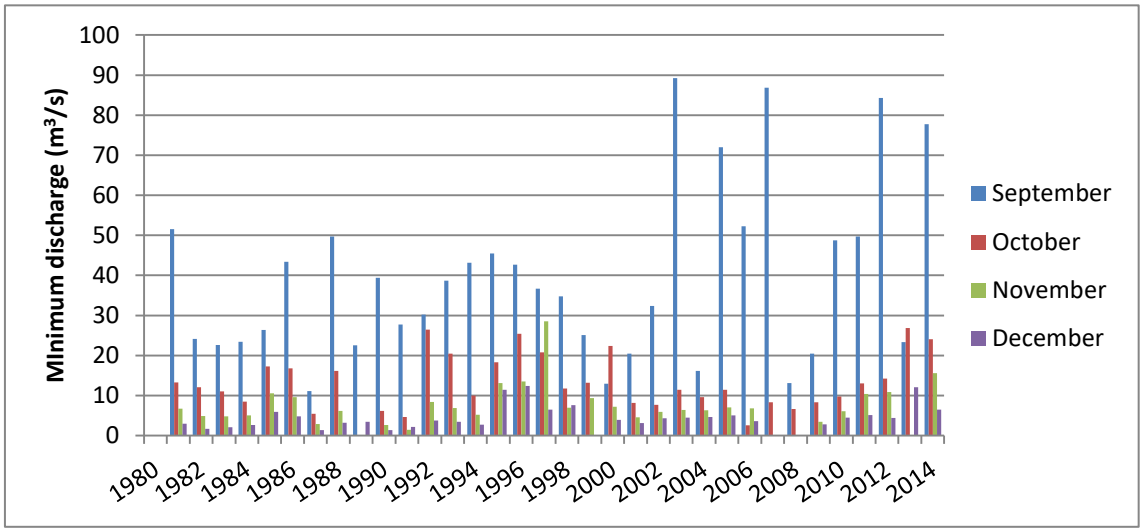

Fig. 4.13: (a) Represents the minimum discharge distribution for the months of January - May in 1980-2014. (b) Illustrates the minimum discharge distribution in September – December in 1980-2014.

4.6. Hydraulic parameters

A description of the dominant sediments and the type of aquifer that occur in the area of which the hydraulic parameters are determined, is provided based on field observations. The upper 15 cm of the well consists of silty clay. Tuff material is dominating the underlying formations consisting of boulders ranging from a few cm up to 20 cm. The aquifer is unconfined because the water table is located deeper than the clay layer. When the hand dug well was almost overflowing, the owner decided to dig a channel of 33 cm deep.

Figure 4.14 represents the position of the diver in the well. The diameter of the hand dug well is 1.44 m. The length of the pipe is 6 m. The diver was put at a depth of 5.42 m. The depth of the well is unknown but is estimated to be 6 m.

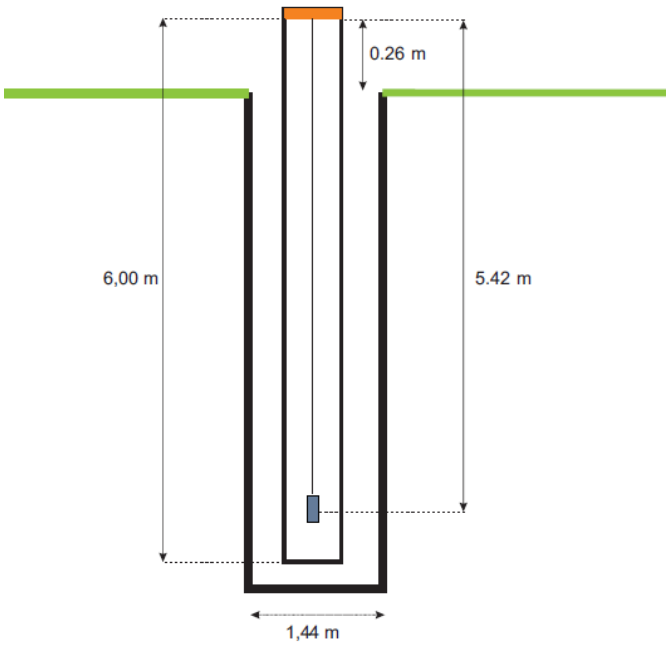

Fig. 4.14: Representation of the position of the diver.

4.6.1. Specific yield and recession rate

As already mentioned in section 3.6, the specific yield is determined for the upstream catchment using the diver data and the daily meteorological measurements. In figure 4.15, the water table is represented in blue, the rainfall data in red. Several fluctuations can be observed but only two water table rises can be used for the calculations. The other rises reach the ground surface and an unknown volume of water has left the aquifer as runoff. If runoff occurs, the equation 3.4 cannot be applied. Using the two water table rises, represented in green on figure 4.15, the specific yield is derived (Table 4.10a). The groundwater table immediately responds to precipitation.

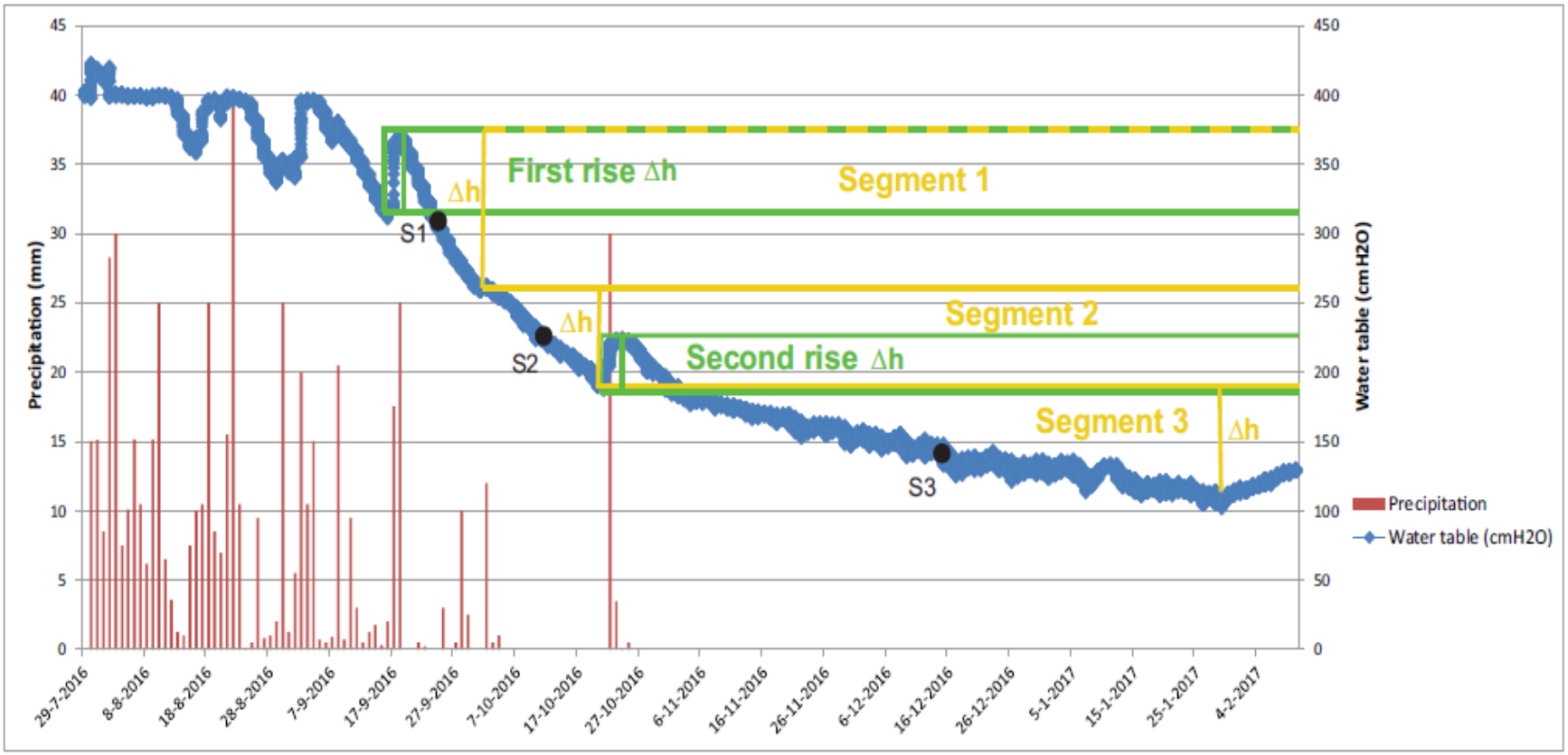

Fig. 4.15: Representing the diver data and the meteorological data.

(a)

	Rise	Date	Precipitation (mm)	PET (mm)	Recharge (mm)	Total recharge	h (cm)	Δh (mm)	Sy (%)
Specific yield	First rise	17-9-2016	17,5	2	15,5	37	320,0	499,7	7,4
		18-9-2016	25	3,5	21,5		370,0		
	Second rise	21-10-2016	30	5,6	24,4	25,9	194,7	282,8	9,2
		22-10-2016	3,5	2	1,5		-		
		24-10-2016	-	-	-	-	223,0		

(b)

GW velocity (mm/day)			
Parameters	Segment 1 (18/09/2016 - 1/10/2016)	Segment 2 (2/10/2016 - 21/10/2016)	Segment 3 (3/11/2016 - 29/01/2017)
hmax	370,0	263,0	186,1
hmin	261,3	194,7	108,0
Δh (mm)	1086,9	683,2	781,4
Δt (day)	13	19	87
v (mm/day)	83,6	36,0	9,0

(c)

GW recession rate (mm/day)			
Parameters	Segment 1	Segment 2	Segment 3
Sy	0,074	0,092	0,092
v (mm/day)	83,6	36	4,07
GW recession rate (mm/dag)	6,186	3,312	0,374

Table 4.10: Used data and results for the calculations.

Two rainfall events have caused the first water table rise having a total recharge of 37 mm (Table 4.10a). These two days rainfall has increased the water table with 499,7 mm. Dividing the values result in a specific yield of 7,4%. The total amount of recharge received in the second rise is 25,9 mm. Two rainfall events have caused a water table rise of 282,8 mm resulting in a specific yield of 9,2 %. The average specific yield in this aquifer is 8,3 %.

Three different recession slopes are characterized in the diver data. They are divided in three different segments on the basis of which the groundwater velocity is determined (Table 4.10b). Figure 4.13 represents the different segments in yellow. The height difference between the minimum and maximum water table in a certain recession slope is determined together with the corresponding time period (Table 4.10b). Segment 1 occurs from 18th September till 1st October. It has a water table difference of 1086,9 mm achieved in a time period of 13 days resulting in a corresponding velocity of 83,6 mm. The water table difference in segment 2 is 683,2 mm obtained between the 2th of October to 21th of October which is 19 days. The velocity of the groundwater is 36 mm/day. Segment 3 has a water table difference of 781,4 mm developed in 87 days between 3th November till 29th January having a groundwater velocity of 9 mm/dag. Segment 1 has a recession rate of 6,18 m/day. A recession rate of 3,31 mm/day and 0.374 mm/day is characterizing segment 2 and segment 3 respectively. The groundwater recessions varies with the time after a precipitation event. With increasing time, the groundwater recession rate tends to be slower.

Based on the collected data, a groundwater recession graph is made for 3 days (24/09/2016, 12/10/2016, 16/12/2016) occurring in the middle of the recession slope assuming that the calculated recession rate is applicable for the expected days (Fig. 4.15; Fig. 4.16; Table 4.11). This represents the rate of change of the

groundwater storage S at time t. S1 is located in segment 1 at a depth of 0,855 m having a groundwater recession rate of 6,186 mm/day. At a depth of 1,71 m, S2 is situated subjected to a groundwater recession rate of 3,312 mm/day. A groundwater recession rate of 0,374 mm/day is characterizing S3, located at 2,56 m depth (Table 4.11). The maximum recession rate is 9,14 mm/day. The recession rate approaches a velocity of zero around a depth of 2,67 m (Fig. 4.16).

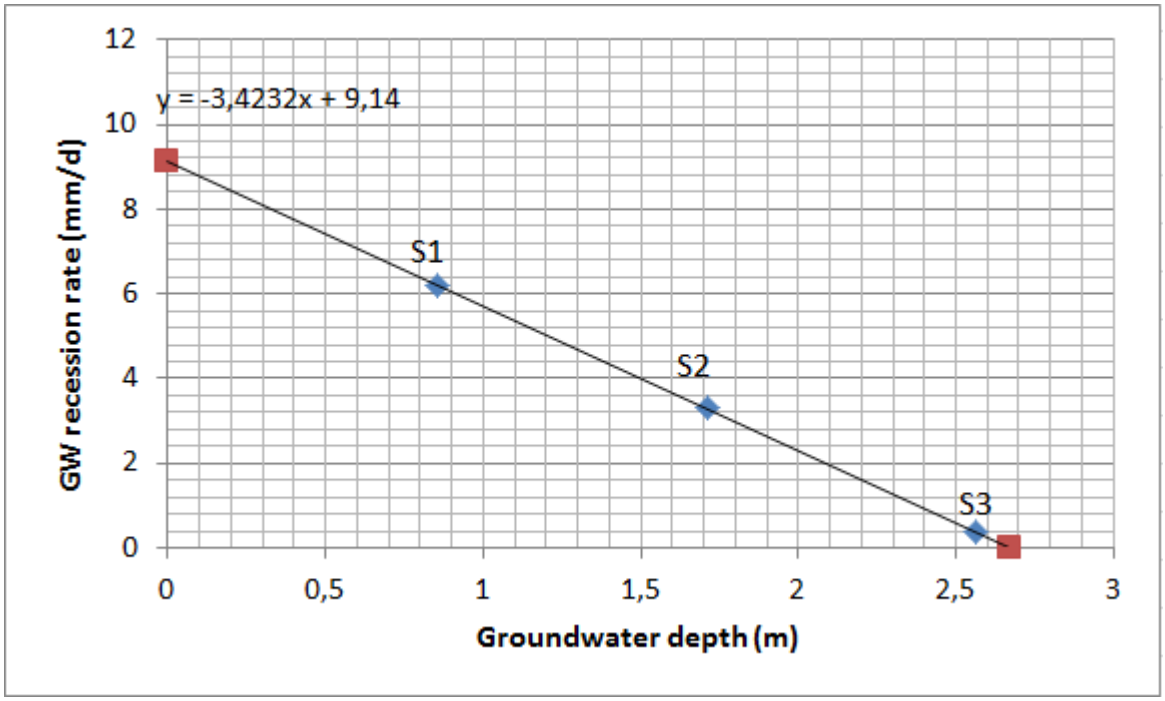

Fig. 4.16: Linear relationship between the recession rate and the groundwater depth.

Location	GW recession rate (mm/dag)	Groundwater depth (m)
S1	6,186	0,855
S2	3,312	1,71
S3	0,374	2,56

Table 4.11: Represents the corresponding groundwater depth and recession rate for the assumed days.

4.6.2. Pumping test

Figure 4.17 shows the complete drawdown and recovery of the performed pumping test. During pumping, springs have been observed in the well around a depth of 2.5 m. Because also recovery was measured, the Theis recovery method can be applied to determine the transmissivity (T) and hydraulic conductivity (K) (Kruseman and de Ridder, 1990).

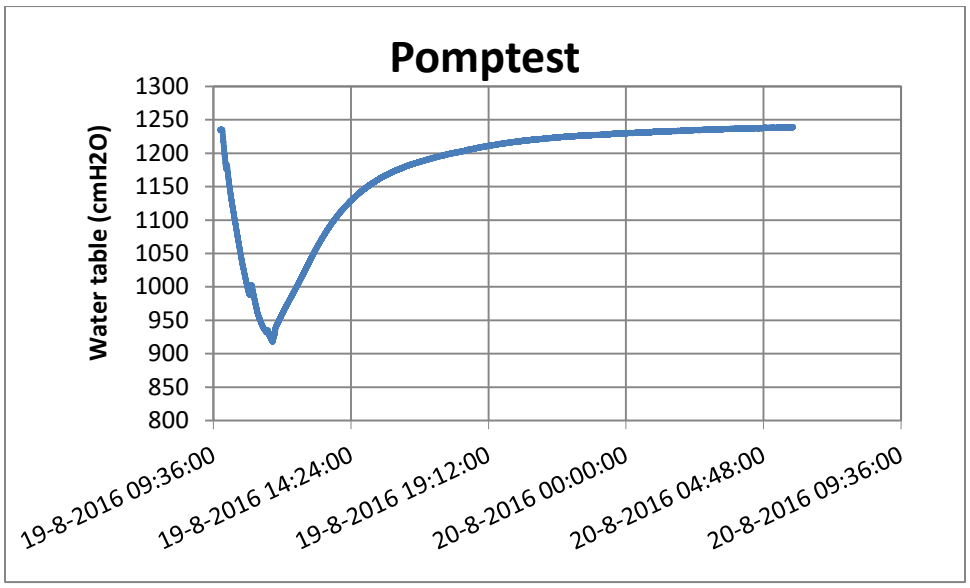

Fig. 4.17: Evolution of the drawdown and the recovery.

Figure 4.18 represents the plot of the residual drawdown (s') over the time ratio (t/t'). The residual drawdown difference (Δ s'), defined as the drawdown difference per log cycle of t/t' is 5,75 m. This value is derived from figure 4.18 and is used to calculate the transmissivity (Eq. 3.8). The transmissivity is 9,35 m²/d (Table 4.12). Dividing the transmissivity over the saturated thickness of the aquifer provides the hydraulic conductivity (Eq. 3.9) which is 1,61 m/d.

Figure 4.19 shows the best obtained fit with the MLU Software between the observed and simulated drawdown. Table 4.13 represents the different used input data and the approached transmissivity and hydraulic conductivity. The hydraulic conductivity is estimated to be 1,6 m/d. The transmissivity is 9,6 m²/d (Table 4.13).

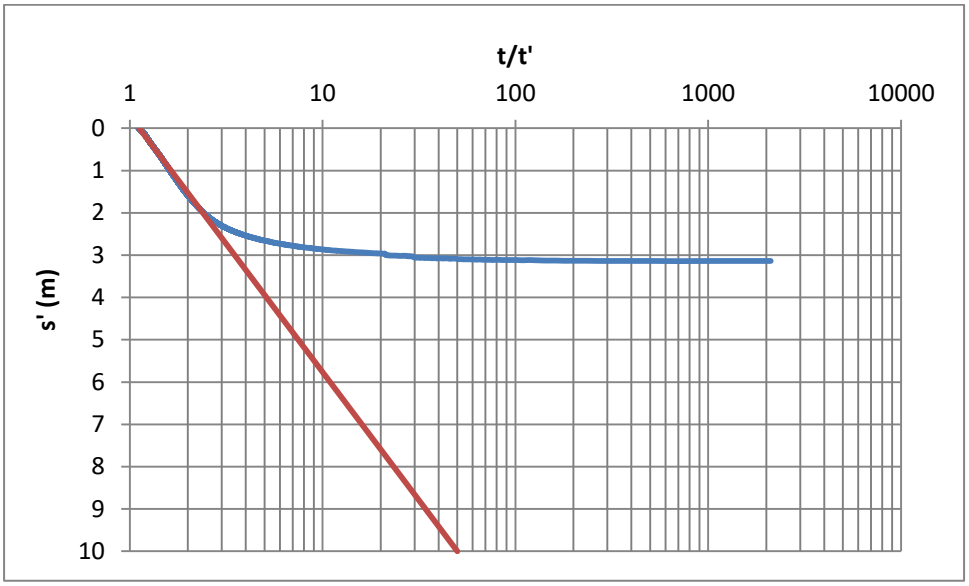

Fig. 4.18: Plot of the residual drawdown (s') over the time ratio (t/t').

Q (m^3/s)	T (m^2/d)	D (m)	K (m/d)
0,0034	9,35	6,00	1,61

Table 4.12: The calculated transmissivity and hydraulic conductivity based on the Theis recovery method.

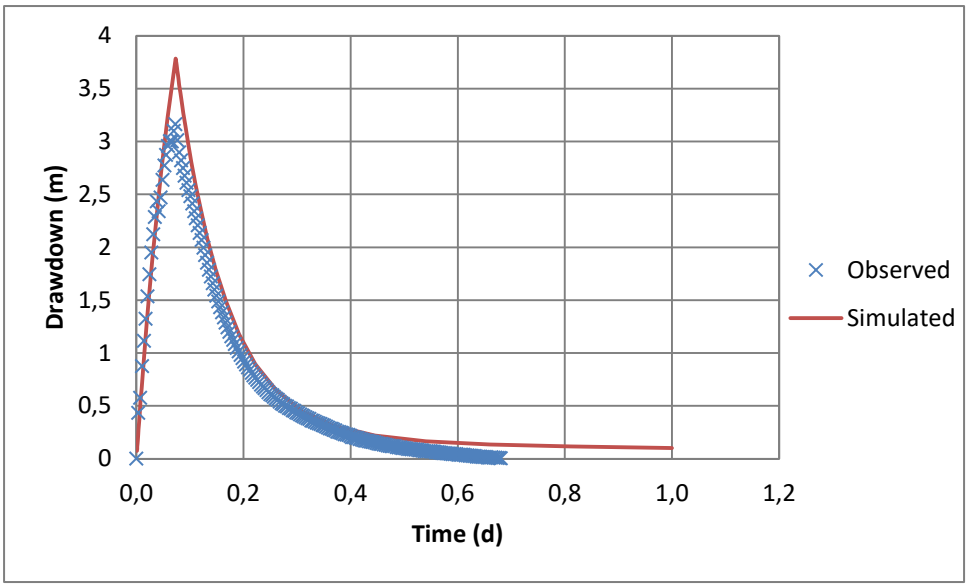

Fig. 4.19: Best obtained fit between the observed and simulated drawdown.

Parameters	Q (m/d)	r (m)	D (m)	Sy	T (m^2/d)	K (m/d)
Input	293,76	0,7	6	0,1	-	-
Output	-	-	-	-	9,6	1,6

Table 4.13: The used input data for the MLU Software and the approached transmissivity (T) and hydraulic conductivity (K).

4.7. Groundwater flow

In section 4.3, the structure of the groundwater reservoir is determined based on several cross-sections (Fig. 4.3). Two different flow directions are distinguished. The local topography is affecting the groundwater flow in the subsurface. The regional groundwater flow occurs in the deeper parts of the groundwater reservoir. Figure 4.20 and 4.21 represent the regional and local groundwater flow directions for the whole catchment.

The equipotential lines approach the estimated piezometric surface at a certain area. On regional scale, the groundwater flows from east to northwest following the general topography. Due to the large topographic differences on local scale, many local groundwater systems are formed (Fig. 4.21a). The groundwater converges in the central, lower parts of the catchment (Fig. 4.20). Another factor having an important contribution to the groundwater flow system is the surrounding geology with its corresponding permeability and porosity. As already mentioned above, volcanic rocks have a large variation in water bearing capacities. The occurrence of massive basalts and tuff layers in the Termaber Basalts create a semi-pervious layer and prevent the large infiltration of groundwater to deeper parts of the catchment. Figure 4.21b-h show the groundwater flow direction for the monitoring wells in a detailed view. Lateral variations in topography are controlling the groundwater flow directions.

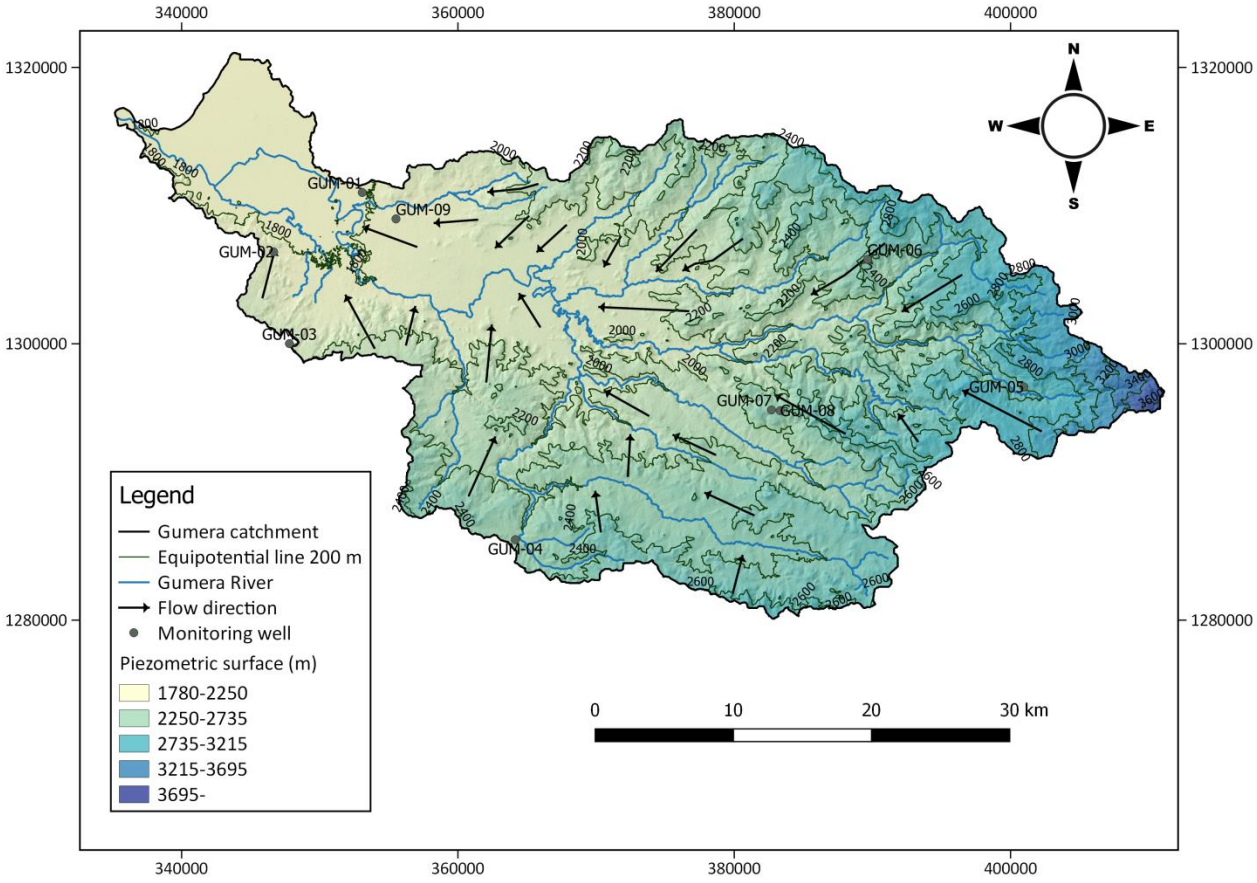

Fig. 4.20: Regional groundwater flow in the catchment.

(a)

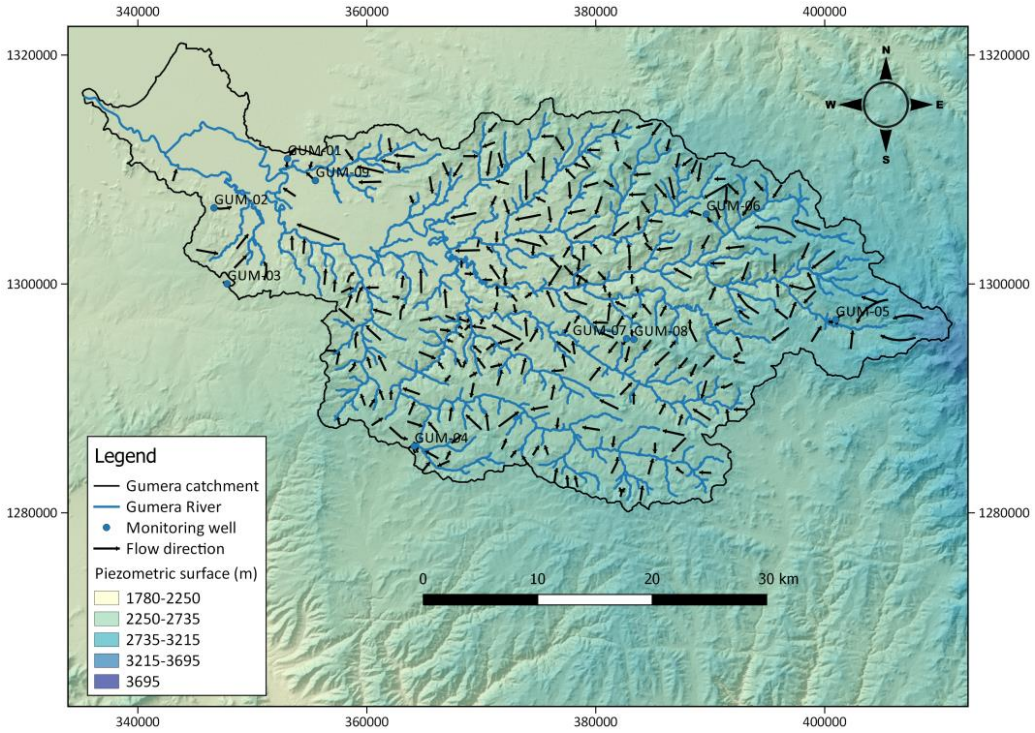

(b)

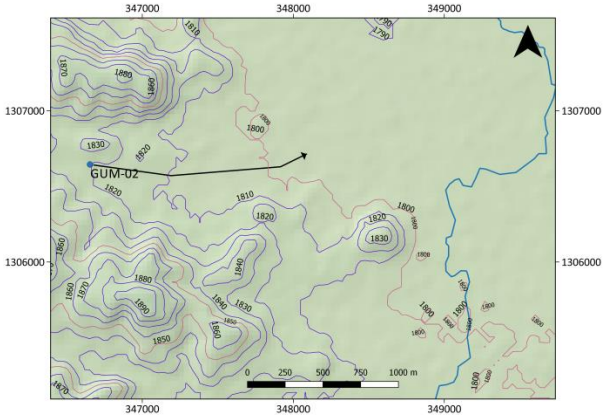
347000
348000
349000
1307000
1306000
GUM-02
0 250 500 750 1000 m

(c)

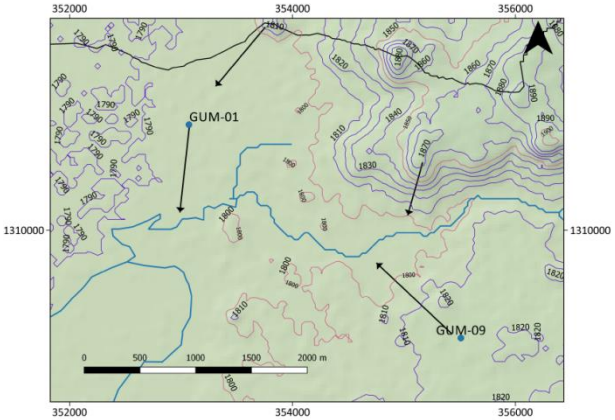
352000
354000
356000
1310000
GUM-01
GUM-09
0 500 1000 1500 2000 m

(d)

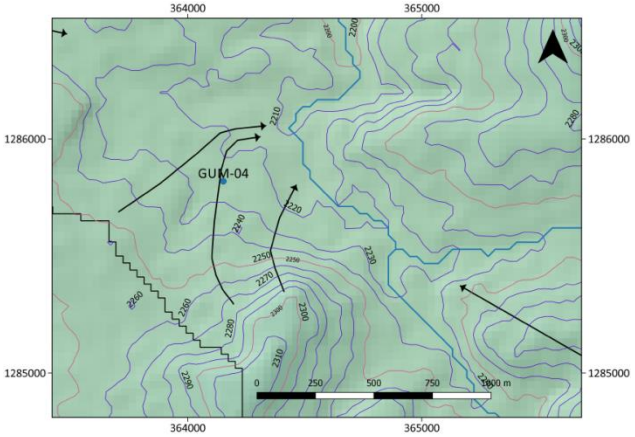
364000
365000
1286000
1285000
GUM-04
0 250 500 750 1000 m

(e)

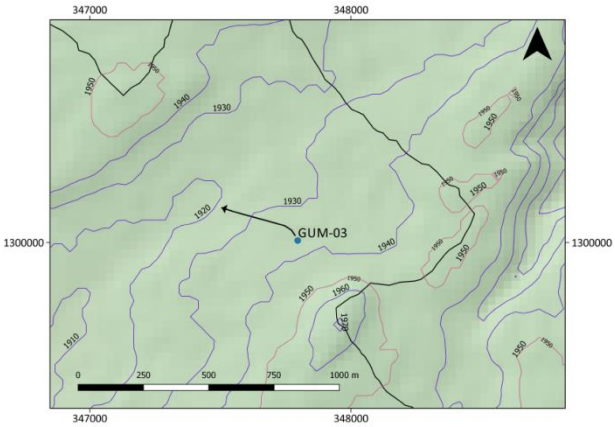
347000
348000
1300000
GUM-03
0 250 500 750 1000 m

(f)

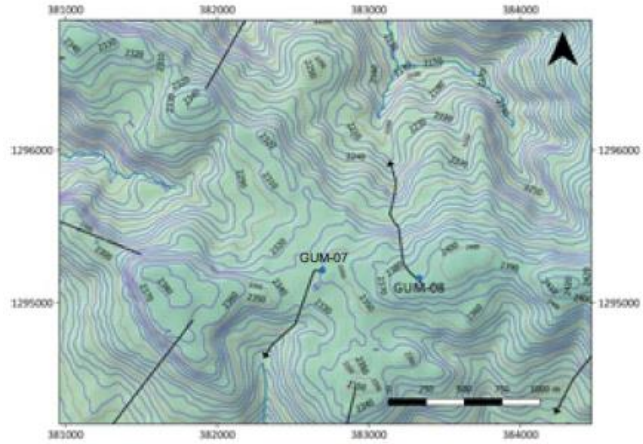
1296000
1295000
GUM-07
GUM-08

(g)

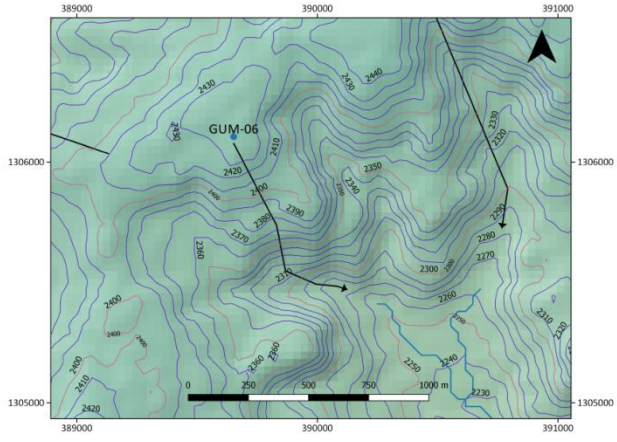
389000
390000
391000
1306000
1305000
GUM-06
0 250 500 750 1000 m

(h)

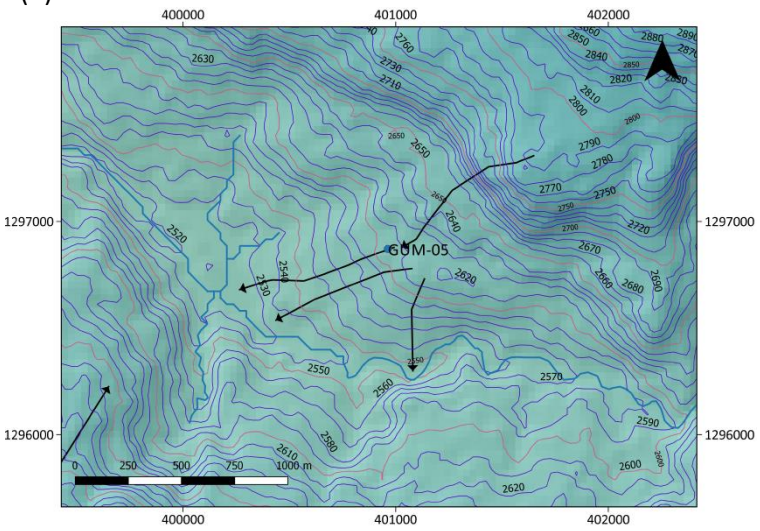

Fig. 4.21: Local groundwater flow with a detailed view on the monitoring wells. (b) GUM-02, (c) GUM-01 and GUM-09, (d) GUM-04, (e) GUM-03, (f) GUM-07 and GUM-08, (g) GUM-06, (h) GUM-05.

4.8. Groundwater recharge

4.8.1. Base flow separation

The obtained total annual recharge based on the base flow separation method is 141,98 mm/year using the monthly base flow values of Gumera River (Table 4.14). The recharge is only 8,6 % of the annual precipitation. This corresponds with approximately 200 million m^3/year recharge in the whole catchment.

Month	Base flow (m^3/s)	Recharge (mm/month)
January	2,80	4,90
February	1,95	3,07
March	1,47	2,56
April	1,09	1,84
May	1,49	2,60
June	2,61	4,43
July	11,31	19,78
August	19,00	33,24
September	15,00	25,40
October	13,39	22,67
November	7,91	13,38
December	4,64	8,11
Total	82,64	141,98

Table 4.14: The calculated recharge based on the approached base flow of Gumera River

4.8.2. Chloride Mass Balance method

The CMB-method is calculated with the arithmetic-geometric averages (Table 4.15) The chloride concentrations in the eleven rainfall samples vary between 0,196 mg/l and 1,548 mg/l having a total arithmetic-geometric average of 0,549 mg/l. The recharge is estimated for the chloride concentrations in the wells and springs separately. The well samples have a chloride concentration between 0,8937 mg/l and 63,851 mg/l whereas the chloride concentrations of the spring samples vary from 0,6689 mg/l to 5,9713 mg/l. The calculated arithmetic-geometric average is 11,198 mg/l and 3,058 mg/l respectively for the well and the spring samples. The average annual precipitation for Bahir Dar and Debre Tabor is 1459,54 mm/year and 1651 mm/year. The annual runoff is 590,66 mm/year. The effective precipitation is 956,57 mm/year and 1060,34 mm/year respectively. The estimated recharges in the spring samples vary from 171,42 mm/year to 190,02 mm/year whereas for the wells, it ranges from 46,81 mm/year to 51,89 mm/year (Table 4.16). Taking into account the surface area of Gumera catchment, this is more than 300 million m^3/year of groundwater recharge over the catchment as based on the spring samples and approximately 100 million m^3/year using the well samples.

The bromide concentrations in the rain samples have an arithmetic-geometric average of 0,143 mg/l. For the well and spring samples, it is respectively 0,3 and 0,116 mg/l. The recharge is estimated to be 455,96-505,43 mm/year for the well samples and 1179,21 – 1307,14 mm/year for the spring samples (Table 4.16). Figure 4.22 shows the relationship between the Cl/Br ratio in function of the Cl^--concentrations. The ratio rises with increasing chloride concentrations.

	Rain sample		Well sample		Spring sample	
	Cl	Br	Cl	Br	Cl	Br
Arithmetic mean	0,651	0,148	15,517	0,364	3,202	0,135
Geometric mean	0,455	0,139	7,587	0,242	2,918	0,099
AGM	0,549	0,143	11,198	0,300	3,058	0,116
median	0,299	0,136	6,305	0,241	3,125	0,081

Table 4.15: The results of the calculated mean values, the median for the rain, sample and spring samples respectively. There is a large variation between the determined recharge values between the well and spring samples. AGM is the Arithmetic-Geometric Mean.

Recharge (mm/year)	Well		Spring	
Based on rainfall from:	Cl	Br	Cl	Br
Debre Tabor	51,89	505,43	171,42	1307,14
Bahir Dar	46,81	455,96	190,02	1179,21

Table 4.16: The estimated recharge for the wells and springs based on precipitation from Bahir Dar and Debre Tabor.

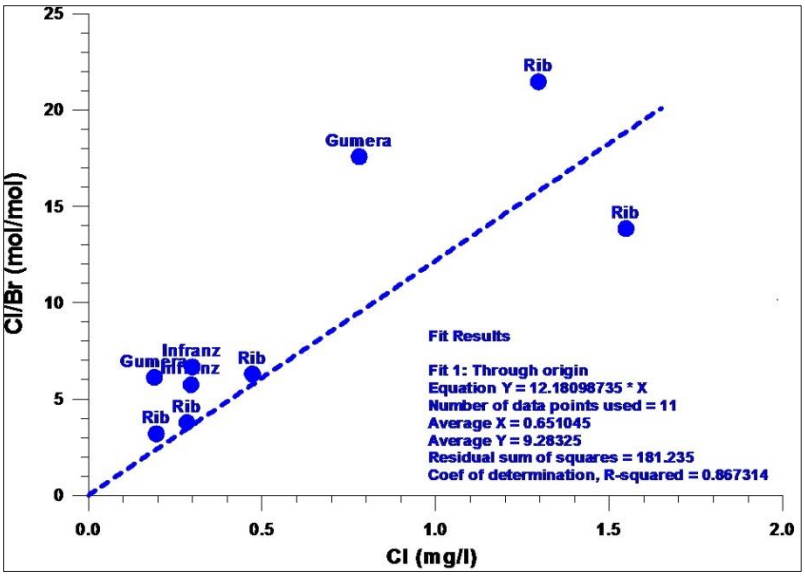

Fig. 4.22: The relation is shown between the Cl/Br ratio and the Cl^--concentrations.

4.8.3. Soil moisture balance: Thornthwaite method

According to Mamo and Jain (2010), the eastern side of the catchment, the highlands, consists of clay and clayey loam, the central part and western part contains mainly clay to silty clay. Moderately deep rooted crops like teff, maize, barley and wheat are the major cultivated crops. Grassland, Eucalyptus and Acacia trees are dominating the highlands. Other land cover types are shrubland, grassland and the cultivation of vegetables. Fan et al. (2016) had measured the rooting depth of the cereals (except for teff) and compared with the maximum rooting depth found in literature. The maximum rooting depth in literature varies between 300 cm and 170 cm although the average maximum rooting depth of cereals observed by the authors is 128 cm. Grasslands and shrubland are thought to have a maximum rooting depth of approximately 2,5 m and 4,7 m respectively. *Eucalypthus sp.* has roots at a maximum depth of 10 m (Canadell et al., 1996).

The plant available water (PAW) is calculated for the different soil textures corresponding to several rooting depths occurring in the catchment (Table 4.17). A rooting depth of 0,8 m coincides with a PAW-value of 96,8 mm, 109,6 mm, 110,4 mm respectively for clay, clay loam and silty clay resulting in a recharge of around 370 mm. Rooting depths ranging from 0,80 m and 4 m corresponds with a recharge varying between 370 mm – 150 mm. The actual evapotranspiration ranges from 519,5 mm to 695,8 mm for PAW-values between 100 to 400 mm respectively (Table 4.17b). Figure 4.23a represents the relationship between the estimated recharge and actual evapotranspiration (AET) the different PAW-values which is rather exponential. Figure 4.23b shows the distribution of the potential evapotranspiration (PET), the effective precipitation and the estimated recharge over 14 years. Highest PET- values occur during March, April and May. The groundwater recharge generally occurs during July and August.

Grassland and forest dominates the highlands with a corresponding soil texture of clay and clayey loam. Assuming an average rooting depth of 2,5 m, this corresponds with a recharge of approximately 235 mm. Moderately deep rooted crops are considered to occur in the central and western parts having an estimated rooting depth of 1,2 m. This area would receive a recharge of approximately 320 mm/year.

(a)

PAW (mm)			
Rooting depth (m)	clay	clay loam	silty clay
0,8	96,8	109,6	110,4
1,2	145,2	164,4	165,6
2	242	274	276
2,5	302,5	342,5	345
3	363	411	414
3,5	423,5	479,5	483
4	484	548	552

(b)

PAW (mm)	AET (mm)	Recharge (mm/year)
50	474,84	425,08
100	519,49	376,70
200	600,50	294,70
300	656,94	235,50
400	695,82	193,04
500	722,08	163,33
550	731,36	281,39

Table 4.17: (a) The calculated PAW for the different soil types and rooting depth. (b) represents the calculated AET and recharge for the corresponding PAW.

(a)

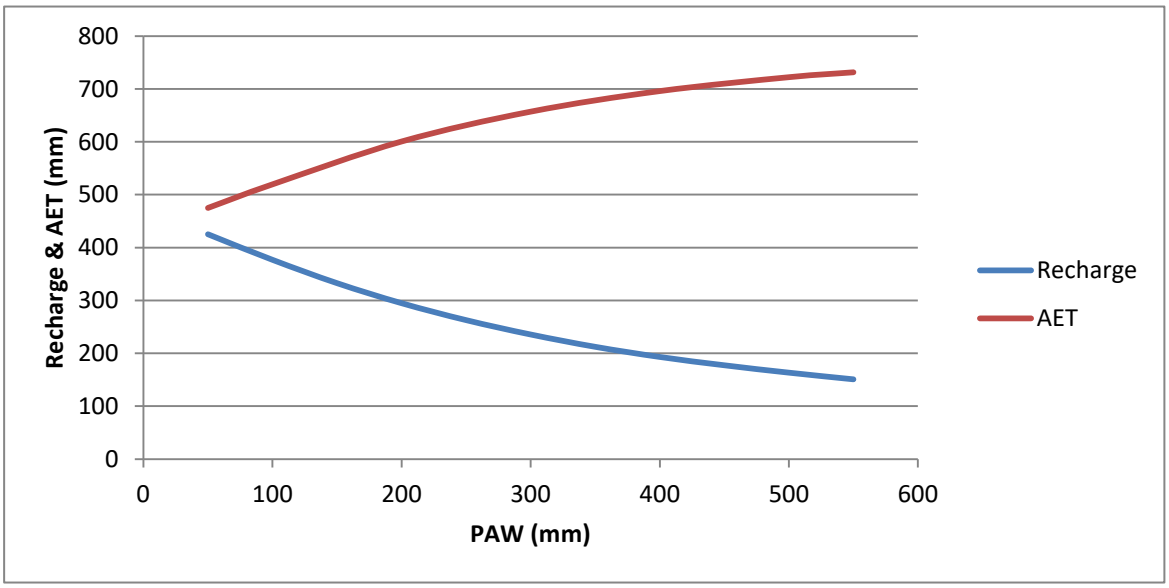

(b)

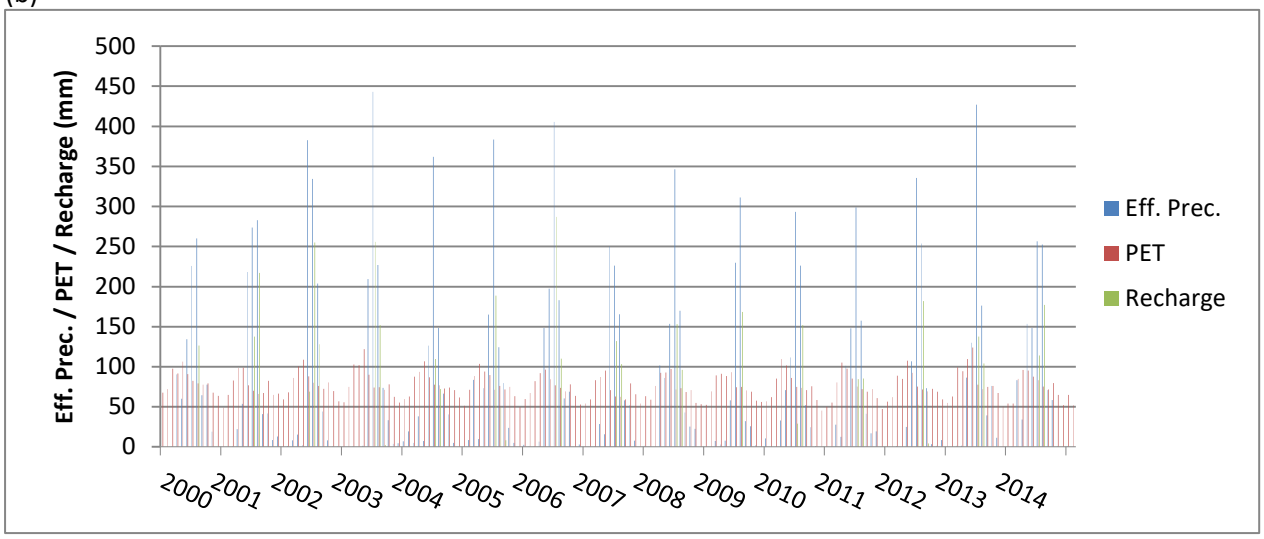

Fig. 4.23: (a) The estimated recharge and AET corresponding to the determined PAW. (d) The assessed recharge, effective precipitation and potential evapotranspiration during 2000 -2014 for a PAW-value of 250 mm.

4.8.4. Water table fluctuation method

Table 4.18 represents the different location, the name of the surrounding geological formation, the water-table rise and the corresponding recharge. The recharge estimations derived from the WTF-method varies from 105,19 mm/year up to 977,74 mm/year (Table 4.18). The specific yield for the lacustrine-alluvial deposits is 3% of which the subsurface is dominated by silty clay. The Termaber Basalts have an average specific yield of 8,3 %. The average recharge is 369,68 mm/year. The calculated recharge is lower for the wells located in the lacustrine-alluvial deposits compared with wells in the Termaber Basalts (Table 4.18).

W-Id	Geological formation	DH (m)	Sy (%)	Recharge (mm/year)
GUM-01	LA	3,85	3	115,5
GUM-02	T	3,1	8,3	257,3
GUM-03	T	11,78	8,3	977,74
GUM-04	T	6,17	8,3	512,11
GUM-05	T	3,69	8,3	306,27
GUM-06	T	3,09	8,3	256,47
GUM-07	T	9,99	8,3	829,17
GUM-08	T	3,86	8,3	320,38
GUM-09	LA	4,74	3	142,2
Diver 1	T	2,94	8,3	244,02
Diver 2	LA	3,51	3	105,19

Table 4.18: The estimated recharge for each specific location, together with the water table rise and the name of the geological formation. LA refers to Lacustrine-Alluvial deposits. T indicates the Termaber Basalts.

4.9. Hydrochemistry

Figure 4.24a shows the different samples sites. The concentrations of the water samples are represented in the appendix (Table 7.5-7.7). The number behind the name of the spring or well refers to the date at which the sample was taken. GIW refer to Gumera Inventorized Well.

4.9.1. Temperature, Total dissolved oxygen (TDS), Electrical Conductivity (EC) and pH

In situ temperature measurements vary from 18,5 °C in the highland, 21°C in the central part of the catchment and 24°C for the lowlands. The pH from the well samples ranges from 5,11-7,2 with an average of 6,1. The spring samples vary between 5,27 and 6,72 with a similar average of 6,1. All the samples have a pH lower than 8,2. No CO_3^{2-} -measurements are performed because all the CO_3^{2-} is transformed to HCO_3^-. The measured TDS in well samples fluctuate between 32,6 mg/l and 685 mg/l having an average value of 188,5 mg/l whereas the minimum and maximum value in the spring samples is 30 mg/l, respectively 205,5 mg/l with an average value of 105,7 mg/l. The relationship between the EC and TDS is linear (Fig. 4.24b). The maximum TDS value of the well samples is much higher compared with the other TDS values (Fig. 4.24b). Excluding this value results in a lower average TDS value of 161.5 mg/l but is still higher compared with the springs (105.7 mg/l). TDS increases with lower elevations (Fig. 4.24c).

(a)

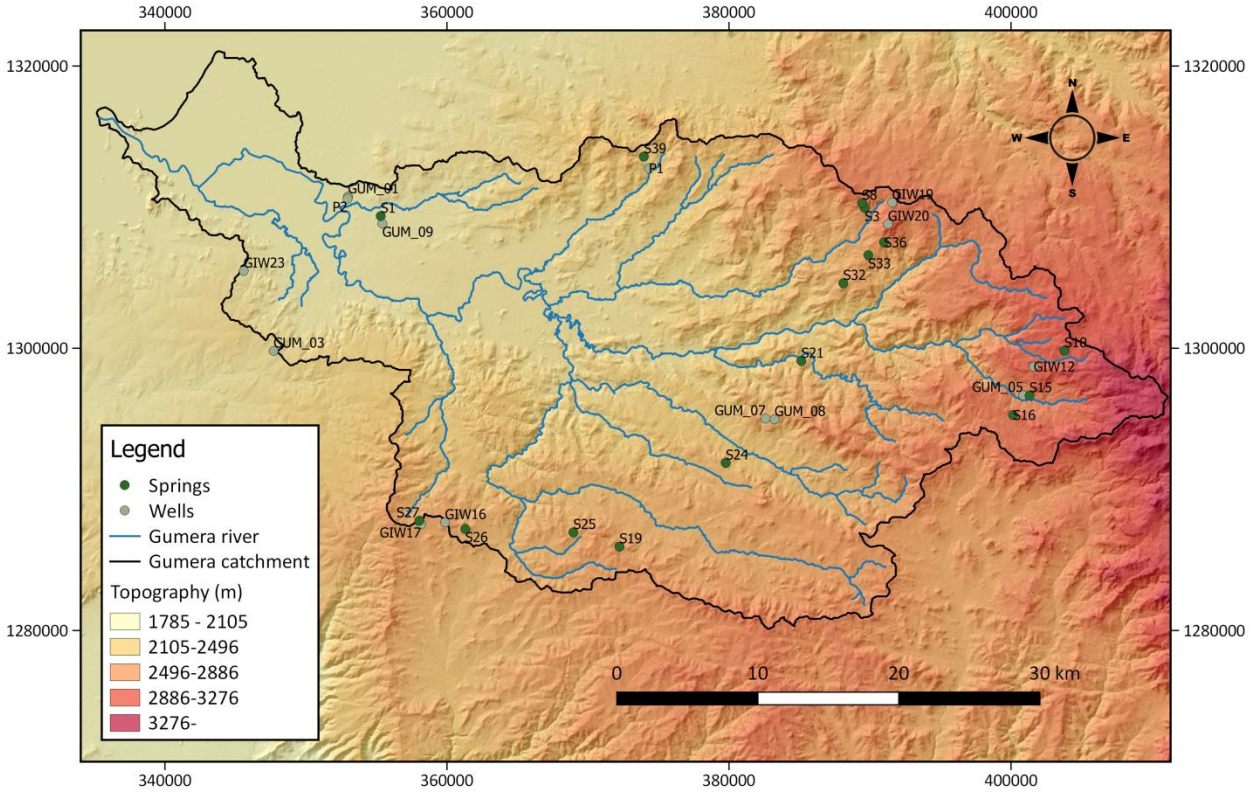

(b)

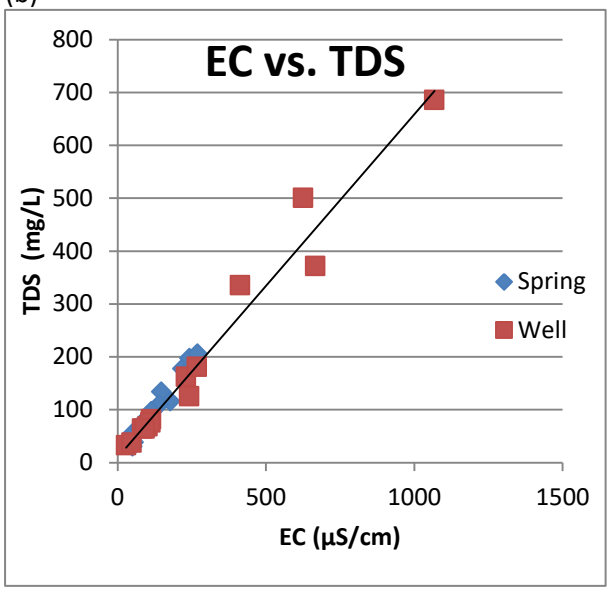

(c)

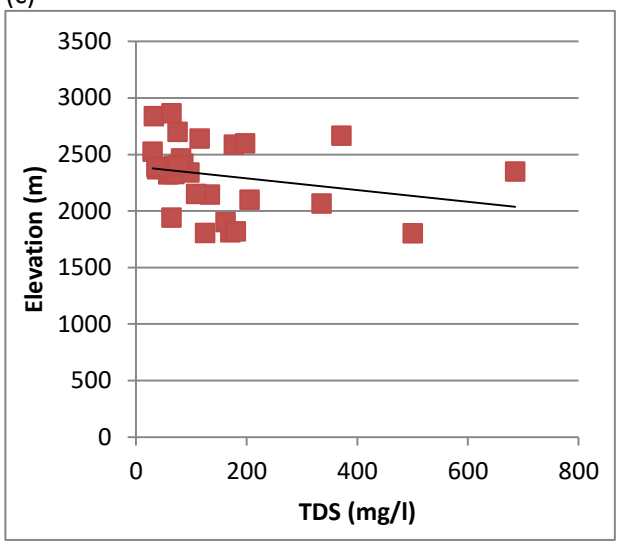

Fig. 4.24: (a) shows the different sample sites. (b) There is a linear relationship between TDS and EC. (c) TDS increases at lower elevation.

4.9.2. Major cation and anion concentrations

For the Piper diagram, the samples are divided in several groups based on their location in the catchment. The highland group incorporates S18, S15, S16, GIW12 and GUM-05. The northern part is the area around Debre Tabor and represents GIW19, GIW20, S8, S36, S33, P1, S39 and S32. The central part of the catchment includes GUM-07, GUM-08 and S21 and S24. The southern part of the catchment incorporates S19, S25, S26, GIW16, S27 and GIW17. The lowlands represent GUM-03, GIW23, P2, GUM-01, S1 and GUM-09. The triangle symbols represent the well samples, the circles show the spring samples.

The results from the Schoeller variant and the Piper diagram show a clustered distribution for the spring samples while the results from the well samples are more scattered (Fig. 4.25 and Fig. 4.26). Figure 4.26b suggests a systematic evolution of the recharge water through the soil and bedrock. Some wells indicate higher chloride concentration compared to the others (Fig. 4.26a). The dominant water type is the calcium-magnesium-bicarbonate type (Ca-Mg-HCO_3.). S1, S3, S39 and S8 have a higher Mg^{2+}-composition compared to the other spring sample (Fig. 4.26b). In general higher Mg^{2+}-concentrations are characterizing the lowlands (Fig. 4.25). Two samples are given the same sample name for two different springs (S10 and S36). To distinguish them, spring 36 is resampled. The hope was that differences in composition could establish which first sample (with both the name GUM-16) corresponds to S36. (Table 7.5. indicated by the dark frame). It seems this is the case for sample taken on 19/08/2016 although this is not completely clear.

Cross plots of HCO_3^- vs. Ca^{2+}, HCO_3^- vs. Mg^{2+}, HCO_3^- vs. Na^+, HCO_3^- vs. K^+ , Br^- vs. Cl^- and pH vs. HCO_3^- for the spring, well and rainfall samples are represented in figure 4.27. The figures 4.27a,b confirm the systematic evolution of the recharge water through the soil and bedrock as observed in figure 4.26b. The plot of HCO_3^- vs. Na^+ indicates a comparable evolution except for some well samples (Fig. 4.27c). This identical phenomenon is observed for the HCO_3^- vs. K^+ plot (Fig. 4.27d). HCO_3^- vs. Ca^{2+}, HCO_3^- vs. Mg^{2+} and HCO_3^- vs. Na^+ indicate a linear trend for the well and spring samples. The linear trend has a larger distribution for the well samples in the Ca^{2+} -plot. The pH increases with increasing HCO_3^-. The precipitation is slightly acidic (Fig. 4.27f). The Br^- vs. Cl^- -plot indicates higher values for the well samples, the springs are clustered while the well samples follow a linear trend (Fig. 4.27e).

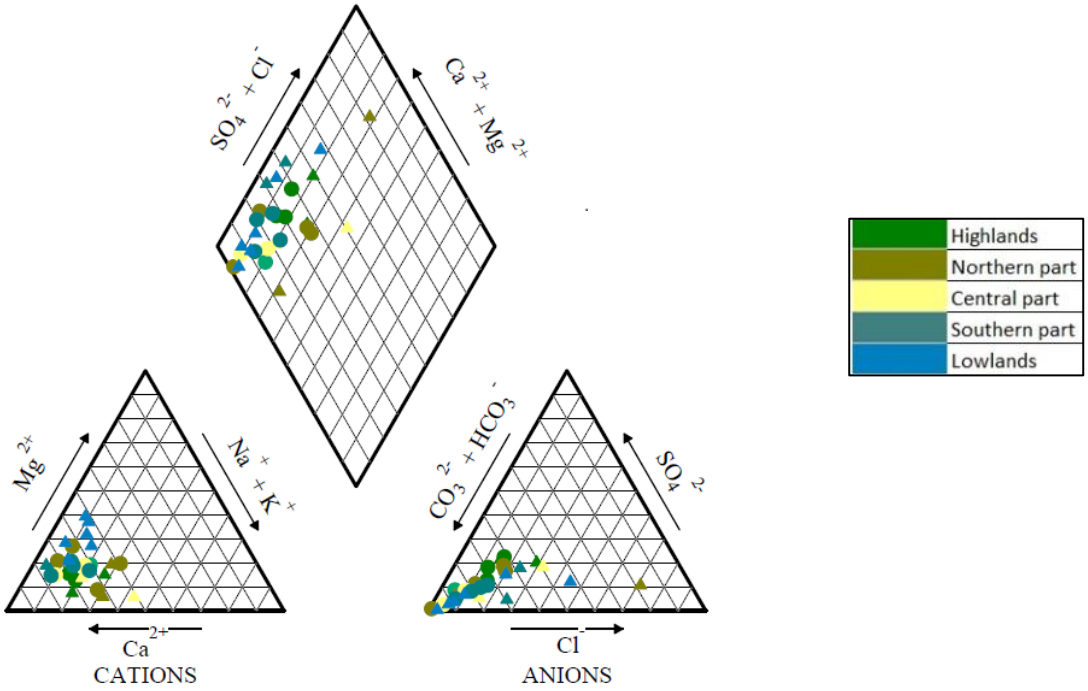

Fig.4.25: Piper diagram shows the distribution of the samples in the catchment. The triangle symbols are representing the well samples, the circles the springs.

(a)

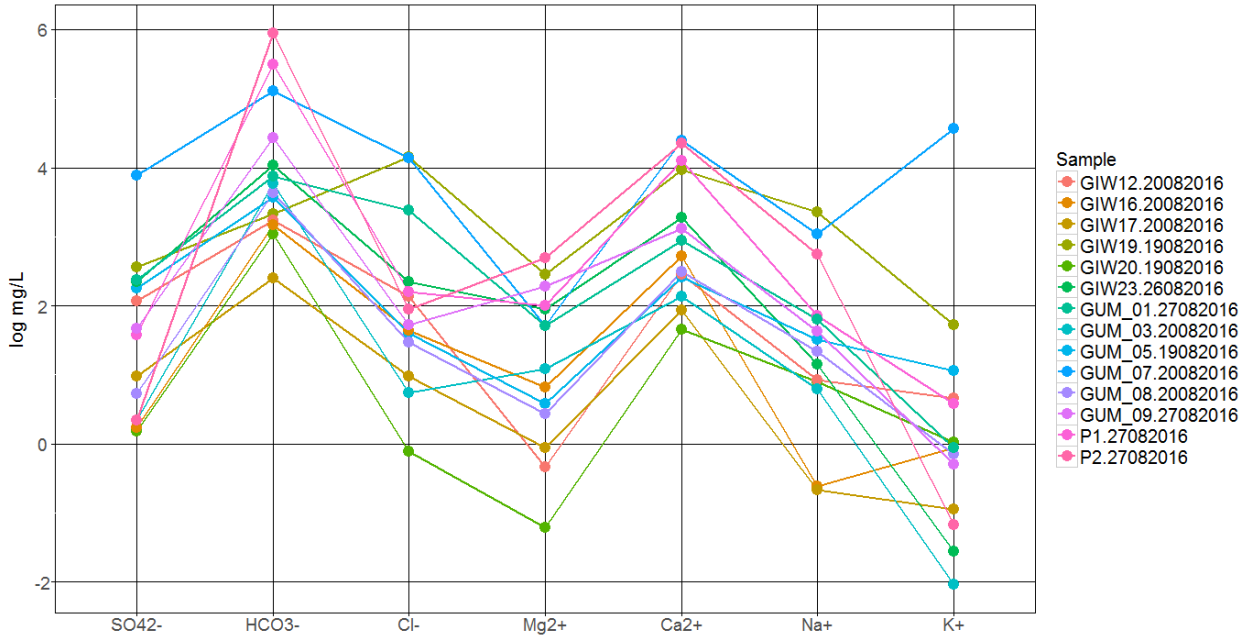

(b)

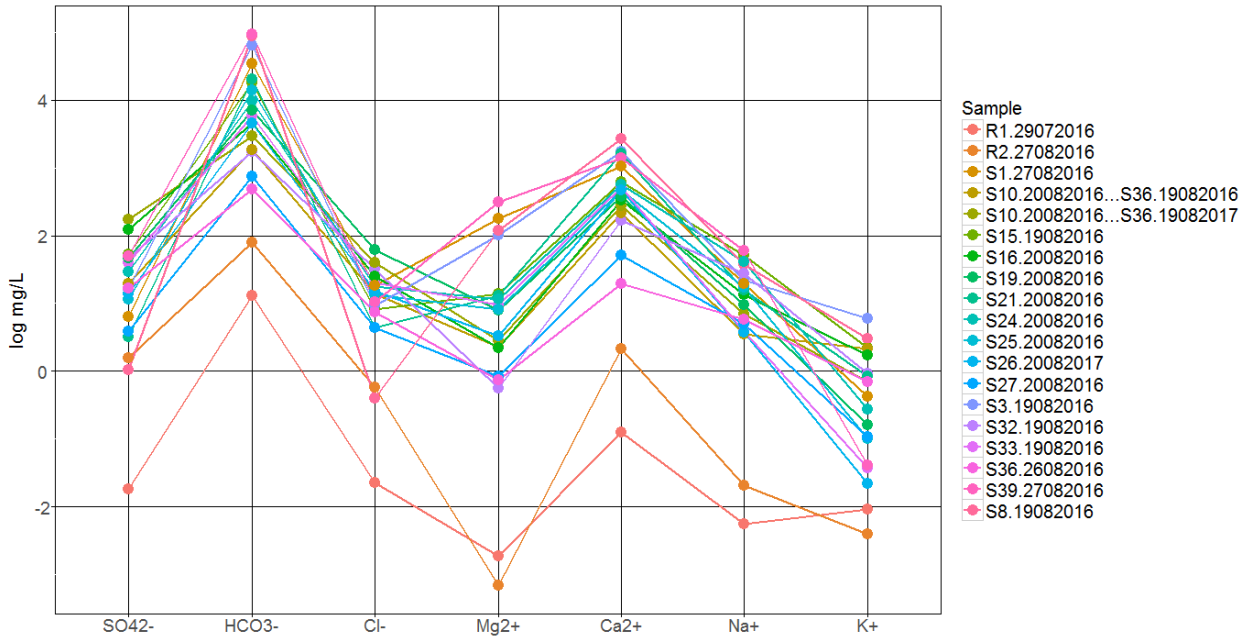

Fig. 4.26: The diagram differs from the Schoeller diagram representing the ion concentrations in mg/l on a logarithmic scale. (a) represents the well samples. (b) shows the spring samples.

(a)

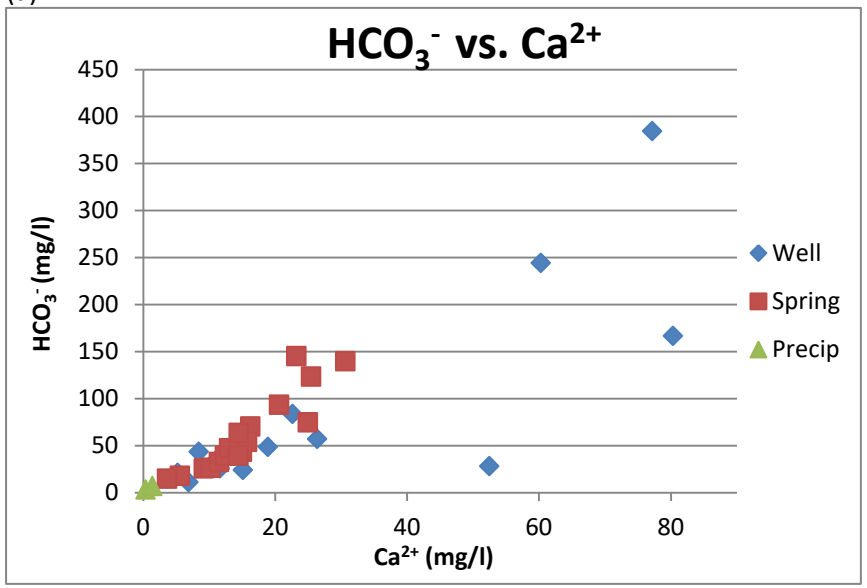
HCO3- vs. Ca2+
HCO3- (mg/l)
Ca2+ (mg/l)
0
50
100
150
200
250
300
350
400
450
0
20
40
60
80
Well
Spring
Precip

(b)

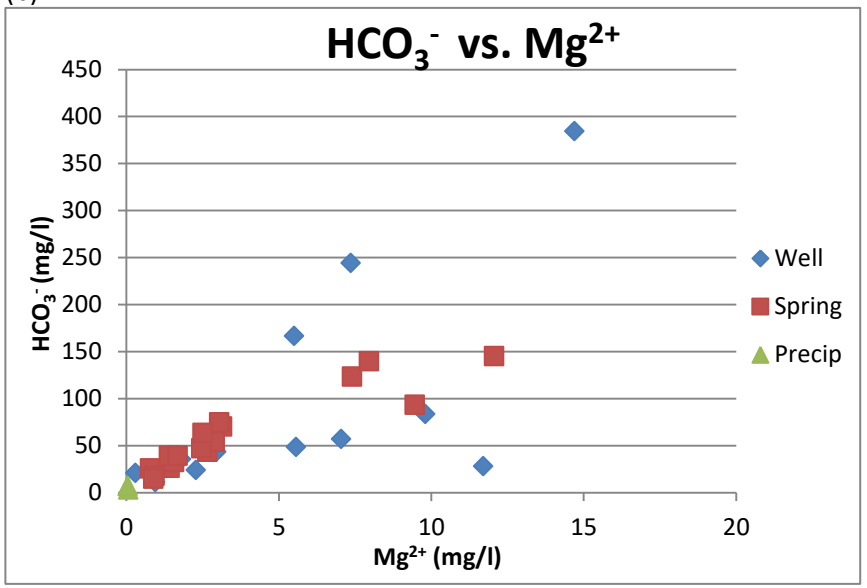
HCO3- vs. Mg2+
HCO3- (mg/l)
Mg2+ (mg/l)
0
50
100
150
200
250
300
350
400
450
0
5
10
15
20
Well
Spring
Precip

(c)

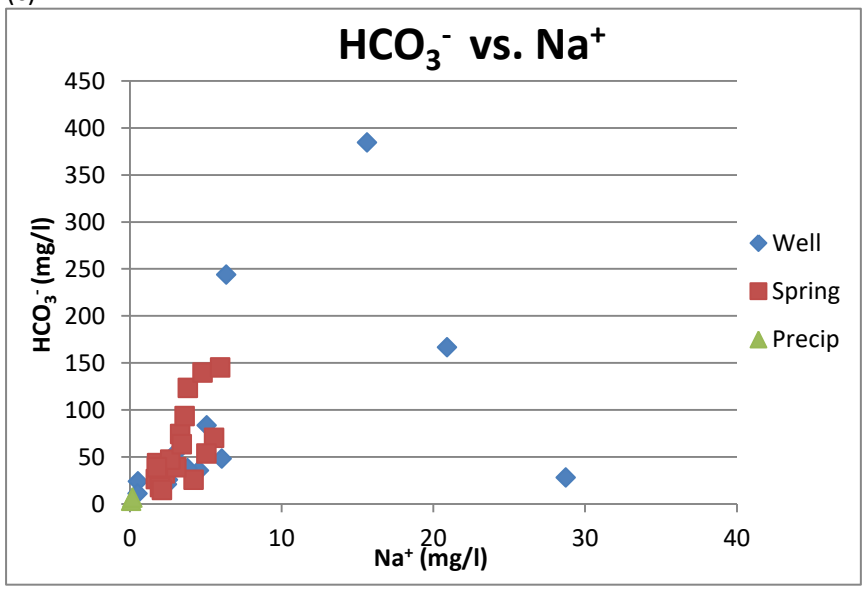
HCO3- vs. Na+
HCO3- (mg/l)
Na+ (mg/l)
0
50
100
150
200
250
300
350
400
450
0
10
20
30
40
Well
Spring
Precip

(d)

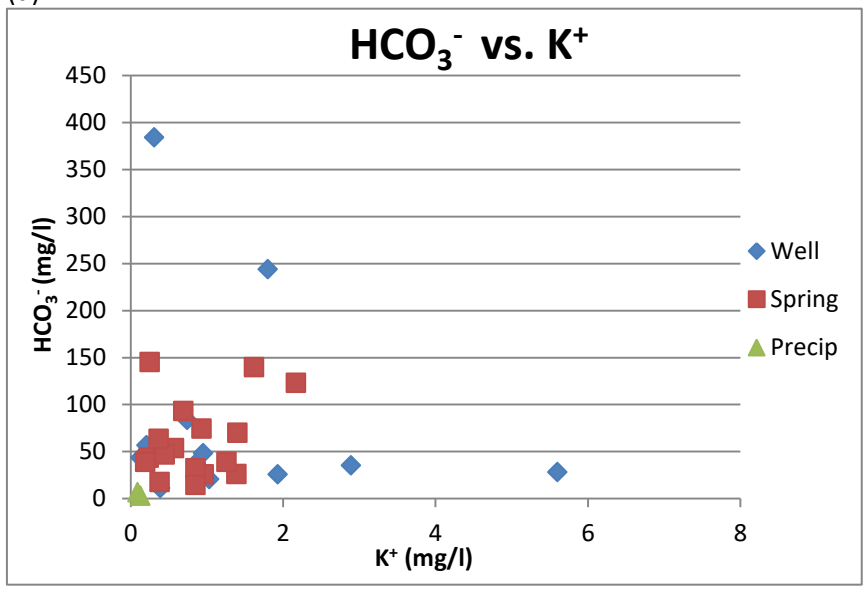
HCO3- vs. K+
HCO3- (mg/l)
K+ (mg/l)
0
50
100
150
200
250
300
350
400
450
0
2
4
6
8
Well
Spring
Precip

(e)

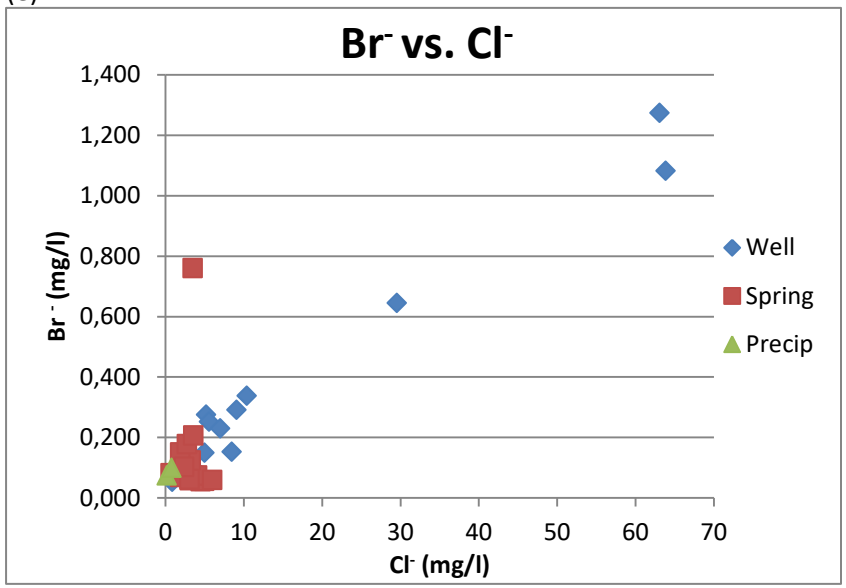

(f)

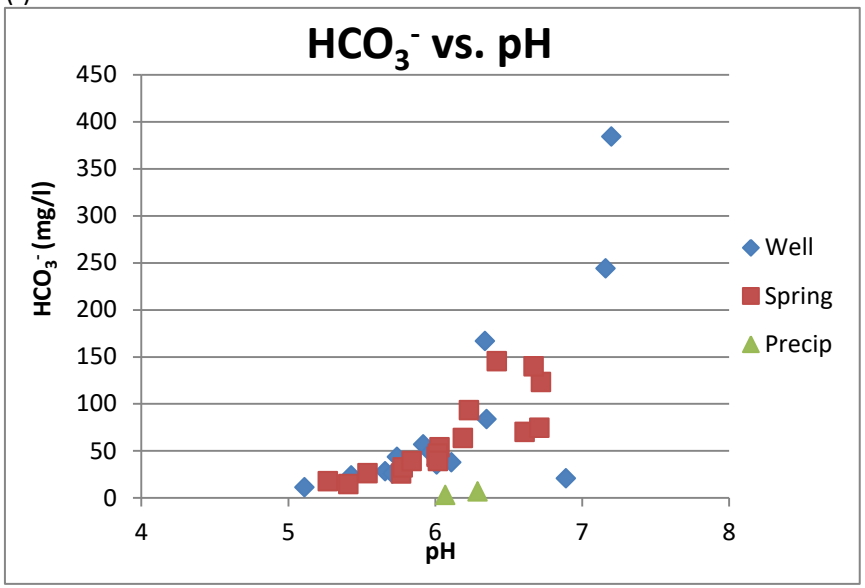

Fig. 4.27: (a) – (e) Cross plots of the cation concentration of the spring, well and rainfall samples. (f) shows the evolution of the HCO_3^- vs. pH.

4.9.3. Water quality evaluation based on the chemical composition

Microbial contamination causes the majority of water-related health problems. Nevertheless, deviations in the chemical composition of water can contribute to poor water qualities (WHO, 2006). In this section, the contribution of the chemical composition to the water quality is verified. Water used for domestic purposes should ideally have no visible color or smell (WHO, 2006). Organic matter and the chemical composition of water affect the color, taste and odor. Health problems can occur after a prolonged time of exposure. Table 4.19 shows the thresholds as indicated by the World Health Organization. Only for the last parameter (PO_4^{3-}) the given threshold is a manual reference value based on the rainfall concentration to estimate the impact of agricultural activities.

Constituents	Threshold WHO (mg/l)
Na^+	200
Ca^{2+}	200
Mg^{2+}	100
Fe^{2+}/Fe^{3+}	0,3
Mn^{2+}	0,1
NH^{4+}	35
Cl^-	250
SO_4^{2-}	250
NO_3^-	50
NO_2^-	3
F^-	1,5
PO_4^{3-}	0,20

Table 4.19: Indication of the taste thresholds defined by the WHO except for PO_4^{3-}.

The concentrations of Na^+, Ca^{2+}, Mg^{2+}, Mg^{2+}, Cl^-, SO_4^{2-}, NO_2^- and F^- in the well and spring samples are always lower than the threshold. Table 4.20 shows the different springs and wells having a concentration larger than the threshold for Fe^{3+}, Mn^{2+}, NO_3^- and PO_4^{3-}.

Name	Fe2+/Fe3+	Mn2+	NO3-	PO43-
Threshold	0,3	0,1	50	0,2
GUM-05	0,63	-	-	-
GIW12	0,41	-	-	0,5088
S3	0,34	-	-	0,5874
S33	0,33	-	-	-
S10	0,73	-	-	-
S16	0,44	-	-	-
S24	0,37	-	-	-
S25	0,66	-	-	-
GUM-07	-	0,128	202,32	0,9006
P1	-	0,367	-	0,29
GUM-01	-	0,219	-	-
GIW19	-	-	168,065	-
S32	-	-	-	0,399
S21	-	-	-	0,464
S15	-	-	-	0,2865
S8	-	-	-	0,2184

Table 4.20: Representation of the wells and springs deviating from the threshold.

5. Discussion

5.1. Topography

Gumera catchment is visualized with Google Earth based on SRTM and Landsat images. The DEM is based on SRTM data. The Landsat images have a spatial resolution of 15 m. A resolution of 30 m is characterizing SRTM images. Similar satellite images explain the small elevation deviations between Google Earth and the DEM. On the field the Garmin GPS displays the spatial resolution of the waypoint which was less than 5 m. Mukul et al. (2016) assessed the vertical accuracy of the SRTM using Ground Control Points concluding a larger error with higher elevations. The calculated average error was 187 m. Removing the outliers resulted in an absolute vertical accuracy of 10,3 m. The GPS data have a higher accuracy compared with the SRTM and Google Earth.

5.2. Meteorological data

The variation in annual rainfall between Debre Tabor and Bahir Dar is explained due to the large topographic difference. Debra Tabor has an elevation of about 2678 m, Bahir Dar 1795 m. Bookhagen and Burbank (2006) investigated the relationship between the topography and the rainfall variations concluding higher precipitation at increased elevation. According to Jemberie et al. (2016), the precipitation varies with latitude and longitude in Tana Basin. Lower rainfall generally occurs in the northern part whereas the highest rainfall is observed in the southern part of the basin. Due to the larger distance and topographic difference between Infranz and Gumera there is no correlation. The little relation between Ribb and Gumera meteorological stations is probably due to the topographic difference.

5.3. Hydrostratigraphical model

Diffuse recharge in the Lacustrine-Alluvial Aquifer can be limited due to the development of thick fine sediments at the subsurface. The groundwater potential will probably decrease closer to the lake due to the increasing amount of fine-grained lacustrine sediments. The groundwater occurrences in the Lacustrine-Alluvial Aquifer will likely increase near contact areas between the scoriaceous Quaternary basalts or the weathered and fractured Tertiary basalt. Groundwater will preferably flow in the fluvial layers of this aquifer referring to the waters strikes observed near the fluvial layers in the Woreta Borehole during drilling.

The occurrence of the groundwater flow in the Termaber Basalt Aquifer depends on the type of surrounding volcanic material. Fractures and weathered rock enhance the aquifer properties. Groundwater prefers to flow through these types of rock while massive basalts and tuff layers will operate as semi-pervious layer resulting in a large variation of groundwater condition in this multi-layered aquifer.

According to Nigate et al. (2017) the groundwater storage is not high near Mount Guna due to the occurrence of steep slopes and the poor pervious nature of the surrounding rocks. Steep slopes intensify runoff and decrease the groundwater storage resulting in very low productive aquifers. They confirm the presence of two different flow systems. A low yield is characterizing the groundwater flow at shallow depth (Nigate et al., 2017).

5.4. Monitoring of groundwater hydraulic heads

The description of the monitoring wells is based on oral information and should be interpreted with caution e.g. depth wells. The large variation in groundwater level for GUM-03, GUM-04 and GUM-07 is probably due to their location relatively close to the hillside. They are located at the onset of a hill

receiving more lateral inflow of the hill side. GUM-09 is located in the lacustrine - alluvial deposits but close to the boundary with the scoriaceous Quaternary Basalts. The lateral inflow from the groundwater flow derived from the Quaternary basalts apparently causes the slightly higher groundwater rise in GUM-09 (Table 4.7). The large groundwater depth of GUM-08 and GUM-06 is due to their position on top of the Hill Top Aquifer (Fig. 4.5). The water table rarely reaches the top of the hill because groundwater prefers to leave the aquifer as spring discharge. The water table may vary during the different seasons.

According to SOGREAH (2012c), the thermal spring (S30) is developed from a fault scarp in the Quaternary basalts. The pH and temperature of the water are 9.5 and 39°C respectively. A borehole of 150 m is drilled but no more information is available.

Spring 1 (S1) is located in the Quaternary basalts but near the lacustrine-alluvial deposits (Fig. 4.3a). Assuming the information about the Bebeks as correct, many springs occur near the boundary between the two aquifers. Due to the difference in permeability between the lacustrine - alluvial deposits (low permeability) and the Quaternary Basalts (medium permeability), the groundwater flow deriving from the Quaternary Basalts Aquifer will deflect to the surface and create many springs at the boundary. It would be interesting to perform discharge estimations of the inventorized springs to investigate the relationship between the topography and the groundwater system.

In the diver data, it is observed that the groundwater reaches a constant level after a certain time period. An equilibrium is reached between the inflow of water from other aquifers and the discharge of the respective aquifer.

5.5. Surface water discharge measurements

Table 5.1 compares the calculated runoff coefficients with the values derived from Jemberie et al. (2016). The authors determined the seasonal runoff based on the HEC-HMS hydrological model using the streamflow data. The seasonal values differ largely for winter and autumn. According to them, the runoff values are generally high for Gumera catchment indicating a high susceptibility to erosion and sedimentation. The runoff coefficient is higher for September although July and August receive the most precipitation. The end of the rainy season explains this higher value. The soil moisture storage is saturated, water tables have risen, many intermittent springs and streams appear and no further infiltration can occur. This result in more runoff during September compared with the receiving precipitation.

Season	Mean calculated runoff coeff.	Runoff coeff. estimated by Jemberie et al. 2016
Winter	0,10	0,30
Spring	0,06	0,09
Summer	0,50	0,55
Autumn	0,37	0,57

Table 5.1: The calculated runoff coefficients compared with the coefficient values obtained from Jemberie et al. 2016. The calculated coefficients are lower.

According to Awulachew et al. (2005), a small irrigation project was under construction in 2002 covering an area of 62 ha for which the river was used as potential water source. The irrigated area is increased to more than 300 ha in 2009. The irrigation areas are all located along Gumera River close the bridge where the river is gauged (Derib, 2015). It can be expected that this lead to a decrease of the minimum discharge after 2002 during winter and spring season, which is not the case (Fig. 4.13a). A change in land use probably explains the increasing trend in the minimum discharge plot of January - May. As already

mentioned earlier, the cultivated land and urban areas expanded with 21.99% (Wubie et al., 2016). Forest land, shrubland and grassland are replaced by agricultural activities. The cultivated crops apparently perform less evapotranspiration resulting in a higher baseflow. An increase in runoff can explain the minimum discharge rise for September in 2003, 2005, 2007, 2012 and 2014.

5.6. Hydraulic parameters

5.6.1. Specific yield

According to Şen (2014), the specific yield is not constant but changes as a function of the water table depth influenced by the physical characteristics of the soil. This is also observed in the tested aquifer. The specific yield, determined at a larger depth, has a larger value (9,2%) compared with the shallower one (7,4%). The groundwater recessions varies exponentially with the time after the occurrence of a precipitation event. With increasing time, the recession tends to be slower. The same observation is recognized and confirmed in streamflow recessions (Zhu et al., 2010). Little recharge in the dry periods reaches the groundwater table.

Johnson (1967) determined the specific yield for unconfined aquifers in unconsolidated sedimentary formations (Table 5.2). For tuff material, a compilation of several studies has been presented, for which the specific yield varies between 3-10% (Johnson, 1967). The calculated specific yields approach the latter value. Comparing the calculated values with the reported specific yields for sedimentary deposits (Johnson, 1967) indicates that the calculated yield is comparable with the specific yield of sand clay, silt and fine sand (Table 5.2).

Material	Minimum	Average	Maximum
Clay	0	0,02	0,05
Sand clay	0,03	0,07	0,12
Silt	0,03	0,18	0,19
Fine sand	0,1	0,21	0,28
Medium sand	0,15	0,26	0,32
Coarse sand	0,2	0,27	0,35
Gravelly sand	0,2	0,25	0,35
Fine gravel	0,21	0,25	0,35
Medium gravel	0,13	0,23	0,26
Coarse gravel	0,12	0,22	0,26

Table 5.2: The specific yields determined by Johnson (1967).

5.6.2. Pumping test

Based on the two methods, the obtained hydraulic parameters are similar because they are calculated with the same method. Two other pumping tests have been performed in the catchment . The hydraulic conductivity determined in Leway, is 7,19 m/d (Kassahun, 2012b). The hydraulic conductivity in Lecha is 2,62 m/d (Kassahun, 2012a). No information about the geological characteristics of the wells is available for these tests. In general, the hydraulic conductivity varies with the geological characteristics throughout the catchment depending on the degree of weathering, density of the fractures and their corresponding width. Kruseman and de Ridder (1990) provide hydraulic conductivity values for different materials (Table 5.3). Large variations in hydraulic conductivities are characterizing volcanic, weathered and fractured rock. Insufficient available information and unevenly distributed boreholes makes it difficult to enable a quantitative evaluation of the aquifer system in Gumera catchment.

Materials	K (m/d)
Clay	10-8 -10-2
Fine sand	1 - 5
Medium sand	5-102
Coarse sand	20- 102
Gravel	102 -103
Sand and gravel mix	5-102
Clay, sand, gravel mixes (e.g. till)	10-3 - 10-1

Rocks	K (m/d)
Sandstone	10-3 -1
Carbonate rock	10-2- 1
Shale	10-7
Dense solid rock	10-5
Fractured or weathered rock	10-1 -302
Volcanic rock	10-1 - 103

Table 5.3: The different estimated hydraulic conductivities for different materials (Kruseman and de Ridder, 1990).

5.7. Groundwater flow

The piezometric map is based on a mathematical approach. The correlation between the groundwater depth and the distance to the closest valley is poor although this relationship is used to generate the map causing some deviations (Fig. 4.7b). The distance to the river was measured using a GIS tool. In the floodplain, only Gumera River occurs. Larger estimated depths are expected at the north- westernmost boundary of the Gumera-Ribb catchment close to Lake Tana. Table 5.4 verifies the piezometric surface of the created map with piezometric surface of the monitoring wells. The largest difference between the two compared values of each monitoring well occurs at the wells located on the hill top, GUM-06 and GUM-08 respectively. Kebede et al. (2005) confirm the convergence of groundwater towards Lake Tana.

The groundwater reservoir is a complex system with a large variation in groundwater flow due to the large lateral topographic variations and volcanic structures e.g. faults. Besides, it is difficult to estimate the groundwater flow path within the different aquifers due to the occurrence of faults and the lateral discontinuity of the fractured and weathered Termaber Basalts. In general the structure and distribution of the geological formation together with the topographic variations determine the occurrence and the availability of groundwater.

W-Id	Average GW depth (m)	Elevation DEM (m)	Piezometric surface (m)	Piezometric surface on map (m)
GUM-01	2,19	1798	1795,81	1797,35
GUM-02	1,70	1828	1826,30	1819,7
GUM-03	7,95	1940	1932,05	No data
GUM-04	4,13	2228	2223,87	2227,5
GUM-05	1,18	2609	2607,82	2607,83
GUM-06	13,73	2443	2429,27	2438,9
GUM-07	2,58	2347	2344,42	2345,31
GUM-08	9,30	2394	2384,70	2391,44
GUM-09	3,51	1820	1816,49	1817,8

Table 5.4: Comparison of the piezometric surfaces.

5.8. Groundwater recharge

The precipitation and potential evapotranspiration values used for the SMB-method may not be representative for the whole catchment. The values are based on data derived from a meteorological station located in Bahir Dar approximately, estimated from the lowlands, 40 km out of the catchment at

an elevation of 1795 m. The runoff coefficients are based on rainfall data from Debre Tabor. This city is situated at the northern boundary having an elevation of 2700 m. The annual rainfall is higher for Debre Taber compared with Bahir Dar, 1651 mm and 1459,5 mm respectively. The study area contains furthermore a large altitudinal range. There is in addition the uncertainty about the different rooting depths and the exact percentage of the respective land use types. In general, a recharge of 235 mm/year is assumed in the highlands. The central and western part of the catchment is characterized by a recharge of 320 mm/year.

A difference in flow path explains the large variation in recharge obtained from several well and spring samples using the Chloride Mass Balance (CMB). The groundwater flow in spring areas is shallower compared to the groundwater flow in wells. A larger residence time is probably characterizing the groundwater in wells resulting in higher chloride concentration causing smaller recharge estimations. The CMB-method cannot be applied to bromide concentration. The estimated recharge is not reliable and not even in the range of the estimations using the chloride-concentration. According to figure 4.20, the relationship between Br^- and Cl^--concentrations is not linearly. In a volcanic soil, an accumulation of bromide can occur due to repeated volcanic eruptions (Fiantis et al., 2010).

A recharge of 141,98 mm/year is estimated for the baseflow. Using table 4.16, a recharge of 141.98 mm/year coincides with a PAW of more than 500 mm. This means that the catchment should be characterized by crops and vegetation having an average rooting depth of 4 m - 4.5 m. Referring to the literature as described in section 4.8.3., this is not possible. The baseflow is probably an underestimation of the recharge.

The recharge estimations based on the water-table fluctuation method indicate a lower recharge in the floodplain due to the dominating lacustrine deposits at the subsurface. The locations in the Termaber Basalt suggest a recharge between 250-320 mm/year except for GUM-03, GUM-04 and GUM-07 having a recharge of respectively 977,74, 512,11 and 829,17 mm/year. GUM-04 and GUM-07 are located at the onset of a hill receiving more lateral inflow of the hill side. GUM-07 is located close to a plateau connecting two hills with each other. This plateau contributes to an accumulation of groundwater explaining the large difference in recharge between the two locations of GUM-07 and GUM-04. (Fig. 4.21df). Two little hills are located near GUM-03. The two groundwater flow paths probably join each other around the area of GUM-03 resulting in an increase of the water-table (Fig. 4.21e). Coincidence or not, but GUM-03 has an estimated recharge almost double of GUM-04 which is located at the onset of one hill. The SMB –method only considers diffuse recharge from precipitation while the WTF – method takes into account other causes than local infiltration of precipitation.

The obtained recharge estimations are compared with the recharge estimated by Abiy et al. (2016). These authors' estimation is based on baseflow separation using a digital filter method. According to them, the groundwater contribution to Lake Tana is 414 mm/year based on data from 1997-2005. This value is significantly higher compared with the results acquired in this study.

5.9. Hydrochemistry

5.9.1. Temperature, Total dissolved oxygen (TDS), Electrical Conductivity (EC) and pH

The similar average pH for the wells and springs is 6.1. Water with a pH ranging from 6.5 to 9.5 is preferable for drinking purposes but a lower pH doesn't cause health problems (WHO, 2006). Most of the samples are acidic having a pH lower than 6.5.

The EC is an indirect factor for the dissolved solids and contributes to determine the quality of the water (Şen, 2014). The higher the dissolved constituents, the higher is the EC. This appears in a linear

relationship between the TDS and EC (Fig. 4.24b). EC levels smaller than 750 µS/cm refer to good water qualities (Şen, 2014).

The TDS in groundwater depends on the different geological formations and anthropogenic influences at the surface (Şen, 2014). TDS concentrations lower than 1000 mg/l are obtained from freshwater resource (WHO, 2006). TDS values smaller than 600 mg/l are assumed to have a good palatability of water (WHO, 2006). All the water samples in Gumera catchment derive from freshwater resources. The higher average TDS value for the wells is related with a higher degree of weathering. The TDS slightly increases with decreasing elevation (Fig. 4.24c). Precipitation that infiltrates in the highland and flows towards lower elevations interacts with the surrounding geological formations resulting in higher dissolved constituents in lower areas. The groundwater has more time to interact with the surrounding environment. Besides, the evapotranspiration is higher in the lowlands due to the occurrence of higher temperatures appearing higher concentration. Samples with TDS values lower than 200 mg/l has been subjected to little interaction with the environment suggesting a shorter flow path in the groundwater reservoir and a small interaction with the surrounding rocks (Nigate et al., in press).

5.9.2. Major cation and anion concentrations

Some wells contain high chloride concentration (GUM-07, GIW 19, GUM-01). GIW 19 and GUM-07 are located in the centre of Debre Tabor and Mahideramariyam, respectively. Both areas are highly populated, although Mahideramariyam has just recently become easily accessible and is not yet urbanized. Cl^- is also an indicator for pollution. The higher chloride concentration in both wells is due to pollution of groundwater as confirmed by the higher observed NO_3^- concentrations (Table 4.20). GUM-01 is situated in the floodplain. Around April the well runs dry during the evening but recovers in the night. There is an accumulation of chloride due to evapotranspiration.

The clustered spring samples in the Br^- vs. Cl^- and the Piper diagram are probably at an early stage of geochemical evolution suggesting a recent discharge and different flow paths between well and spring samples. The flow path of springs is probably shallower compared with the flows occurring at well depth. The larger variations in concentration of the well samples are probably due to a longer path way. The recharge water has more time to react with the surrounding geology. Although this is in contrast with the observed TDS values, whereby a TDS level < 200 mg/l refers to little rock interaction and a shorter flow path (Nigate et al., in press). The samples located in the lowlands have a higher concentration in Mg^{2+} compared to the other samples probably indicating less dilution by local recharge and a higher rock-groundwater interaction. This also explains the higher Mg^{2+}-concentration observed in S1.

S3 and S8 are both located near Debre Tabor. The spring water in S3 comes to the surface under pressure, probably along a vesicular tube as observed in the field, suggesting a deeper pathway and intensified weathering. Little dikes are collecting the water in spring 8. In the field there was a discussion about the classification of S39 to classify it as a spring or as a well. The rural people name it a spring but no free outflow is observed and the water level only decreases with 1 meter in winter season. Both S39 and S8 have probably a higher Mg-concentration due to in-situ weathering.

5.9.3. Hydrochemistry evolution process

Oxygen and carbon dioxide are the most important dissolved gases present in groundwater. CO_2 enhances the solubility of minerals and is stored in the atmosphere and in the soil after oxidation of organic matter (Fetter, 2000). CO_2 will dissolve in water and produces dissolved CO_2, which reacts with water resulting in the HCO_3^--ion.

$$CO_2 + H_2O \leftrightarrow H^+ + HCO_3^-$$

Due to the presence of CO_2 in the atmosphere, the precipitation is slightly acidic. Dissolved CO_2 enhances the dissolution of cations along its flow path (Şen, 2014). The HCO_3^- - ion is the dominant anion type in Gumera catchment as indicated in the Piper diagram (Fig. 4.25). Previous studies in Infranz and Gilgel-Abbay catchment, south-southwest of Tana Basin indicate mainly the dissolution and hydrolysis of silicate minerals as the controlling factor for the hydrochemical evolution of groundwater (Nigate et al., 2016; Fenta et al., in press). Volcanic rocks are dominating the study area whereby the same processes are assumed to occur in Gumera catchment. Hydrolysis is a chemical weathering process between water and silicate minerals. New minerals are formed due to the removal of the dominant cation in the current mineral. The following equations are considered based on the assumption that olivine and feldspar belong to the dominant minerals occurring in the volcanic formations (Fenta et al., 2016).

$$\text{Orthoclase: } 2KAlSi_3O_8 + 2H^+ + 9H_2O \leftrightarrow Al_2Si_2O_5(OH)_4 + 4H_4SiO_4 + 2K^+$$

$$\text{Albite: } 2NaAlSi_3O_8 + 2H^+ + 9H_2O \leftrightarrow Al_2Si_2O_5(OH)_4 + 4H_4SiO_4 + 2Na^+$$

$$\text{Anorthite: } CaAl_2Si_2O_8 + 2H^+ + H_2O \leftrightarrow Al_2Si_2O_5(OH)_4 + Ca^{2+}$$

$$\text{Forsterite: } 5Mg_2SiO_4 + 8H^+ + 2H_2O \leftrightarrow Mg_6(OH)_8Si_4O_{10} + H_4SiO_4 + 4Mg^{2+}.$$

Hydrolysis of anorthite is probably responsible for the increase of Ca^{2+}-concentrations (Fig. 4.27a). The rise in Mg^{2+} is likely due to forsterite weathering (Fig. 4.27b). Some albite weathering and little orthoclase weathering occurs (Fig. 4.27cd) although the Piper diagram indicates sometimes similar concentrations of Mg^{2+}, and Na^+ (Fig. 4.25). According to Şen (2014), Na^+ ions are easily soluble and remain in solution. On the other hand, K^+ occurs generally in rocks having a large resistance against weathering. In addition, K^+ easily takes part in precipitation reactions. Therefore, Na^+-concentration generally occurs in higher amounts in groundwater compared to K^+. According to Nigate et al. (in press), the increasing HCO_3^--concentrations are related with CO_2-dissolution together with the open-system dissolution of silicates. The SO_4^{2-} can originate as weathering products from some magmatic rocks (Şen, 2014). The Cl^- is assumed as conservative ion that only derives from precipitation except for the specific cases where it is added due to pollution. An increase in Cl^--concentrations is related with evapotranspiration. In general, the chemistry of groundwater varies spatially and temporally. The spatial variations cause an impact on different water utilization programs such as domestic water supply, irrigation, industry,.. (Ludi et al., 2013)

5.9.4. Water quality evaluation based on the chemical composition

As already mentioned in section 5.3.1, TDS values smaller than 600 mg/l enhance the palatability of water. Farmland is surrounding most of the wells and springs deviating from the threshold (Table 4.19). A high influence of agricultural activity is suggested related with the use of fertilizers and pesticides decreasing the water quality. In densely populated areas, domestic pollution occurs indicated by higher NO_3^- and Cl^- -concentrations. Higher Fe^{2+} and Mn^{2+} -concentrations suggest reduced conditions of the groundwater. Spring 10 and Spring 16 show a trouble color based on field observations. The water of GUM-07 is sold in bottles of 10 l, although it is one of the most polluted areas. This will affect the health of the consumers in the future.

6. Conclusion

The groundwater reservoir of Gumera catchment is a complex system with a large variation in groundwater flow due to lateral topographic variations and volcanic structures. In general, two different flow systems have been distinguished. The shallow groundwater flow is subjected to a shorter travel distance. It appears to the surface as springs or contributes to river valleys. Large topographic variations result in many local groundwater systems. The deeper groundwater flow indicates a regional extent of the groundwater system flowing in the catchment from east to northwest following the general topography. The groundwater converges in the central, lower parts of the catchment and flow further towards Lake Tana.

In line with the geology and geomorphology, the catchment contains at least five different aquifer types with a corresponding recharge/discharge mechanism. For each aquifer type the permeability, the porosity type, the extent of the flow system and the continuity of the aquifers are determined. The dominant aquifer is the Termaber Basalt Aquifer that consists of weathered/fractured rocks alternating with tuff layers and massive basalts of which the latter operate as semi-pervious. The presence of fractured and weathered rocks enhances the aquifer properties. The Quaternary Basalt Aquifer occurs in the central lower part of the catchment consisting of scoriaceous and fractured basalts. The Lacustrine-Alluvial Aquifer near Lake Tana provides an additional potential aquifer due to the occurrence of sand and sandy gravel in fine sediments. Fine sediments characterize the Hill Top Aquifer resulting in a low to medium permeability. The River Valley Aquifer consists of medium to coarse sediments having a medium to high permeability. The dominant recharge type for the whole catchment is diffuse recharge from precipitation. The mountain front recharge appears in the River Valley Aquifers. Discharge mainly occurs as spring, runoff, evapotranspiration and percolation to other aquifers.

It is difficult to estimate the groundwater flow path within the different aquifers due to the occurrence of faults and the lateral discontinuity of the fractured and weathered basalts. In general the structure and distribution of the geological formation together with the topographic variations determine the occurrence and the availability of groundwater.

A spatial variability in recharge is characterizing the catchment. The amount of recharge varies mainly with the topography, local geology, vegetation type, soil texture and the amount of rainfall as indicated with the SMB-method and WTF-method. The floodplain receives less recharge due to the occurrence of a thick package of silty clay. The estimated recharge is suggested between 250 and 320 mm/year, based on the WTF-method for the wells located in the Termaber Basalts. Some wells indicate a higher recharge but this is due to specific circumstances. The recharge determined with the base flow separation method is 141,98 mm/year. The recharge estimated with the SMB-method is assumed to be 235 mm/year for the highlands and 320 mm/year for the central and western part of the catchment. This was based on yearly precipitation, the dominant vegetation and soil texture. The CMB-method indicates a large variation in recharge between the springs and the wells assuming a different flow path and the influence of anthropogenic activity.

The hydrochemistry of the groundwater depends on its location in the catchment. The dominant water type is the Ca-Mg-HCO_3-type. The dissolution and hydrolysis of silicate minerals are the controlling factors for the hydrochemical evolution of the groundwater. In general, higher Mg^{2+}-concentrations occur in the lowlands indicating less dilution by local recharge and a higher rock-groundwater interaction. Spring samples indicate an early stage of geochemical evolution suggesting a recent recharge and different flow paths between well and spring samples. Precipitation that infiltrates in the highland and flows towards lower elevations interacts with the surrounding geological formations. This results in higher dissolved constituents in lower areas.

In general, the water resources in the study area are suitable for domestic purposes. Although, densely populated areas indicates higher NO_3^- and Cl^- -concentrations due to domestic pollution affecting the health of the consumers in the future. The influence of agricultural activity is observed in some water samples related with the use of fertilizers and pesticides decreasing the water quality. Controlling mechanisms should be performed in the near future to sustain the quality of the water and identify areas, sensitive to anthropogenic pollution.

The specific yield is determined in the upper part of the catchment, in dominantly tuff deposits, and has an average value of 8,3 %. The hydraulic conductivity is 1,61 m/d for the same environment. Large variations in hydraulic conductivity are characterizing volcanic, weathered and fractured rocks. A quantitative evaluation of the aquifer system in the Gumera catchment is difficult because of insufficient available information and unevenly distributed boreholes.

7. References

Abate, M., Nyssen, J., Steenhuis, T. S., Moges, M. M., Tilahun, S. A., Enku, T., & Adgo, E. (2015). Morphological changes of Gumara River channel over 50 years, upper Blue Nile basin, Ethiopia. *Journal of Hydrology*, *525*, 152-164.

Abiy, A. Z., Demissie, S. S., MacAlister, C., Dessu, S. B., & Melesse, A. M. (2016). Groundwater Recharge and Contribution to the Tana Sub-basin, Upper Blue Nile Basin, Ethiopia. In: Landscape Dynamics, Soils and Hydrological Processes in Varied Climates (A. M. Melesse & W. Abtew, eds). *Springer International Publishing,* 463-481.

Alemayehu, T., McCartney, M., & Kebede, S. (2010). The water resource implications of planned development in the Lake Tana catchment, Ethiopia. *Ecohydrology & Hydrobiology*, *10*, 211-221.

Awulachew, S. B., Merrey, D., Kamara, A., Van Koppen, B., Penning de Vries, F., & Boelee, E. (2005). Experiences and opportunities for promoting small-scale/micro irrigation and rainwater harvesting for food security in Ethiopia . *International Water Management Institute*, 86.

Ayele, H. S., Li, M. H., Tung, C. P., & Liu, T. M. (2016). Impact of Climate Change on Runoff in the Gilgel Abbay Watershed, the Upper Blue Nile Basin, Ethiopia. *Water*, *8*, 380.

Bakundukize, C., Van Camp, M., & Walraevens, K. (2011). Estimation of groundwater recharge in Bugesera region (Burundi) using soil moisture budget approach. *Geologica Belgica*, *14*, 85-102.

Beyene, A., & Abdelsalam, M.G. (2005). Tectonics of the Afar Depression: A review and synthesis: *Journal of African Earth Sciences*, 41, 41–59.

Bookhagen, B., & Burbank, D. W. (2006). Topography, relief, and TRMM-derived rainfall variations along the Himalaya. *Geophysical Research Letters*, *33*.

Canadell, J., Jackson, R. B., Ehleringer, J. B., Mooney, H. A., Sala, O. E., & Schulze, E. D. (1996). Maximum rooting depth of vegetation types at the global scale. *Oecologia*, *108*, 583-595.

Chebud, Y. A., & Melesse, A. M. (2009). Modelling lake stage and water balance of Lake Tana, Ethiopia. *Hydrological Processes*, *23*, 3534-3544.

Chesworth, W. (2008). Encyclopedia of soil science. *Springer International Publishing,* 845.

Chorowicz, J., Collet, B., Bonavia, F. F., Mohr, P., Parrot, J. F., & Korme, T. (1998). The Tana basin, Ethiopia: Intra-plateau uplift, rifting and subsidence. *Tectonophysics*, 295, 351-367.

Conway, D. (2000). The Climate and hydrology of the Upper Blue Nile River, *The Geographical Journal*., 166, 49–62.

Davis, P.M., & Slack, P.D. (2002). The uppermost mantle beneath the Kenya dome and relation to melting, rifting and uplift in East Africa. *Geophysical Research Letters*, 29, 211-214.

Demlie, M. (2015). Assessment and estimation of groundwater recharge for a catchment located in highland tropical climate in central Ethiopia using catchment soil–water balance (SWB) and chloride mass balance (CMB) techniques. *Environmental Earth Sciences*, *74*, 1137-1150.

Derib, S. D. (2015). Balancing Water Availability and Water Demand in the Blue Nile: A case Study of Gumara Watershed in Ethiopia. *Zentrum für Entwicklungsforschung*.

Dessie, M., Verhoest, N.E.C., Admasu, T., Pauwels, V.R.N., Poesen, J., Adgo, E., Deckers, J., Nyssen, J. (2014a). Effects of the floodplain on river discharge into Lake Tana (Ethiopia). *Journal of Hydrology,* 519, 699-710.

Dessie, M., Verhoest, N.E.C., Pauwels, V.R.N., Admasu, T., Poesen, J., Adgo, E., Deckers, J., Nyssen, J. (2014b). Analyzing runoff processes through conceptual hydrological modelling in the Upper Blue Nile basin, Ethiopia. *Hydrology Earth System Sciences*, 18, 5149-5167.

Dessie, M., Verhoest, N.E.C., Pauwels, V.R.N., Adgo, E., Deckers, J., Poesen, J., Nyssen, J., (2015). Water balance of a lake with floodplain buffering: Lake Tana, Blue Nile Basin, Ethiopia. *Journal of Hydrology* 522, 174-186.

De Vries, J. J., & Simmers, I. (2002). Groundwater recharge: an overview of processes and challenges. *Hydrogeology Journal*, *10*, 5-17.

Eriksson, E., & Khunakasem, V. (1969). Chloride concentration in groundwater, recharge rate and rate of deposition of chloride in the Israel Coastal Plain. *Journal of Hydrology*, *7*, 178-197.

Fan, J., McConkey, B., Wang, H., & Janzen, H. (2016). Root distribution by depth for temperate agricultural crops. *Field Crops Research*, *189*, 68-74.

Fetter, C. W. (2000). Chapter 5: Water Quality and Groundwater Contamination. In: Applied hydrogeology. *Prentice hall*, 615.

Fiantis, D., Nelson, M., Shamshuddin, J., Goh, T. B., & Van Ranst, E. (2010). Determination of the geochemical weathering indices and trace elements content of new volcanic ash deposits from Mt. Talang (West Sumatra) Indonesia. *Eurasian Soil Science*, *43*, 1477-1485.

Gani, N.D., & Abdelsalam, M.G. (2006). Remote sensing analysis of the Gorge of the Nile, Ethiopia with emphasis on Dejen–Gohatsion region. *Journal of African Earth Sciences*, 44, 135-150.

Gani, N. D., Gani, M. R., & Abdelsalam, M. G. (2007). Blue Nile incision on the Ethiopian Plateau: Pulsed plateau growth, Pliocene uplift, and hominin evolution. *GSA today*, *17*.

Healy, R. W., & Cook, P. G. (2002). Using groundwater levels to estimate recharge. *Hydrogeology Journal*, *10*, 91-109.

Hemker, K., & Post, V. (2011). MLU for Windows. *MLU Users Guide*.

Hofmann, C., Courtillot, V., Feraud, G., Rochette, P., Yirgu, G., Ketefo, E., and Pik, R. (1997). Timing of the Ethiopian flood basalt event and implications of Plume birth and global change. *Nature*, 389, 838-841.

Jemberie, M. A., Awass, A. A., Melesse, A. M., Ayele, G. T., & Demissie, S. S. (2016). Seasonal Rainfall-Runoff Variability Analysis, Lake Tana Sub-Basin, Upper Blue Nile Basin, Ethiopia. In: Landscape Dynamics, Soils and Hydrological Processes in Varied Climates. *Springer International Publishing,* 341-363.

Johnson, A.I. (1967). Specific yield - compilation of specific yields for various materials. *U.S. Geological. Survey Water Supply Paper 1662-D*, 74.

Jones, J. B., and Mulholland, P. J. (2000). Streams and groundwater. *Academic Press*.

Kassahun, M. (2012a). Pump test report of Lucha deep well. *Water Well Drilling Enterprise* (ANRS WWDE), 12.

Kassahun, M. (2012b). Pump test report of Leway deep well. *Water Well Drilling Enterprise* (ANRS WWDE), 13.

Kebede, S. (2013). Groundwater in Ethiopia: Features, Numbers and Opportunities. *Springer*.

Kebede, S., Travi, Y., Alemayehu, T., Ayenew, T. (2005). Groundwater recharge, circulation and geochemical evolution in the source region of the Blue Nile River, Ethiopia. *Applied Geochemistry*, 20, 1658–1676.

Kebede, S., Travi, Y., Alemayehu, T., & Marc, V. (2006). Water balance of Lake Tana and its sensitivity to fluctuations in rainfall, Blue Nile basin, Ethiopia. *Journal of Hydrology*, *316*, 233-247.

Kieffer, B., Arndt, N., Lapierre, H., Bastien, F., Bosch, D., Pecher, A. & Keller, F. (2004). Flood and shield basalts from Ethiopia: magmas from the African super swell. *Journal of Petrology*, *45*, 793-834.

Kim, U., Kaluarachchi, J. J., & Smakhtin, V. U. (2008). Generation of monthly precipitation under climate change for the upper blue Nile river basin, Ethiopia. *Journal of the American Water Resources Association* (JAWRA) 44, 1231-1247.

Korecha, D., & Barnston, A. G. (2007). Predictability of June–September rainfall in Ethiopia. *Monthly Weather Review*, *135*, 628-650.

Kruseman, G. P., & Ridder, N. A. (1990). Chapter 13: Recovery tests. In: Analysis and evaluation of pumping test data. *International Institute for Land Reclamation and Improvement*, 193-197.

Ludi, E., Terefe, B., Calow, R., & Birhane, G. (2013). Ethiopia's water resources, policies, and institutions. In: Achieving Water Security: Lessons from Research in Water Supply, Sanitation and Hygiene in Ethiopia (R. Calow, E. Ludi and J. Tucker, eds). *Practical Action Publishing*, Rugby.

Mamo, K. H. M., & Jain, M. K. (2013). Runoff and sediment modeling using SWAT in Gumera catchment, Ethiopia. *Open Journal of Modern Hydrology*, 3, 10.

Mason, N., MacDonald, A., Mtisi, S., Haylamicheal, I. D., & Abebe, H. (2013). Sustainability of water services in Ethiopia. In: Achieving Water Security: Lessons from Research in Water Supply, Sanitation and Hygiene in Ethiopia (R. Calow, E. Ludi and J. Tucker, eds). Practical Action Publishing, Rugby.

Mohr, P. A. (1968). The Cainozoic volcanic succession in Ethiopia. *Bulletin of Volcanology*, *32*, 5-14.

Mukul, M., Srivastava, V., & Mukul, M. (2016). Accuracy analysis of the 2014–2015 Global Shuttle Radar Topography mission (SRTM) 1 arc-sec C-Band height model using international Global Navigation Satellite System Service (IGS) network. *Journal of Earth System Science*, *125*, 909-917.

Nigate, F., Ayenew, T., Belete, W., & Walraevens, K. (2017). Overview of the Hydrogeology and Groundwater Occurrence in the Lake Tana Basin, Upper Blue Nile River Basin. In: Social and Ecological System Dynamics . *Springer International Publishing*, 77-91.

Nigate, F., Van Camp, M., Kebede, S., & Walraevens, K. (2016). Hydrologic interconnection between the volcanic aquifer and springs, Lake Tana basin on the Upper Blue Nile. *Journal of African Earth Sciences*, *121*, 154-167.

Nigate, F., Van Camp, M., & Walraevens, K. Hydrogeology and water chemistry of Infranz catchment springs, Bahir Dar Area, Lake Tana Basin, Ethiopia. *Land Degradation & Development*, (in press).

Pereira, A. R., & De Camargo, A. P. (1989). An analysis of the criticism of Thornthwaite's equation for estimating potential evapotranspiration. *Agricultural and Forest Meteorology*, *46*, 149-157.

Poppe, L., Frankl, A., Poesen, J., Admasu, Teshager, Dessie, Mekete, Adgo, Enyew, Deckers, J., Nyssen, J. (2013). Geomorphology of the Lake Tana basin, Ethiopia. *Journal of Maps*, 9, 431–437.

Schad, P., & Spaargaren, O. (2006). World Reference Base for Soil Resources 2006: A Framework for International Classification, Correlation and Communication. *Food and agriculture organization of the United Nations (FAO).*

Şen, Z. (2014) Practical and applied hydrogeology. *Elsevier,* 424*.*

Şengör, A.M.C. (2001). Elevation as indicator of mantle-plume activity. In: Mantle Plumes: Their identification through time (R.E., Ernst and K.L., Buchan, eds). *Geological Society of America Special Paper,* 352, 183–225.

Setegn, S. G., Rayner, D., Melesse, A. M., Dargahi, B., & Srinivasan, R. (2011). Impact of climate change on the hydroclimatology of Lake Tana Basin, Ethiopia. *Water Resources Research*, *47*.

Seyoum, M., van Andel, S. J., Xuan, Y., & Amare, K. (2013). Precipitation forecasts for rainfall runoff predictions. A case study in poorly gauged Ribb and Gumara catchments, upper Blue Nile, Ethiopia. *Physics and Chemistry of the Earth, 61*, 43-51.

SOGREAH, (2012a). Final Stage 1 Report – Part 3: Geological and Geomorphological Survey, *Ministry of Water and Energy*.

SOGREAH, (2012b). Final stage 1 Report – Part 4: Geophysical Survey, *Ministry of Water and Energy*.

SOGREAH, (2012c). Final stage 1 Report – Part 6: Hydrogeological Survey, *Ministry of Water and Energy.*

Sun, H., Grandstaff, D. & Shagam, R. (1999). Land subsidence due to groundwater withdrawal: potential damage of subsidence and sea level rise in southern New Jersey, USA*. Environmental Geology,* 37, 290-296.

Theis, C. V. (1935). The relation between the lowering of the Piezometric surface and the rate and duration of discharge of a well using ground-water storage. *Eos, Transactions American Geophysical Union*, *16*, 519-524.

Thornthwaite, C. W., & Mather, J. R. (1957). Instructions and tables for computing potential evapotranspiration and the water balance. *Laboratory of Climatology*, 254.

Ting, C. S., Kerh, T., & Liao, C. J. (1998). Estimation of groundwater recharge using the chloride mass-balance method, Pingtung Plain, Taiwan. *Hydrogeology Journal*, *6*, 282-292.

Van Koppen, B., Smits, S., Moriarty, P., Penning de Vries, F., Mikhail, M., and Boelee, E. (2009) Climbing the Water Ladder – Multiple-Use Water Services for Poverty Reduction, *IRC International Water and Sanitation Centre and International water Management Institute*,213.

Wagena, M. B., Sommerlot, A., Abiy, A. Z., Collick, A. S., Langan, S., Fuka, D. R., & Easton, Z. M. (2016). Climate change in the Blue Nile Basin Ethiopia: implications for water resources and sediment transport. *Climatic Change*, 139, 229-243.

White, W. B., Culver, D. C., Herman, J. S., Kane, T. C. & Mylroie, J. E. (1995). Karst lands. *American Scientist,* 83, 450–459.

Wilson, J. L., & Guan, H. (2004). Mountain-Block Hydrology and Mountain-Front Recharge. *The American Geopysical Union*, 113-137.

Woldesenbet, T. A., Elagib, N. A., Ribbe, L., & Heinrich, J. (2017). Hydrological responses to land use/cover changes in the source region of the Upper Blue Nile Basin, Ethiopia. *Science of The Total Environment*, *575*, 724-741.

World Health Organization. (2006). Guidelines for drinking-water quality. *World Health Organization*.

World Health Organisation (WHO) (2016) Key country indicators [website] <http://apps.who.int/gho/data/node.cco.ki-ETH?lang=en> [accessed 9 April 2017].

Wubie, M. A., Assen, M., & Nicolau, M. D. (2016). Patterns, causes and consequences of land use/cover dynamics in the Gumara watershed of Lake Tana basin, Northwestern Ethiopia. *Environmental Systems Research*, *5*, 8.

Zhu, R., Zheng, H., & Liu, C. (2010). Estimation of groundwater residence time and recession rate in watershed of the Loess Plateau. *Journal of Geographical Sciences*, *20*, 273-282.

8. Appendix

Date	Rainfall_Infranz	Rainfall_Gumera	Rainfall_Ribb
30-Jul-16	8	15	No_measurement
31-Jul-16	19	15,1	2,5
1-Aug-16	17	8,5	1
2-Aug-16	1,75	28,3	15,4
3-Aug-16	0,3	30	7
4-Aug-16	3,5	7,5	3
5-Aug-16	7,5	10,1	1,5
6-Aug-16	22	15,15	2
7-Aug-16	22	10,5	15,3
8-Aug-16	1,75	6,2	0
9-Aug-16	15	15,15	30,2
10-Aug-16	21	25	3,5
11-Aug-16	0,3	6,5	0,4
12-Aug-16	30	3,6	0,2
13-Aug-16	20	1,25	0,1
14-Aug-16	0	1	0
15-Aug-16	0	7,5	6
16-Aug-16	0	10	15
17-Aug-16	3	10,5	4,5
18-Aug-16	9,5	25	15,2
19-Aug-16	40	8,5	20,2
20-Aug-16	10	7	0,1
21-Aug-16	12	15,5	15,4
22-Aug-16	20	40,2	1,5
23-Aug-16	0	10,5	4
24-Aug-16	1,25	0,1	0
25-Aug-16	21	0,5	0
26-Aug-16	45	9,5	0
27-Aug-16	1,23	0,8	10,3
28-Aug-16	10	1	0
29-Aug-16	7	2	3
30-Aug-16	5	25	15,3
Total	374,08	372,45	192,6

Table 7.1: The daily rainfall measurements to assess the correlation between different catchments for August.

(a)

W-Id	X	Y	Z	reference level	27-5-2016	10-6-2016	24-6-2016	8-7-2016	17-7-2016	23-7-2016	30-7-2016	13-8-2016	20-8-2016	26-8-2016	3-9-2016	17-9-2016
GUM-01	352978	1310739	1803	0,43	4,06	4,32	4,53	2,77	1,91	1,53	0,92	1,06	1,25	1,35	1,4	1,15
GUM-02	346561	1306439	1825	0,93	3,11	3,15	1,56	1,37	1,03	0,59	0,1	1,32	1,95	2,5	1,95	1,78
GUM-03	347703	1299802	1939	0,6	14,92	15,14	15,25	7,34	5,44	4,5	4,36	3,47	5,05	5,99	6,5	7,48
GUM-04	364059	1285613	2232	0,6	8,23	8,31	8,28	4,46	3,2	2,85	2,32	2,3	2,14	2,38	2,45	2,62
GUM-05	400870	1296665	2462	0,33	3,6	3,64	3,69	0,3	0,54	0,62	0	0	0,1	0	0,42	1,22
GUM-06	389559	1305899	2461	-	14,89	14,92	14,96	14,72	14,87	14,91	14,77	12,6	12,4	11,97	11,87	11,9
GUM-07	382602	1295007	2347	0,86	9,21	9,51	9,7	1,1	0,94	0,31	0,13	0	0,01	0	0	0,08
GUM-08	383239	1294956	2399	0,59	11,18	11,17	11,21	9,11	8,57	8,36	7,94	8,21	7,41	9,04	9,55	9,82
GUM-09	355418	1308829	1819	0,75	6,25	6,32	6,4	4,63	3,58	3,4	2,64	1,9	1,75	1,66	1,75	1,82

(b)

W-Id	X	Y	Z	Reference level	5-10-2016	22-10-2016	5-11-2016	20-11-2016	3-12-2016	16-12-2016	5-1-2017	24-1-2017	10-2-2017	25-2-2017	11-3-2017
GUM-01	352978	1310739	1803	0,43	1,415	2,11	2,02	3,2	4,02	4,25	4,27	4,33	4,39	4,77	4,67
GUM-02	346561	1306439	1825	0,93	1,71	2,57	2,17	2,33	2,47	2,48	2,6	2,61	2,85	3,2	3,05
GUM-03	347703	1299802	1939	0,6	8,365	9,85	9,11	11,16	9,93	11,35	11,66	11,93	12,79	13,67	14,75
GUM-04	364059	1285613	2232	0,6	2,915	3,81	4,33	5,25	6,1	6,54	7,06	7,9	7,73	7,87	7,99
GUM-05	400870	1296665	2462	0,33	1,34	1,79	2,08	2,17	2,52	-	-	-	-	-	-
GUM-06	389559	1305899	2461	-	12,1	12,3	12,85	13,41	13,6	13,78	13,94	14,12	14,3	14,42	14,4
GUM-07	382602	1295007	2347	0,86	1,335	3,45	4,09	6,67	7,35	8,39	6,29	9,99	9,74	9,39	9,95
GUM-08	383239	1294956	2399	0,59	9,97	10,71	10,76	10,88	11,03	10,96	11,13	11,09	11,27	10,14	11,2
GUM-09	355418	1308829	1819	0,75	1,785	2,5	2,795	3,09	3,35	3,51	-	4,5	4,85	-	4,45

Table 7.2: Representation of the weekly groundwater level measurements. (a) from 27-05-2016 to 17-9 -2016. (b) from 5-10-2016 to 11-03-2017.

ID	Easting	Northing	Elevation (m)	Location
S1	355301	1309364	1808	Wanzaye
S2	391391	1310031	2640	Debra Tabor
S3	389633	1309932	2585	Abuti
S4	389492	1309989	2581	Abuti
S5	388538	1308260	2373	Abuti
S6	388467	1308192	2360	Abuti
S7	389629	1309373	2481	Abuti
S8	389451	1310287	2596	Abuti
S9	404307	1299743	2847	Garavane
S10	403796	1299819	2909	Garavane
S11	403946	1299835	2903	Garavane
S12	400645	1298623	2831	Jezus
S13	400835	1298537	2835	Jezus
S14	401729	1297399	2809	Telikmeda
S15	401320	1296638	2638	Telikmeda
S16	400154	1295262	2697	Liwaye Ashama Gedayat
S17	398480	1294693	2681	Liwaye Ashama Gedayat
S18	384275	1288788	2389	Shemagile Giyorigis
S19	372236	1285931	2369	Gelawudiwos
S20	385282	1300152	2076	Genamechawecha
S21	385138	1299084	2142	Genamechawecha
S22	384894	1296252	2348	Mahideramariyam
S23	382556	1294717	2325	Mahideramariyam
S24	379775	1291860	2150	Ginda Temem
S25	368965	1286945	2338	Gelawudiwos
S26	361301	1287191	2324	Sheme Mariyam
S27	358036	1287771	2367	Sheme Mariyam
S28	348654	1298790	1979	Kusheshilame
S29	346553	1300954	1946	Kusheshilame
S30	355777	1303279	1783	Wanzaye
S31	355557	1310144	1802	Wanzaye
S32	388115	1304603	2323	Werken
S33	389887	1306593	2418	Werken
S34	390321	1306476	2440	Werken
S35	390227	1307009	2474	Debra Tabor
S36	391010	1307497	2522	Debra Tabor
S37	390679	1309209	2616	Debra Tabor
S38	391181	1308587	2785	Debra Tabor
S39	373962	1313578	2099	Chalmana Mantura

Table 7.3: Representation of the location and elevation of the inventorized springs

Well	Easting	Northing	Elevation	Location
GIW1	355492	1308661	1821	Wanzaye
GIW2	355476	1308647	1821	Wanzaye
GIW3	355522	1308625	1822	Wanzaye
GIW4	355538	1308606	1822	Wanzaye
GIW5	355634	1308406	1823	Wanzaye
GIW6	355404	1308410	1821	Wanzaye
GIW7	354242	1310502	1812	Wanzaye
GIW8	347583	1307017	1806	Zarina Jegina
GIW9	347677	1306782	1807	Zarina Jegina
GIW10	389251	1309420	2498	Abuti
GIW11	388285	1308276	2364	Abuti
GIW12	401621	1298691	2861	Garavane-Jezus (Mynet)
GIW13	400678	1298341	2856	Jezus (Mynet)
GIW14	383155	1294979	2354	Mahideramariyam
GIW15	383121	1295032	2349	Mahideramariyam
GIW16	359861	1287645	2401	Sheme Mariyam
GIW17	358165	1287515	2388	Sheme Mariyam
GIW18	355636	1302564	1845	Wanzaye
GIW19	391585	1310324	2664	Debra Tabor
GIW20	391285	1308793	2836	Debra Tabor
GIW21	391536	1308867	2822	Debra Tabor
GIW22	391606	1309728	2709	Debra Tabor
GIW23	345579	1305471	1899	Zarina Jegina
GIW24	374477	1312599	2058	Amboras

Table 7.4: Representation of the location and elevation of the inventorized wells. GIW refers to Gumera Inventorized Well.

Name	P1-27082016	P2-27082016	R1-29072016	R2-27082016	S1-27082016	S3-19082016	S8-19082016	S36-19082016	S10-20082016	S36-26082016	S15-19082016	S16-20082016
PH	7,16	7,2	6,07	6,29	6,23	6,72	6,67	5,54	5,78	5,41	6,61	5,84
EC (µS /cm)	413	626	11,1	26,2	232	219	243	51,3	73,1	50,4	177,4	87
Na^{+}(mg/l)	6,36	15,63	0,105	0,185	3,62	3,84	4,8	1,72	2,31	2,13	5,56	3,08
K^{+} (mg/l)	1,8	0,31	0,13	0,09	0,69	2,17	1,62	1,39	0,85	0,85	1,4	1,26
Ca^{2+}(mg/l)	60,28	77,203	0,406	1,389	20,64	25,46	30,64	10,235	11,52	3,62	16,23	12,42
Mg^{2+} (mg/l)	7,36	14,7	0,065	0,042	9,46	7,4	7,96	1,42	1,56	0,88	3,14	1,4
Fe^{2+}/Fe^{3+} (mg/l)	0,16	0,1	0,06	0,13	0,1	0,34	0,1	0,73	0,13	0,13	0,11	0,44
Mn^{2+} (mg/l)	0,367	0,022	0,009	0,003	0,007	0,016	0,003	0,036	0,01	0,011	0,003	0,025
NH_4^{+} (mg/l)	0,1608	0,0023	0,2571	1,1847	0	0	0	0	0,0373	0	0	0,0001
Cl^{-} (mg/l)	9,0704	7,0228	0,1916	0,7831	3,557	2,6301	0,6689	3,125	4,944	2,3879	2,4848	4,0724
SO_4^{2-} (mg/l)	4,8604	1,3993	0,1756	1,2057	2,2282	3,3595	1,0185	3,6283	9,321	3,4043	5,6221	8,0415
NO_3^{-} (mg/l)	0,647	0	0	1,236	36,794	8,0673	10,624	6,3116	2,954	1,8235	10,32	5,6326
NO_2^{-} (mg/l)	0,0508	0,0046	0,0187	0,0274	0,0086	0,0247	0,0008	0,0234	0,0725	0,0144	0,0154	0,0417
HCO_3^{-} (mg/l)	244	384,3	3,05	6,71	93,33	123,22	139,69	26,23	32,33	14,64	70,15	39,04
PO_4^{3-} (mg/l)	0,2915	0	0,0053	0,0225	0,0501	0,5874	0,2184	0,1085	0,3565	0,082	0,2865	0,0544
TDS (mg/l)	335,408	500,69	4,473	13,008	170,4849	177,115	197,344	54,958	66,395	29,973	115,322	75,508
Li^{+} (mg/l)	0	0	0	0	0	0	0	0	0	0	0	0
Sr^{2+} (mg/l)	0,911	1,886	0	0	0,175	1,134	1,024	0,286	0	0,216	0,783	0,249
F^{-} (mg/l)	0,134	0,437	0,011	0,013	0,0501	0,11	0,121	0,066	0,081	0,031	0,125	0,038
Br^{-} (mg/l)	0,291	0,229	0,074	0,099	0,206	0,083	0,081	0,058	0,056	0,102	0,1	0,074

Table 7.5: Concentrations of the ions in the spring samples.

Name	S19-20082016	S21-20082016	S24-20082016	S25-20082016	S26-20082016	S27-20082016	S32-19082016	S33-19082016	S39-27082016
PH	6,02	6,71	6,03	6,19	6,02	5,27	5,77	6,01	6,42
EC (µS /cm)	96,8	147,6	139,8	114,1	80,6	54,4	63,2	105,5	270
Na^{+}(mg/l)	2,67	3,32	5,06	3,43	1,78	1,99	4,2	1,8	5,95
K^{+} (mg/l)	0,45	0,93	0,57	0,37	0,19	0,38	0,96	0,24	0,25
Ca^{2+}(mg/l)	13,06	25	15,76	14,52	14,46	5,56	9,2	15	23,26
Mg^{2+} (mg/l)	2,46	3,04	2,9	2,5	1,68	0,92	0,78	2,66	12,06
Fe^{2+}/Fe^{3+} (mg/l)	0,32	0,11	0,37	0,66	0,21	0,11	0,21	0,33	0,21
Mn^{2+} (mg/l)	0,01	0,009	0,008	0,006	0,009	0,012	0,005	0,006	0,095
NH_4^{+} (mg/l)	0	0	0	0	0	0	0	0,0104	0,0248
Cl^{-} (mg/l)	5,9713	1,8968	3,4844	3,0832	3,2665	1,9003	4,5324	3,6677	2,7546
SO_4^{2-} (mg/l)	5,3421	1,6569	4,334	2,8666	3,1467	1,8025	5,2748	4,9724	5,4317
NO_3^{-} (mg/l)	5,053	22,823	22,712	5,62	5,5959	7,624	7,56	13,567	10,245
NO_2^{-} (mg/l)	0,0316	0,0066	0,018	0,0178	0,0119	0,0098	0,0268	0,0204	0,0194
HCO_3^{-} (mg/l)	46,97	74,42	53,68	63,44	39,04	17,69	25,62	43,31	145,18
PO_4^{3-} (mg/l)	0,1785	0,464	0,0784	0,1404	0,1717	0,0188	0,399	0,0194	0,012
TDS (mg/l)	82,517	133,676	108,975	96,654	69,562	38,017	58,768	85,603	205,493
Li^{+} (mg/l)	0	0	0	0	0	0	0	0	0
Sr^{2+} (mg/l)	0,225	0,365	0,356	0,26	0,229	0	0,248	0,253	0,512
F^{-} (mg/l)	0,056	0,054	0,061	0,044	0,054	0,022	0,089	0,089	0,079
Br^{-} (mg/l)	0,059	0,069	0,76	0,061	0,124	0,15	0,055	0,072	0,178

Table 7.6: Concentrations of the ions in the spring samples.

Name	GIW12-20082016	GIW16-20082016	GIW17-20082016	GIW19-19082016	GIW20-19082016	GIW23-26082016	GUM-01-27082016	GUM-03-20082016	GUM-05-19082016	GUM-07-20082016	GUM-08-20082016	GUM-09-27082016
PH	5,71	5,43	5,11	5,66	6,89	5,92	5,97	5,74	6,01	6,34	6,11	6,35
EC (µS /cm)	82,7	110,5	46,9	667	28,5	231	241	91,7	112,7	106,8	101,5	267
Na^{+}(mg/l)	2,52	0,54	0,516	28,74	2,46	3,18	6,06	2,2	4,56	20,92	3,82	5,08
K^{+} (mg/l)	1,93	0,94	0,39	5,6	1,03	0,21	0,95	0,13	2,89	96	0,86	0,74
Ca^{2+}(mg/l)	11,63	15,12	6,9	52,5	5,23	26,4	18,92	8,45	11,23	80,34	12,16	22,65
Mg^{2+} (mg/l)	0,72	2,28	0,94	11,7	0,299	7,04	5,56	2,95	1,8	5,5	1,54	9,8
Fe^{2+}/Fe^{3+} (mg/l)	0,41	0,07	0,29	0,03	0,05	0,09	0,27	0,13	0,63	0,18	0,12	0,09
Mn^{2+} (mg/l)	0,026	0,02	0,017	0,007	0,001	0,006	0,219	0,005	0,014	0,128	0,005	0,011
NH_4^{+} (mg/l)	0,0197	0,1331	0,1611	0	0	0	0	0	0,006	0	0	0
Cl^{-} (mg/l)	8,4755	5,1896	2,6577	63,851	0,8937	10,412	29,54	2,087	4,992	63,09	4,3629	5,5874
SO_4^{2-} (mg/l)	7,9631	1,2649	2,6762	12,992	1,1977	10,461	10,696	1,417	9,542	48,69	2,0563	5,286
NO_3^{-} (mg/l)	4,4703	26,058	11,75	168,065	0,6532	47,352	4,5376	3,5623	10,553	202,32	5,1983	47,872
NO_2^{-} (mg/l)	0,0482	0,0187	0,0105	0,0325	0,003	0,0107	0,0312	0,0083	0,043	0,882	0,0077	0,0086
HCO_3^{-} (mg/l)	25,62	23,79	10,98	28,06	20,74	56,73	48,19	43,31	35,38	166,53	37,82	83,57
PO_4^{3-} (mg/l)	0,5088	0,1735	0,0734	0,0219	0,0096	0,0593	0,1232	0,0673	0,0925	0,9006	0,4296	0,0323
TDS (mg/l)	64,342	75,598	37,362	371,599	32,567	161,951	125,1	64,317	81,734	685,481	68,38	180,727
Li^{+} (mg/l)	0	0	0	0	0	0	0	0	0	0	0	0
Sr^{2+} (mg/l)	0	0,28	0	2,181	0	0,485	0,503	0,232	0,456	2,068	0,291	0,4
F^{-} (mg/l)	0,032	0,022	0,021	0,043	0,044	0,038	0,044	0,034	0,108	0,063	0,048	0,049
Br^{-} (mg/l)	0,152	0,275	0,176	1,082	0,053	0,337	0,645	0,105	0,149	1,274	0,079	0,252

Table 7.7: Concentration of the ions in the well samples

sample_name	Name_date_sampling	Type	Easting	Northing	Elevation	Depth (m)	Others characteristics
GHP1	P1-27082016	Hand pump	374326	1312748	2065		Surrounded by farmland and grassland
GHP2	P2-27082016	Hand pump	352952	1310599	1802		Surrounded by farmland and grassland
GUM-08	GUM_05-19082016	Well	400870	1296665	2462	5	Surrounded by grassland, farmland and trees
GUM-09	S15-19082016	Spring	401320	1296638	2638	-	Enhanced spring, surrounded by grassland and trees
GUM-10	S3-19082016	Spring	389633	1309932	2585	-	Surrounded by farmland
GUM-11	S8-19082016	Spring	389451	1310287	2596	-	Surrounded by farmland
GUM-12	GIW20-19082016	Well	391285	1308793	2836	29	No agriculture, surrounded by grassland
GUM-13	GIW19-19082016	Well	391585	1310324	2664		Inside Debra Tabor, surrounded by many houses
GUM-14	S32-19082016	Spring	388115	1304603	2323	-	Surrounded by farmland
GUM-15	S33-19082016	Spring	389887	1306593	2418	-	Fractured rock, Surrounded by farmland
GUM-16	S10-19082016	Spring	403796	1299819	2909	-	Surrounded by farmland, no discharge
GUM-16 / GUM-31	S36-19082016 / S36-26082016	Spring	391010	1307497	2522	-	Enhanced spring, fractured rock
GUM-17	GIW12-20082016	Well	401621	1298691	2861		Surrounded by farmland
GUM-18	S16-20082016	Spring	400154	1295262	2697	-	Surrounded by farm- and grassland
GUM-19	S21-20082016	Spring	385138	1299084	2142	-	Enhanced spring, surrounded by grassland and trees
GUM-20	GUM_08-20082016	Well	383239	1294956	2399	8	Occurs on a hill top, surrounded by farmland

Table 7.8: Description of the different water samples (part 1).

sample_name	Name_date_sampling	Type	Easting	Northing	Elevation	Depth	Others characteristics
GUM-21	GUM_07-20082016	Well	382602	1295007	2347	10 m	Occurs in city
GUM-22	S24-20082016	Spring	379775	1291860	2150	-	Surrounded by farmland
GUM-23	S19-20082016	Spring	372236	1285931	2369	-	Surrounded by farmland
GUM-24	S25-20082016	Spring	368965	1286945	2338	-	Enhanced spring, surrounded by farmland
GUM-25	S26-20082017	Spring	361301	1287191	2324	-	Surrounded by forest and farmland
GUM-26	GIW16-20082016	Well	359861	1287645	2401		Hill top
GUM-27	GIW17-20082016	Well	358165	1287515	2388	23 m	Hill top, surrounded by grassland
GUM-28	S27-20082016	Spring	358036	1287771	2367	-	Contact spring, small forest and farmland
GUM-29	GUM_03-20082016	Well	347703	1299802	1939	17 m	Surrounded by farmland and grassland
GUM-30	GIW23-26082016	Well	345579	1305471	1899	7,5 m	Surrounded by farmland and grassland
GUM-33	S39-27082016	Spring	373962	1313578	2099	-	Surrounded by agricultural
GUM-34	GUM_09-27082016	Well	355418	1308829	1819	8,5 m	Surrounded by farmland and grassland
GUM-35	S1-27082016	Spring	355301	1309364	1808	-	In small village, vesicular basalts
GUM-36	GUM_01-27082016	Well	352978	1310739	1803	7 m	Surrounded by farmland and grassland
RDT	R1-29072016	Rain	391494	1311117	2706	-	-
RFOGARA	R2-27082016	Rain	352759	1310660	1796	-	-

Table 7.9: Description of the different water samples (part 2).